eman ta zabal zazu

Universidad del País Vasco

Euskal Herriko Unibertsitatea

Size-dependent electronic properties of metal nanoparticles

Memoria para optar al grado de

Doctora en Ciencias físicas presentada por:

Marina Quijada Van den Berghe

Directores:

Ricardo Díez Muiño

Pedro Miguel Echenique Landiribar

Donostia - San Sebastián, 2015

Contents

1 Introduction

1.1 General context of this Thesis

Nanoscience is a term broadly used, coined to name the study of matter at the nanometer scale. One nanometer (nm) is one billionth of a meter (10^{-9} meters). Typical interatomic distances in solids are of few tenths of nm. This means that, beyond single atoms, the arrangement of a few atoms in a composed system (molecule, cluster, etc.) already belongs to the nanoscale. In a more general way, nanosystems are considered those systems with dimensions ranging between few nm to several hundreds of nm. To better understand the dimensions of the nanoscale, let us mention that one sheet of paper is about 100000 nm thick, a red blood cell is about 8000 nm, and viruses may vary in diameter from 20 nm to 400 nm.

Nanoscience is a highly multidisciplinary activity, in which concepts originated in scientific fields such as physics, chemistry, materials sciences, or biology are used, and often at the same time. In the nanometer scale, the physical, chemical and biological properties of matter differ in fundamental ways from the properties of individual atoms and molecules, as well as from the properties of bulk matter. A textbook example of this is the chemical and optical behaviour of gold. Chemically, gold becomes a good catalyzer in the nanoscale and thus is not noble anymore [1]. Optically, the yellowish color of gold is lost for nanometer-sized particles and different colors arise depending on the exact size of the system.

The understanding of nanosystems is becoming increasingly possible thanks to the development of new experimental tools. Characterization techniques based on scanning microscopies with atomic resolution and fabrication processes such as molecular beam epitaxy are emblematic examples of this point. But the understanding of the nanoscale has been also possible because of unprecedented advance in computational science. Huge efforts in the improvement of theoretical methods and numerical algorithms, together with the fast progress of computing capabilities, have allowed theoretical scientists to describe the properties of nanosystems up to an accuracy with no match in history.

The rising popularity of nanoscience is intimately linked to the vast potential applications that systems of nanometer size may have in technology. Research in nanotechnology is directed towards understanding and creating improved materials, devices, and systems that exploit novel properties

emerging in the nanoscale. For this purpose, a precise control of the fabrication and characterization techniques of nanosystems is required. Fabrication techniques are usually classified into the "bottom-up" and "top-down" approaches. In the former, the systems are built from molecular components which assemble themselves chemically. In the latter, the systems are built from larger entities without atomic-level control. A final goal in this research activity is to design and fabricate systems in these tiny scales with properties at wish: One important consequence of the tunable morphology of nanosystems in terms of shape, size, and environment is the possibility to adapt and tailor their properties relative to bulk crystals.

A crucial point in the scenario described above is thus to understand how the properties of a given system of nanometer size depend on its size. If the final goal is the design of objects with fit properties, an accurate control and understanding of the variability of these properties on size and shape will be necessary. Framed in this general context, this is the main goal of the research activity presented in this manuscript: the analysis of the dependence in size of some given electronic properties in metallic nanoparticles of variable size.

In the history of science, the dependence of a given property on the size of a system of nanoscale dimension is not a recent discovery. The first educated speculation on this issue is probably due to Faraday in 1857 [2]. Faraday was the first to talk about the optical properties of what later become known as metallic nanoparticles, in the context of his research on gold colloids. Faraday discovered that the optical properties of gold colloids differed from those of the corresponding bulk metal, and that the color itself could be easily modified by adding certain salts. Faraday attempted to explain this conspicuous change by saying that *"a mere variation in the size of [gold] particles gave rise to a variety of resultant colours"*. Faraday's work was presumably the first reported observation of quantum size effects. The controlled variation of a given physical property just by modifying the size of the system in the nanoscale could be considered to be the birth of nanoscience.

Another milestone in the control of the nanoscale, again in the field of optics, is the work developed in the 20s and 30s of the XXth century by Irving Langmuir and Katharine B. Blodgett. The two scientists developed a methodology to deposit organic coatings on top of a surface. The big advantage of these so-called Langmuir Blodgett films was that the adsorbed material was deposited layer by layer, making it possible to control accurately the number of layers (and hence the size) of the coating. In this way, the

optical properties of the coatings could be carefully prepared, leading to spectacular practical applications, such as non-reflecting glasses.

Focusing now into the main topic of this work, namely, gas-phase clusters, the development of mass spectrometer ion sources and later molecular beam setups triggered the interest on these systems. Laser vaporization technique enabled to produce clusters of virtually any element in the periodic table, exciting the curiosity of a large community of researchers that eventually bloomed in the 1980s. The term *cluster* was then and is still used in scientific literature to denote an aggregate containing from few atoms up to a few thousand atoms (i.e., from 0.1 nm to 5 nm). It was coined for the first time by the chemist F. A. Cotton in the early 1960s when referring to compounds containing metal-metal bonds. Currently, however, it refers to compounds in a broader perspective. Indeed, the type of chemical bonding established among the cluster constituents can be used to classify the clusters in different categories and metallic clusters, Van der Waals clusters, clusters of ionic materials, or molecular clusters, for instance, can be distinguished [3, 4].

In the field of clusters, size effects have been a matter of continuous investigation. One of the first clear signatures of size effects in gas-phase clusters were the measurements of Schmidt-Ott *et al.* on the photoemission yield from particles with radii smaller than 5 nm [5]. Schmidt-Ott and coworkers showed that the number of photoelectrons reaching the detector strongly depended on the size of the particles and explained their findings in terms of surface/volume ratios.

In the particular case of metal clusters, another relevant finding to push the field was the discovery of electronic shell structure in free alkali clusters by Knight *et al* [6, 7]. As a consequence of this shell structure, clusters with filled electronic shells are more stable and less reactive than clusters with open shells. This is similar to the behavior of atoms in the periodic table, with noble gases being an example of low reactive systems.

The dependence on size of the electrical, optical and mechanical properties in nanometer-sized metal clusters is not always predictable. A small variation in size (an addition of a single atom, in some cases) can change dramatically some of these properties. One of the reasons for this fluctuating behavior is that the geometry of clusters is often difficult to elucidate, in particular for small sizes. In a simplified picture, one could define two different regimes [8]:

- The scalable regime, in which the material properties and functionality differ from the bulk counterpart, but the change is gradual with size and/or

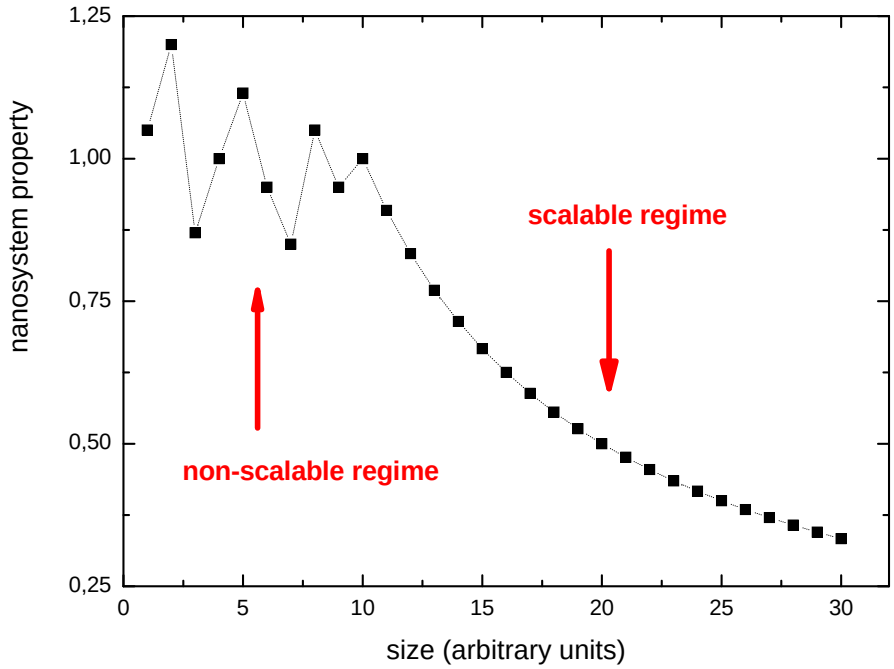

Figure 1.1: Scalability of a given property in a nanosized particle as a function of size: Illustrative behavior

shape.

- The non-scalable regime, in which the material properties change with every new atom added or subtracted from the syste, quantum size effects come into play and the properties exhibit discontinuous behavior.

The regime of interest for possible applications is, in general, that in which the properties vary smoothly and the variation is predictable. A question which still lacks a convincing answer in many cases is the following: how many atoms are needed in a cluster to behave like bulk matter? Furthermore, as will be proven in this work, the answer to this question may depend on the particular property under study.

1.2 Motivation for this Thesis work

The above section may be considered as a general and historical context for this thesis work. Our goal in this research activity has been to study the dependence on size of some electronic properties in metallic nanoparticles and

to understand the reasons of those features that set a difference in behavior with respect to bulk properties. We have focused into two different kind of processes, both of which are linked to electronic excitations in the system.

Decay of electronic excitations

The first of the problems that we address in this thesis work is the decay time of electronic excitations in metal nanoparticles. This is a problem of large interest in the fields of optical spectroscopy and photochemistry. While structural properties of materials depend on ground state features, electronic and optical properties are largely determined by their electronic excitations. Excited electrons are one of the most useful tools in physics to transfer charge and energy. Photoexcited electrons convert light into chemical energy in the photosynthesis process and light into electrical energy in solar cells. For these processes and others to happen, the survival time of these electronic excitations needs to be long enough to avoid the dissipation of the excitation energy into heat.

Electronic excitations in metallic media can decay through various mechanisms. In general, the most important of them are electron-electron (*e*-*e*) and electron-phonon (*e*-*ph*) scattering. In practice, the scattering of the electrons at defects can also be an important mechanism for the decay. Over the last years, a large amount of theoretical and experimental work has been devoted to understand and predict the time evolution of these excitations in solids [9, 10, 11, 12, 13] and at surfaces [14, 15, 16, 17, 18]. This has been helped by the development of new experimental techniques based on femtosecond lasers: Electronic excitations with energies of few eV usually decay in a time scale of the order of femtoseconds, making their analysis by other techniques particularly difficult.

Scientific literature and understanding on electron scattering rates in bulk and surfaces is broad, but the study and control of similar processes in finite size systems is much reduced, partially because of the complexity of the process. The drastic modifications in electronic properties that size variation can induce make it involved to find some general leading trends. However, the size-tuning of the electronic properties of metal systems and the subsequent change in the lifetime of electronic excitations is not a question of purely academic interest, but has important implications for many technological applications. In photochemistry, for instance, electronically excited states can act as intermediate steps in various chemical processes.

Either enhancement or reduction of the reaction rate should be thus possible through a proper design of the intermediate step lifetime. Finite systems of nanometer size are very attractive for this purpose.

From a theoretical point of view, the decay of electronic excitations in a metallic system is a tough many-body problem. The dynamic screening of electrons in an interacting Fermi liquid lies behind the concept of quasiparticle, one of the most useful models to describe theoretically electronic excitations [19]. The interaction between quasiparticles determines the time scales in which the corresponding quantum states retain their identity. A quasiparticle is said to have a lifetime, which sets the duration of the excitation. Furthermore, the lifetime determines the mean free path of the quasiparticle, a measure of the range of influence of the excitation.

For any given system, two are the key features that determine the rate at which electronic excitations decay: the dynamic screening among the medium electrons and the density of electronic states at energies close to the Fermi level. These two effects actually work in opposite directions and there is a delicate balance between them. As summarized in Fig.1.2, a large density of states at the Fermi level implies a large phase space for the electronic excitations to decay, increasing the scattering rate. In parallel, a large density of states at the Fermi level also implies an enhanced screening of the Coulomb interaction between the medium electrons, decreasing the scattering rate. In the first self-consistent calculation of the electron-electron scattering rates in a free electron gas (FEG) perfomed by Quinn and Ferrell [20], it was shown that the screening factor is actually stronger than the density of states argument for the infinite system. Reference [20] showed that the lifetime τ scales with the electronic density parameter r_s as $\tau \propto r_s^{-5/2}$ in the case of the infinite FEG.

Focusing now into the particular case of clusters, the density of states and the screening properties of metallic systems are profoundly affected by their dimensionality. Confinement and surface effects are, among others, two features that can drastically reduce the electronic screening as compared with the bulk case. Confinement in finite systems brings forth an additional effect relevant for the evaluation of lifetimes, namely, the quantization of levels and the subsequent reduction in the number of initial and final states available for the excitation and decay processes respectively. The interplay between these two effects makes the analysis of electron dynamics in clusters and nanoparticles both intricate and appealing.

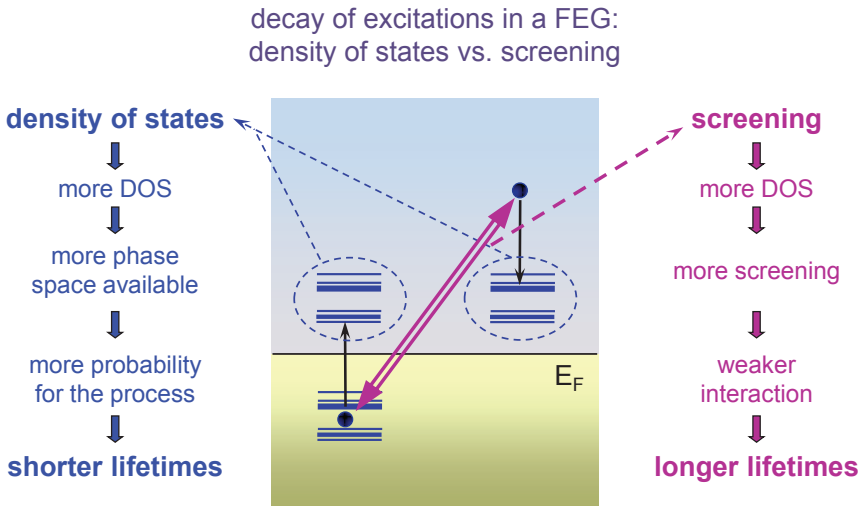

Figure 1.2: Schematic picture of the electron-electron scattering process in a free electron gas (FEG). The two most relevant features determining the rate, i.e., the dynamic screening among the medium electrons and the density of states (DOS) in the vicinity of the Fermi level, are singled out.

The difference between the dynamics of hot electrons in nanoparticles and in bulk has to be discussed taking into account the above mentioned effects. First, the electron lifetime can be enhanced in metal nanoparticles as compared to the bulk situation because of the discretization of levels that reduces the number of final states to which the electronic excitation can decay. However, the electron lifetime can decrease in the nanoparticle because of the general reduction of dynamic screening. The latter effect is due to the relatively lower mobility of the screening electrons in a finite system, as well as to the time spent by the electrons in the vicinity of the surface. There are no *a priori* reasons to choose any of these two effects as more important than the other. Otherwise said, there is no *a priori* reason to predict whether the lifetime of electronic excitations in clusters and nanoparticles is longer than in bulk or not.

From the experimental point of view, collected information does not help much either. Electron dynamics in metal clusters and nanoparticles is usually addressed using laser-based techniques [21], although the acquired knowledge is still scarce as compared to solids and surfaces. Particular attention has been paid to the dependence on size of the electron-electron interaction

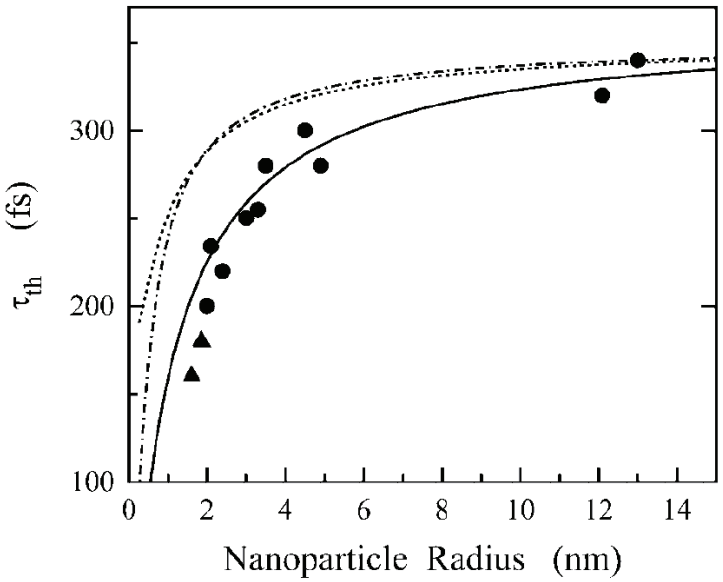

Figure 1.3: Size dependence of the electron thermalization time for Ag nanoparticles. Figure extracted from Ref. [22]. Dots and triangles show the measured values in different matrices. Full line shows a calculated thermalization time, computed taking into account both the spillout (dash-dotted line) and d-electron (dotted line) localization effects. See Ref. [22] for details.

processes [22, 23, 24, 25]. However, some of the conclusions extracted from these works are puzzling. Let us give below a couple of examples.

Voisin *et al.* showed more than one decade ago that the electron thermalization rate (i.e., a quantity that is very much linked, although in an integrated manner, to the inverse of the electron-electron lifetime) is increased for Ag nanoparticles of size smaller than 5 nm, as compared with the bulk reference value [22]. Figure 1.3 shows the measured thermalization times. The decrease of the deexcitation time with the nanoparticle size was attributed to the induced reduction of the Coulomb interaction screening at the nanoparticle surface [22]. In other words, the electron-electron interaction in small nanoparticles is stronger due to large surface regions and this is the effect that determines the rate.

Merschdorf *et al.*, however, measured electron lifetimes in supported Ag nanoparticles appreciably higher than those obtained for Ag bulk or Ag

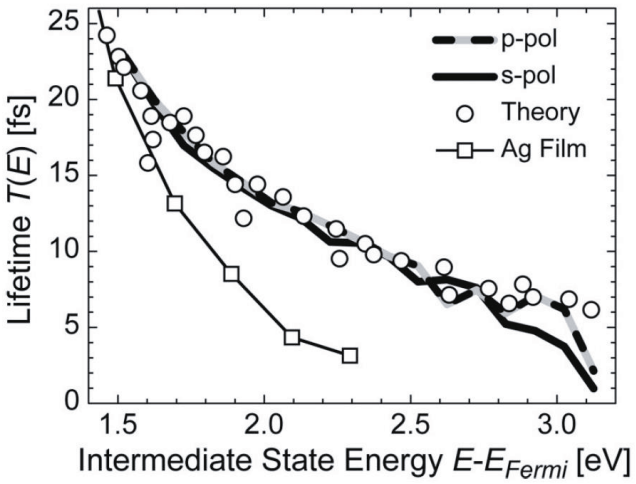

Figure 1.4: Inelastic electron lifetime as a function of the initial state energy above the Fermi level. Figure extracted from Ref. [25]. The two different experimental datasets correspond to data acquired with different polarizations in the excitation. Theoretical predictions and experimental results for a 15 nm thick Ag film are shown for comparison. See Ref. [25] for details.

films [25]. Figure 1.4 shows the measured electronic lifetimes as a function of the initial state energy above the Fermi level and compares them with the corresponding quantities in Ag thin films, which can be considered as a reference for the bulk. The results of Merschdorf *et al.* imply that the deexcitation times in nanoparticles are larger than the corresponding ones in bulk, at least for the range of energies considered. This is a conclusion contradictory to the one discussed in the previous paragraph. It shows well both the complexity of the problem of lifetimes in nanoparticles and the necessity of further research on the subject.

Energy loss problems

The second process that we study is the energy loss of charged particles colliding with metallic systems of nanometer size. Energy loss problems belong to a large tradition in solid-state physics and have relevant connections to some microscopy techniques, as well as important implications in medical physics. The slowing down of charged particles in matter is a key phenomenon in applied materials science, in medical physics, as well as

being an important ingredient in many experimental techniques used in fundamental research on solids, surfaces, and nanostructures. Among many others, let us mention here Low Energy Ion Scattering, Rutherford Back Scattering, and Elastic Recoil Detection Analysis. All these experimental techniques provide information about the structural and electronic properties of materials, as well as about the interaction process itself. Charge exchange and electron emission are other important processes in which electronic excitations of a few eV arise for incident ion energies in the keV/u range.

However, and despite numerous attempts, the complexity of the dynamic interaction between charges and solids has made it difficult to apply theoretical schemes at the level of accuracy achieved in other condensed matter problems. For such accuracy, a detailed description of electronic excitations, dynamic screening, and possible charge transfer processes is required. In the case of metals, a common theoretical approach to describe the electron excitation spectrum of the material is the use of the free electron gas model (FEG).

In the weak coupling limit, first order approaches, such as first Born approximation to treat the scattering and linear response to treat the dynamic screening, are well justified. The weak coupling limit is achieved for fast particles when their charge is much smaller than their velocity (in atomic units). In first-order of perturbation theory, the energy loss per unit path length suffered by such a particle in a free electron gas can be written in terms of the dielectric function of the medium in which the particle moves (in our case, the dielectric function of the FEG) [26], and is given by an integral over the spectrum of excitations defined by energy and momentum.

In the strong coupling limit, when the velocity of the projectile is much smaller than its charge, neither linear response theory to treat the screening nor first-order Born approximation for the scattering process are justified. A combination of scattering theory with the results of static DFT can successfully describe the energy loss in this case [27, 28, 29, 30, 31]. The starting point is the DFT formalism as applied to a static impurity of charge that of the projectile embedded in a free electron gas [32, 33], and the stopping power at low velocities can be written in terms of the transport cross section at the Fermi level, or alternatively the so-called friction coefficient [33, 34].

The above mentioned are well-established approaches to obtain the energy loss in two well-defined limits, namely, the quasi-static situation and the linear regime. Until very recently, there was no quantal self-consistent

theoretical framework able to describe the stopping power of solids for charged projectiles over a wider range of velocities. Only theories based on classical mechanics [35, 36] had been applied. The case in which the projectile velocity is similar to the Fermi velocity v_F of the target electrons is particularly challenging. But in this velocity range, quasi-static or perturbative approximations break down even for unit-charge projectiles.

The development of time-dependent methods in recent years has opened new perspectives in this respect. In particular, time-dependent density functional theory (TDDFT) provides a self consistent, non-perturbative, time-domain treatment of electron dynamics in many body systems. TDDFT has been successfully applied to the calculation of energy transfer in collisions between charged atomic particles and small molecules and clusters in the gas phase [37, 38, 39, 40, 41]. Two-dimensional targets of finite size [42] and metal surfaces [43] have been addressed as well.

In addition to these works, there is a growing interest on ultra-fast processes triggered by the development of femto- and atto-second lasers. Experimental work on this topic naturally puts forward the question on how the electronic excitations caused by external radiation or an intruder in a metallic system evolve in time. It has been demonstrated, for example, that the screening response, one of the basic property of the electron media, needs finite time to be established.

For targets of nanometer size, the interaction time between the projectile and the target electrons might be much shorter than the time needed for the electronic density excitation created in the target to reach its boundaries. The latter time scale can be also interpreted as the characteristic time needed for the many-body excited modes of the nano- object to completely develop. From the point of view of the moving projectile the finite size object would then behave in this time scale as an infinite system in which there will be no quantum size effect for the projectile stopping. From the quantum mechanical point of view, an alternative view would be that, if the spectrum of the perturbation is broad enough to overlap many of the discrete excited states of the system, the continuum limit is retrieved.

The time-domain study of the collision process of projectiles with nanoparticles of variable size is not only a problem of interest in the context of this thesis, but it will also allow us to calculate related properties over a wide range of velocities, so far not achieved. This might give light to the question of the similarities and differences of the slowing down of charges in solids and that occurring in finite-sized systems.

1.3 Outline of this Thesis

This thesis is presented in the form of compilation of publications. Chapter 2 and Chapter 3 contain the fundamentals of the main theory frameworks in which this work has been carried out. The main body of the research activity is presented and discussed in detail in Chapters 4 to 7. Each chapter includes the particular conclusions.

Chapter 2 summarizes the fundamentals of density functional theory and its application to the characterization of metal clusters. In this work, the description of metal clusters is simplified by means of the jellium approximation. One of the main obstacles to obtain meaningful results in the study of size effects is the necessity of analyzing systems of very different size under the same approximation grounds. The jellium approximation allows us cover a wide range of cluster radii under the same theoretical scheme.

Chapter 3 gives an overview of time dependent density functional theory and its application to spherical jellium clusters under the action of a time-dependent external potential with axial symmetry. TDDFT is treated in this work in a fully non-perturbative way. The jellium model is used to calculate the initial state of the system. Then real-time propagation is performed to calculate the evolution of the electronic density of the system.

Chapters 4 and 5 are devoted to the study of the lifetimes of electronic excitations in metal clusters, calculated within linear response theory and the self-energy formalism. Chapter 4 contains a detailed description of the theory employed and first results on the study of size effects. Chapter 5 complements the study on the size dependence of lifetimes, including TDDFT tools for the characterization of the one-electron states describing electronic excitations. The energy dependence of the lifetimes in nanoparticles is analysed as well, obtaining an unexpected result intrinsically different to the corresponding one in bulk materials.

The study of the interaction of charged particles colliding with metallic nanoparticles is addressed in Chapter 6. In this chapter, we calculate the energy loss of protons and antiprotons traversing aluminium clusters. The trajectory of the projectiles crosses the geometrical center of the (jellium) cluster, so axial symmetry is fulfilled. In contrast to results extracted from Chapter 4 and 5, we find out that the energy loss in bulk materials and in nanosized systems have a comparable value.

To complete the study of the collision process of charges with nanoparticles, we addres the calculation of the energy loss of charged

projectiles colliding with metallic thin nanoshells. This is done in Chapter 7.

Last but not least, the general conclusions extracted from this work are provided in Chapter 8. A complete list of the publications resulting from this PhD. work can be found as well at the end of the manuscript.

Atomic units will be used throughout this work unless otherwise stated.

References

[1] H. Häkkinen, S. Abbet, A. Sanchez, U. Heiz, and U. Landman, *Angew. Chem. Int. Ed.* **42**, 1297 (2003).

[2] M. Faraday, *Phil. Trans. R. Soc. London 147* **145** (1857).

[3] Alonso J A and Balbás L C 1996 *Topics in Current Chemistry* vol 182 (Springer-Verlag, Berlin-Heidelberg) p 119

[4] Alonso J A *Structure and Properties of Atomic Nanoclusters* (Imperial College Press, London, 2005)

[5] A. Schmidt-Ott, P. Schurtenberger, and H. C. Siegmann, *Phys. Rev. Lett.* **45**, 1284 (1980).

[6] Knight W D, Clemenger K, de Heer W A, Saunders W A, Chou M Y and Cohen M L 1984 *Phys. Rev. Lett.* **52** 2141

[7] Knight W D, Clemenger K, de Heer W A and Saunders W A, 1985 *Phys. Rev. B* **31** 2539

[8] U. Landman, *PNAS* **102** 6771 (2005).

[9] M. Aeschlimann, M. Bauer, S. Pawlik, W. Weber, S. Burgermeister, D. Oberli, H. C. Siegmann, Phys. Rev. Lett. **79** (1997) 5158.

[10] H. Petek, S. Ogawa, Prog. Surf. Sci. **56** (1997) 239.

[11] E. Knoesel, A. Hotzel, M. Wolf, Phys. Rev. B **57** (1998) 12812.

[12] R. Knorren, K. H. Bennemann, R. Burgermeister, M. Aeschlimann, Phys. Rev. B **61** (2000) 9427.

[13] E. V. Chulkov, A. G. Borisov, J. P. Gauyacq, D. Sánchez-Portal, V. M. Silkin, V. P. Zhukov, P. M. Echenique, Chem. Rev. **106** (2006) 4160.

[14] U. Höfer, I. L. Shumay, Ch. Reuß, U. Thomann, W. Wallauer, T. Fauster, Science **277** (1997) 1480.

[15] M. Weinelt, J. Phys.: Condens. Matter **14** (2002) R1099.

[16] P. M. Echenique, R. Berndt, E. V. Chulkov, Th. Fauster, A. Goldmann, U. Höfer, Surf. Sci. Rep. **52** (2004) 219.

[17] J. Kröger, L. Limot, H. Jensen, R. Berndt, S. Crampin, E. Pehlke, Prog. Surf. Sci. **80** (2005) 26.

[18] J. Güdde, U. Höfer, Prog. Surf. Sci. **80** (2005) 49.

[19] D. Pines and P. Nozières, *The Theory of Quantum Liquids* (Benjamin, New York, 1966).

[20] J. J. Quinn and R. A. Ferrell, *Phys. Rev.* **112**, 812 (1958).

[21] Vajda Š, Bartelt A, Lupulescu C and Wöste L 2003 *Progress in Experimental and Theoretical Studies of Clusters*, Advanced Series in Physical Chemistry vol 13 (Edited by Kondow T and Mafuné F, World Scientific Publishing, Singapore) c 4

[22] C. Voisin, D. Christofilos, N. Del Fatti, F. Vallée, B. Prével, E. Cottancin, J. Lermé, M. Pellarin, M. Broyer, Phys. Rev. Lett. **85** (2000) 2200.

[23] N. Pontius, G. Lüttgens, P. S. Bechthold, M. Neeb, W. Eberhardt, J. Chem. Phys. **115** (2001) 10479.

[24] P. Gerhardt, M. Niemietz, Y. Dok Kim, G. Ganteför, Chem. Phys. Lett. **382** (2003) 454.

[25] M. Merschdorf, C. Kennerknecht, W. Pfeiffer, *Phys. Rev. B* **70**, 193401 (2004).

[26] P. M. Echenique, F. Flores and R. H. Ritchie, in *Solid State Physics: Advances in Research and Applications*, edited by H. Ehrenreich and D. Turnbull (Academic, New York, 1990), Vol. 43, p. 229.

[27] P. M. Echenique, R. M. Nieminen, and R. H. Ritchie, Solid State Commun. **37**, 779 (1981).

[28] I. Nagy, A. Arnau, P. M. Echenique, and E. Zaremba, Phys. Rev. B **40**, R11983 (1989).

[29] A. H. Sørensen, Nucl. Instrum. Methods B **48**, 10 (1990).

[30] A. Närmann, R. Monreal, P. M. Echenique, F. Flores, W. Heiland, and S. Schubert, Phys. Rev. Lett. **64**, 1601 (1990).

[31] A. Salin, A. Arnau, P. M. Echenique, and E. Zaremba, Phys. Rev. B **59**, 2537 (1999).

[32] E. Zaremba, L. M. Sander, H. B. Shore, and J. H. Rose, J. Phys. F **7**, 1763 (1977).

[33] P. M. Echenique, R. M. Nieminen, and R. H. Ritchie, Solid State Commun. **37**, 779 (1981).

[34] A. Salin, A. Arnau, P. M. Echenique, and E. Zaremba, Phys. Rev. B **59**, 2537 (1999).

[35] P. Sigmund and A. Schinner, Eur. Phys. J. D **12**, 425 (2000).

[36] F. Grüner, F. Bell, W. Assmann, and M. Schubert, Phys. Rev. Lett. **93**, 213201 (2004).

[37] K. Yabana, T. Tazawa, Y. Abe, and P. Bozek, Phys. Rev. A **57**, R3165 (1998).

[38] U. Saalmann and R. Schmidt, Phys. Rev. Lett. **80**, 3213 (1998).

[39] T. Kunert and R. Schmidt, Phys. Rev. Lett. **86**, 5258 (2001).

[40] R. Baer and N. Siam, J. Chem. Phys. **121**, 6341 (2004).

[41] T.A. Niehaus, D. Heringer, B. Torralva, and Th. Frauenheim Eur. Phys. J. D **35**, 467 (2005).

[42] A. G. Borisov, J. I. Juaristi, R. Díez Muiño, D. Sánchez-Portal, and P. M. Echenique, Phys. Rev. A **73**, 012901 (2006).

[43] M. Lindenblatt, E. Pehlke, A. Duvenbeck, B. Rethfeld, and A. Wucher, Nucl. Instrum. Methods B **246**, 333 (2006).

2 DFT description of the ground state of a jellium cluster

2.1 Fundamentals of density functional theory

Density functional theory (DFT) is currently the most widely used method to perform accurate calculations of electronic properties in solid-state physics. Recently, it has become popular in quantum chemistry as well. The main reason for that is that DFT offers a reasonable balance between precision and computational effort. Therefore it allows to treat systems of size larger than those usually targeted in quantum chemistry. In addition, the sophisticated wavefunction-based methods used in quantum chemistry, when applied to small systems, can be ideal benchmarks to test the accuracy of DFT calculations.

DFT is a theory to calculate the properties of the ground state of an interacting system, with an external potential $v_{\rm ext}$ applied. Although more general than that, the main success of DFT lies on its treatment of the electronic many-body problem. Instead of focusing into the calculation of the N-electron wave function $\Psi(\mathbf{r}_1, \mathbf{r}_2, ..., \mathbf{r}_N)$, as other *ab-initio* methods do, DFT is based on the calculation of a different basic quantity, namely, the electronic density of the system $n(\mathbf{r})$. An obvious advantage of this choice is that $n(\mathbf{r})$ is a function that depends only on three cartesian coordinates $\mathbf{r}$, simplifying very much the calculation.

The rigorous demonstration that the ground state properties of an interacting system, and in particular the total energy E, can be obtained from the density $n(\mathbf{r})$ was given by Hohenberg and Kohn [1]. These authors prove that the exact energy of the ground state of the system can be written in terms a functional $E[n(\mathbf{r})]$, which has a minimum value for the exact density of the ground state. In addition, Hochenberg-Kohn theorem states that there is a unique external potential $v_{\rm ext}$ (to within a constant) and a unique ground state wave function (to within a phase factor) corresponding to this density $n(\mathbf{r})$. The variational principle can be expressed as:

$$\frac{\delta}{\delta n(\mathbf{r})}\left[E[n(\mathbf{r})] - \lambda \int n(\mathbf{r}) d\mathbf{r}\right] \;=\; 0 \;, \tag{2.1}$$

where the Lagrange multiplier λ is defined so that the density is normalized to the total number of particles N in the system.

In the particular case of a many-electron system moving in the field of a static external potential, the functional $E[n(\mathbf{r})]$ can be written as:

$$E[n(\mathbf{r})] = F_{\mathrm{HK}}[n(\mathbf{r})] + \int v_{\mathrm{ext}}(\mathbf{r}) n(\mathbf{r}) d\mathbf{r} \ , \tag{2.2}$$

where $F_{\mathrm{HK}}[n(\mathbf{r})]$ is a universal funcional of the density $n(\mathbf{r})$, which applies to all electronic systems in their ground state regardless of the external potential v_{ext}.

Using this definition in Eq. 2.1, the variational principle by Hochenberg and Kohn leads to the Euler equation:

$$\lambda = \frac{\delta E[n(\mathbf{r})]}{\delta n(\mathbf{r})} = v_{\mathrm{ext}}(\mathbf{r}) + \frac{\delta F_{\mathrm{HK}}[n(\mathbf{r})]}{\delta n(\mathbf{r})} \ . \tag{2.3}$$

Although the Hohenberg-Kohn theorem provides a rigorous basis for treating a many-electron system in terms of its electronic density, it does not give a recipe to obtain the density itsef. The main difficulty lays in the determination of the universal funcional $F_{\mathrm{HK}}[n(\mathbf{r})]$, which accounts for the kinetic energy of the electrons and the one associated to the electron-electron Coulomb interaction.

In 1965, Kohn and Sham developed a method in which the intricate many-body problem of interacting particles was mapped into a comparatively easier problem of non-interacting particles [2]. The method asserts the existence of a single-particle effective potential $v_{\mathrm{eff}}[n(\mathbf{r})]$ such that the ground state density of the real system $n(\mathbf{r})$ equals to that of a fictitious system of independent particles. In this scheme, the wave function of the full system is a simple product of one-electron wave functions $\varphi_i(\mathbf{r})$, satisfying the KS equations:

$$\left\{ -\frac{1}{2}\nabla^2 + v_{\mathrm{eff}}[n] \right\} \varphi_i = \varepsilon_i \varphi_i \ , \tag{2.4}$$

where ϵ_i are the corresponding KS eigenvalues.

KS equations have to be solved in a self-consistent manner. At every step of the iterative process, the density $n(\mathbf{r})$ can be directly constructed from the following sum over occupied KS wave functions:

$$n(\mathbf{r}) = \sum_{i \in \mathrm{occ.}} |\varphi_i(\mathbf{r})|^2 \ , \tag{2.5}$$

and the effective potential $v_{\mathrm{eff}}[n]$ is calculated from $n(\mathbf{r})$. Once the procedure is converged, the KS wave functions yield not only the electronic density of

the non-interacting KS system $n(\mathbf{r})$, but also the electronic density of the real system, which coincides with it. The KS wave functions do not have a strict physical sense. However, they can be used in many cases as good approximations to the one-electron wave functions of the electrons in the system.

At first sight, KS equations seem to solve the difficult problem of the many-body interacting system. KS equations are a set of single-particle equations, much easier to solve than the coupled Schrödinger equation, especially for large numbers of electrons. They are exact and unique, and yield the exact density. However, the crucial point of the KS method is the definition of the effective potential v_{eff} and, more precisely, of one of its components, the exchange-correlation potential v_{xc} which, in general, is unknown.

In the Kohn-Sham scheme, the total energy of the system E can be written as the sum of three terms:

$$E \;=\; T + E_{\text{coul}} + E_{\text{xc}} \;, \tag{2.6}$$

where T is the kinetic energy of the non interacting system, formally:

$$T \;=\; \sum_i \epsilon_i \;-\; \int d\mathbf{r}\; n(\mathbf{r})\; v_{\text{eff}}(\mathbf{r}) \;, \tag{2.7}$$

E_{coul} is the electrostatic energy:

$$E_{\text{coul}} \;=\; \int d\mathbf{r}\; n(\mathbf{r}) \;\left\{ v_{\text{ext}}(\mathbf{r}) + \frac{1}{2} \int d\mathbf{r}' \frac{n(\mathbf{r}')}{|\mathbf{r}-\mathbf{r}'|} \right\} \;, \tag{2.8}$$

and E_{xc} is the exchange and correlation energy, which is formally defined as:

$$E_{\text{xc}} \;=\; \int d\mathbf{r}\; n(\mathbf{r})\; \epsilon_{\text{xc}}[n(\mathbf{r})] \;. \tag{2.9}$$

Here, $\epsilon_{\text{xc}}[n(\mathbf{r})]$ is the so-called exchange and correlation energy density.

The effective potential v_{eff} is given by:

$$v_{\text{eff}} \;=\; v_{\text{ext}} + v_{\text{H}} + v_{\text{xc}} \;, \tag{2.10}$$

where v_{ext} is the external potential in which the electrons move, v_{H} is the Coulomb potential created by the electronic density

$$v_{\text{H}}(\mathbf{r}) = \int d\mathbf{r}' \frac{n(\mathbf{r}')}{|\mathbf{r}-\mathbf{r}'|} \;, \tag{2.11}$$

and $v_{\rm xc}$ is the exchange and correlation potential, which is formally defined as the functional derivative of the exchange-correlation energy $E_{\rm xc}$ with respect to the density $n(\mathbf{r})$:

$$v_{\rm xc}(\mathbf{r}) = \frac{\delta E_{\rm xc}[n(\mathbf{r})]}{\delta n(\mathbf{r})} \ . \tag{2.12}$$

The exact form of the functional $E_{\rm xc}[n(\mathbf{r})]$ is not known. Otherwise, we would be able to solve all Coulomb-interacting electronic problems exactly. A large number of approximations have been developed to account for this term. The simplest and easiest one is the local density approximation (LDA), in which the exchange-correlation energy is obtained as:

$$E_{\rm xc}^{LDA}[n(\mathbf{r})] = \int d\mathbf{r}\ n(\mathbf{r})\ \epsilon_{\rm xc}(n(\mathbf{r}))\ , \tag{2.13}$$

where $\epsilon_{\rm xc}(n(\mathbf{r}))$ is the exchange-correlation energy density of a uniform electron gas with density equal to the local electronic density at point $\mathbf{r}$. Until the early 90's, the LDA was the standard approach for all density functional calculations. By construction, it is a good approximation for those systems with slow varying density. Unexpectedly, it has shown to be a reasonable approximation even for some realistic and very inhomogeneous systems. However, it does not provide sufficiently accurate values of quantities such as semiconductor band gaps and energies of chemical reactions.

It can be shown that the LDA is in fact the first term in a systematic expansion of the exchange-correlation functional in terms of spatial derivatives with respect to the density. Inclusion of an additional term in this expansion (the gradient of the density $\nabla n(\mathbf{r})$) leads to the generalized gradient approximation (GGA). By specifying different forms of the pair-correlation function of the many-electron system and determining the parameters in this function by sum rules and other constraints, several GGA functionals have been proposed. These GGA functionals have led to large improvements in molecular binding energies, as well as in atomic and molecular adsorption energies at surfaces, as compared to LDA calculations.

Modern state-of-the-art calculations in DFT use exchange-correlation functionals that go beyond GGA. Generally speaking, improvements in the exchange-correlation terms follow two different and complementary schemes: either designing more accurate functionals without modifying the variables on which the functional depends or designing more accurate functionals increasing the number of variables on which the functional depends [3].

2.2 DFT and spherical jellium cluster

Valence electrons in metal clusters can be described as occupying discrete levels determined by the cluster size and geometry. In the limit of very large clusters, the difference in energy between the discrete levels becomes negligible and the density of electronic levels can be safely approximated by a continuum of states, as in bulk. Electronic shells similar to those of atomic and molecular systems appear. Metallic clusters in closed-shell configurations are more stable, as measured in pioneering experiments in the field [4]. Certain "magic numbers" of constituent atoms are thus more abundant than others.

Because of their relatively simple electronic structure, the spherical jellium model has been widely used in the description of small metallic clusters [5, 6]. The jellium model is simple enough to be applied to the description of metal clusters with sizes up to several thousand atoms, but is still able to reproduce in a qualitative (and often also in a quantitative) way many of their electronic properties [7]. Its success in describing the complex 'supershell' structure in large alkali clusters [8], superimposed over the standard shell structure, is a good example of this.

A quite complete set of calculations for the electronic properties of metallic clusters using the jellium model were performed in the '80s of last century by W. Ekardt [9, 10, 11, 12]. In these seminal works, Ekardt used the jellium model to show that the ionization potential of clusters presents a strong oscillatory behaviour with size. Whenever an electronic shell is completely filled, the ionization potential is at a maximum, due to the strong binding of the last electron filling this shell. The oscillations are damped with size and the ionization potential ends up converging into the work function of the corresponding metallic surface. The convergence to the surface work function, however, is rather slow because of the high orbital degeneracy for large values of the angular momentum l.

In the spherical jellium model, the background of positive ions is smeared out over the cluster volume, and the valence electrons move in the attractive potential created by the ionic background. The cluster is assumed to have a spherical shape of radius R, and the positive background charge density $n^+(\mathbf{r})$ is given by:

$$\begin{aligned} n^+(\mathbf{r}) &= n_0 \qquad r \leq R \\ n^+(\mathbf{r}) &= 0 \qquad r > R. \end{aligned} \tag{2.14}$$

For the cluster to be neutral, the following relation holds:

$$\frac{1}{n_0} = \frac{4\pi r_s^3}{3}, \tag{2.15}$$

where $r_s = R/N^{1/3}$ is the so called average *one-electron radius* in the cluster, and N is the number of electrons in the system.

The external potential in which the electrons move is obtained by direct integration of:

$$v_{\rm ext}(\mathbf{r}) = \; -\int \mathbf{dr}' \frac{\mathbf{n}^+(\mathbf{r}')}{|\mathbf{r}-\mathbf{r}'|}, \tag{2.16}$$

which yields an attractive external potential with parabolic behaviour up to the cluster surface, and standard Coulomb-type decay from the surface up to infinity.

With this specific external potential, we use Density Functional Theory and the Kohn-Sham equations (2.4) to calculate the ground state properties of spherical jellium clusters. The exchange and correlation potential $v_{\rm xc}(\mathbf{r})$ is calculated in the local density approximation (LDA) with the parametrization of Reference [13].

Due to spherical symmetry, the KS wave functions are characterized by the radial quantum number k, the angular momentum quantum number l and the quantum number describing the angular momentum projection, m. Expansion of the KS wavefunctions $\varphi_i(\mathbf{r})$ in the spherical-harmonic basis set $Y_{lm}(\Omega)$:

$$\varphi_i(\mathbf{r}) \;=\; R_{kl}(r) Y_{lm}(\Omega) \tag{2.17}$$

where the index i stands for the full set of indexes (k, l, m), leads to the radial KS equation:

$$\left\{ -\frac{1}{2}\frac{\partial^2}{\partial r^2} + \frac{l(l+1)}{2r^2} + v_{\rm eff}(r) \right\} u_{kl}(r) \;=\; \varepsilon_{kl} u_{kl}(r), \tag{2.18}$$

in which the radial wave function has been transformed into $R_{kl}(r) = u_{kl}(r)/r$.

Jellium clusters are finite-size objects in which the electrons are confined. The spectrum of KS energy levels ε_i is thus discrete. Due to angular and spin degeneracy, the energy levels are distinguished by k and l quantum numbers. Each (k, l) shell accepts up to $2(2l+1)$ electrons.

The set of KS equations are solved using an iterative process. For that purpose, we define a one-dimensional grid of equidistant points in the radial

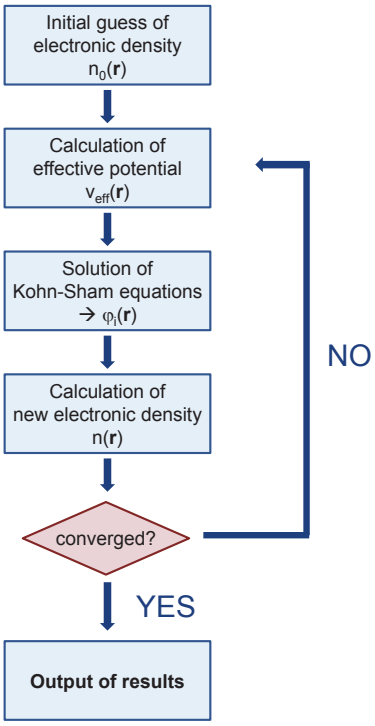

Figure 2.1: Flow chart of the self-consistent process when solving Kohn-Sham equations.

coordinate that extends far beyond the cluster radius R. In each iteration, the radial KS equation (Eq. 2.18) has to be solved. Either the Numerov algorithm [14] or direct diagonalization of the Hamiltonian matrix after Fourier expansion of all quantities [15] have been used for this purpose. Once the KS wave functions and energies are calculated, the radial electronic density of the cluster $n(r)$ and the effective potential $v_{\text{eff}}(r)$ are recalculated. The iterative procedure is stopped when the total energy of the system E converges up to a certain tolerance (typically 10^{-4} a.u.). A simplified flowchart illustrating the numerical self-consistent procedure is shown in Fig. 2.1.

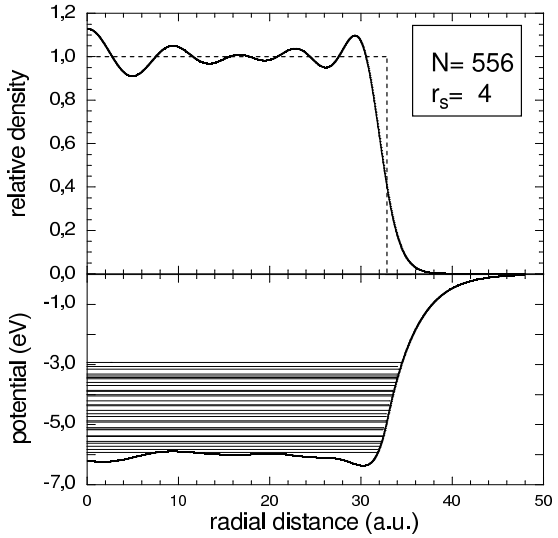

Figure 2.2: Density functional calculation of a jellium cluster with $N = 556$ electrons and density parameter $r_s = 4$. The upper panel shows the electronic density in units of $n_0 = 3/(4\pi r_s^3)$ as a function of radial distance (in a.u.). A dashed vertical line indicates the cluster surface. The lower panel shows the Kohn-Sham potential (in eV) as well as the occupied Kohn-Sham levels.

2.3 Description of the ground state of a jellium cluster

During the development of this PhD. work, we have characterized clusters ranging from a few to thousands of electrons and various screening radii, e.g. $r_s = 2.07$ (aluminum clusters) and $r_s = 4$ (sodium clusters). The scheme and numerical procedure is the aforementioned, where we have taken care that electronic closed shell configurations are formed in the converged systems. We include here a brief description of the main features of jellium clusters, which set the basis for the studies presented in the following chapters.

Figure 2.2 shows the DFT calculation of a sodium cluster with $N = 556$ electrons. The upper panel shows the electronic density $n(\mathbf{r})$, in units of the average electronic density $n_0 = 3/(4\pi r_s^3)$, as a function of radial distance from the center of the cluster. In general terms, the electronic density inside the cluster is close to the average value n_0. Friedel oscillations are observed as a consequence of electron confinement, and an exponential decay of the electronic density at the surface of the cluster is found as well. In the lower

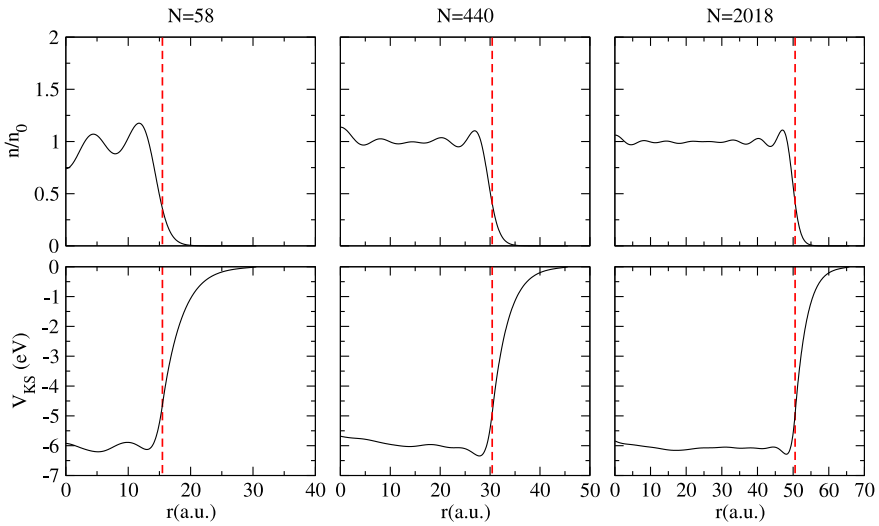

Figure 2.3: electronic density and Kohn-Sham or effective potential for several metal clusters with electron density parameter $r_s = 4$ (sodium clusters)

panel, the effective potential potential $v_{\text{eff}}(r)$ and the occupied KS electron levels are represented, the upper level corresponding to the Fermi energy of the system. Being the electronic density almost constant inside the cluster, the Coulomb potential created by the electronic density and the Coulomb potential of the positive background roughly compensate. Thus, inside the cluster, the value of $v_{\text{eff}}(r)$ is mostly determined by the exchange-correlation potential $v_{\text{xc}}(r)$.

Figure 2.3 shows the evolution of the electronic density and the effective potential for several Na clusters ($r_s = 4$) of increasing size. One can observe that the oscillations in the electronic density, which appear due confinement effects, diminish with increasing cluster size. The electronic density at the center of the sphere is controlled by the number of s ($l = 0$) electrons in the cluster. Because of the boundary conditions of the KS wave functions at the origin, all other electrons with $l > 0$ are repelled from the center region. When a given s-shell is eventually filled, the electronic density at $r = 0$ decreases.

As the cluster grows in size, the discrete spectrum of energy levels is densified. Otherwise said, the average energy step between two different

energy levels is reduced. This effect is graphically shown in Fig. 2.4, in which the energy level diagrams of Na clusters of increasing size are plotted. For the smallest cluster, $N = 58$, the diagram is similar to a molecular level diagram. For the largest one, $N = 2018$, the diagram shows nearly a continuum of states, what is expected of bulk materials. To complete

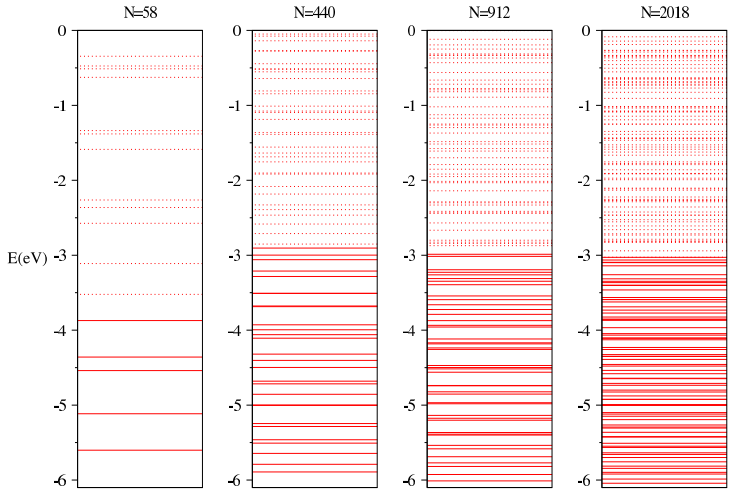

Figure 2.4: Energy level diagrams for several sodium clusters ($r_s = 4$) with increasing number of electrons. Discontinous (continuous) lines represent unnocupied (occupied) energy levels

the description of the ground state of a metal cluster, we show the radial one-electron wave functions calculated for sodium clusters of very different size, namely $R = 15.48$ a.u. (N=58 electrons) and $R = 50, 55$ a.u. (N=2018 electrons). This is shown in Figures 2.5 and 2.6 respectively. The right panels show the diagram (k, l) energy shells with information of the angular momentum l. In this representation, several branches appear, grouping wave functions with a given number of nodes. These are represented on the left panels. As we can observe in the figures, the one-electron wave functions have an appreciable weight around the cluster surface, which will prove to have an influence in the lifetime of electronic excitations. This will be addressed to in Chapter 5.

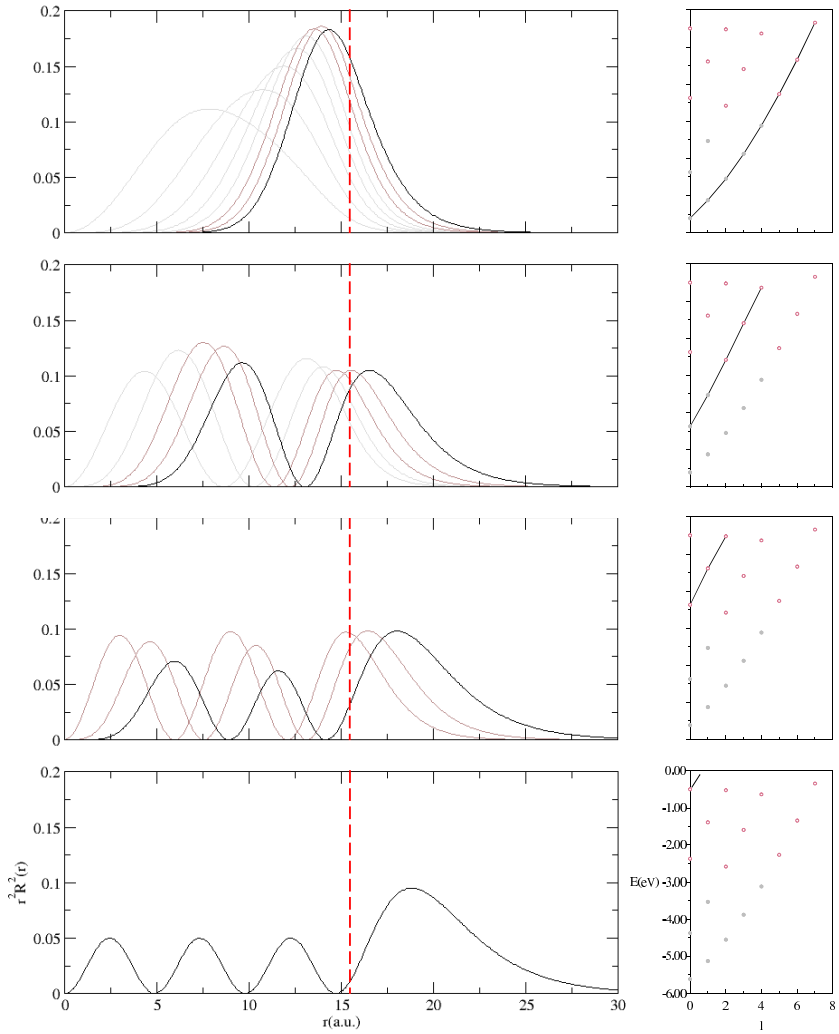

Figure 2.5: wavefunctions of a cluster with N=58 electrons and $r_s = 4$. Occupied states are displayed in grey, unoccupied states in brown, and the outer unoccupied state in black. The right panel shows the branches of the energy versus angular momentum graphs whose wavefunctions are represented on the left panel.

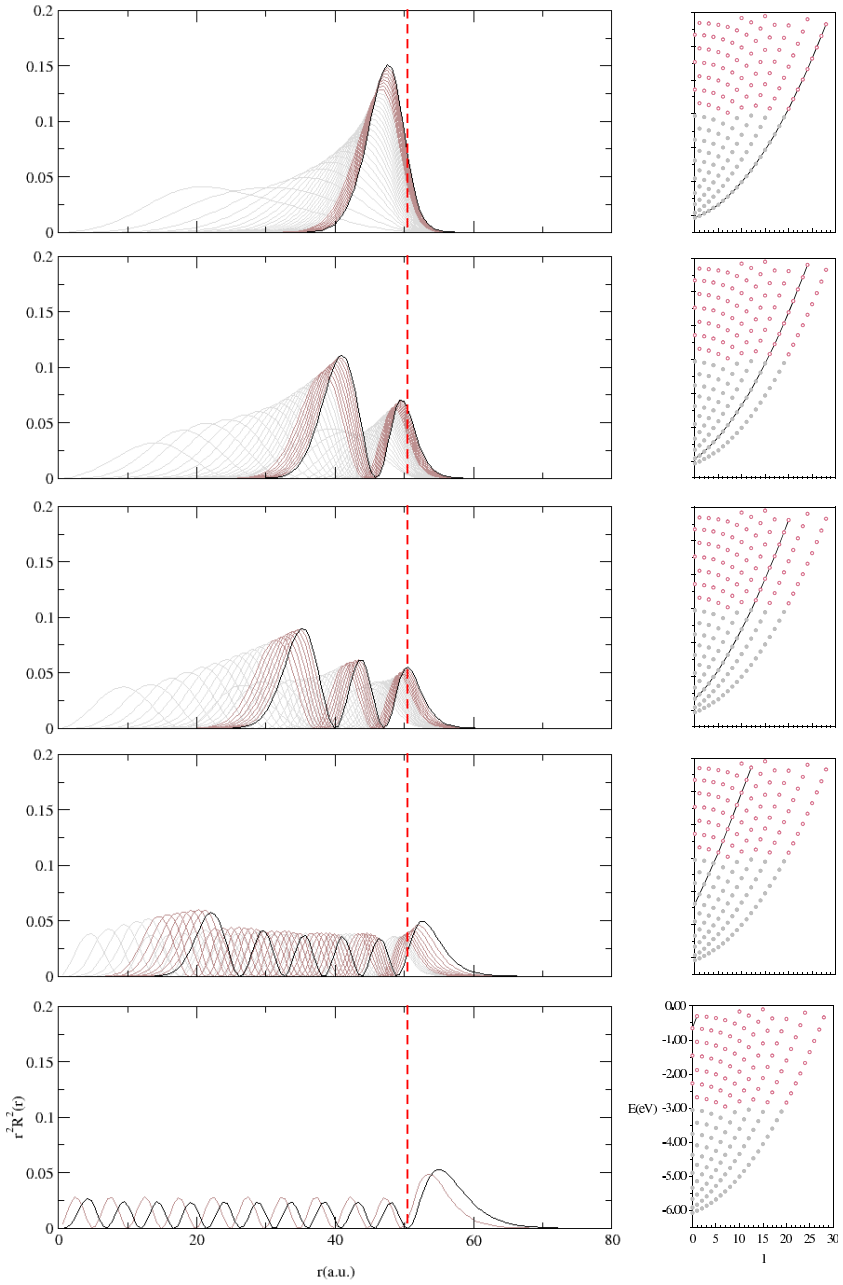

Figure 2.6: wavefunctions of a cluster with N=2018 electrons and $r_s = 4$. Occupied states are displayed in grey, unoccupied states in brown, and the outer unoccupied state in black. The right panel shows the branches of the energy versus angular momentum graphs whose wavefunctions are represented on the left panel.

References

[1] P. Hohenberg and W. Kohn, Phys. Rev. **136**, B864 (1964).

[2] W. Kohn and L. J. Sham, Phys. Rev. **140**, A1133 (1965).

[3] M. E. Casida, J. of Molec. Struc.: THEOCHEM **914**, 3 (2009).

[4] Knight W D, Clemenger K, de Heer W A, Saunders W A, Chou M Y and Cohen M L, *Phys. Rev. Lett.* **52** 2141 (1984).

[5] Alonso J A and Balbás L C, *Topics in Current Chemistry* vol 182, Springer-Verlag, Berlin-Heidelberg (1996) p 119.

[6] Brack M 1993 *Rev. Mod. Phys.* **65** 677

[7] W. A. de Heer, Rev. Mod. Phys. **65**, 611 (1993).

[8] E. Koch and O. Gunnarsson, Phys. Rev. B **54**, 5168 (1996).

[9] W. Ekardt, Phys. Rev. B **29**, 1558 (1984).

[10] W. Ekardt, Phys. Rev. Lett. **52**, 1558 (1984).

[11] W. Ekardt, Phys. Rev. B **31**, 6360 (1985).

[12] W. Ekardt, Phys. Rev. B **37**, 9993 (1988).

[13] Gunnarsson O and Lundqvist B I 1976 *Phys. Rev. B* **13** 4274

[14] F. Calogero, *Variable phase approach to Potential Scattering*, Academic press, New York (1967)

[15] R.Kosloff, J.Phys.Chem. **92**, 2087 (1988).

3 TDDFT description of excited states in a jellium cluster

3.1 Fundamentals of time-dependent density functional theory

The response of an interacting many-particle system to a time-dependent field can be often treated within linear response theory. However, this is not always the case. Let us mention as an example the interaction of matter with ultra-short laser pulses of very high intensity, a tool which has become available in recent years thanks to the advances in the field of laser physics. When a system interacts with a laser of these characteristics, perturbation theory is no longer valid to treat the dynamics of the system. Another example in which linear response fails is the study of collision processes with slow atomic charges, a topic which will be addressed in Chapter 6.

The non-perturbative quantum mechanical description of many-body systems moving in a strong time-dependent external field is becoming a problem of increasing interest in theoretical physics. In principle, this problem requires a full solution of the time-dependent Schrödinger equation for many-body systems, which is an exceedingly difficult task. In view of the success of DFT in the treatment of the ground state of many-body systems, a time-dependent version of density functional theory appears highly desirable.

One of the first steps towards a time-dependent Kohn-Sham scheme was taken by Zangwill and Soven [1] although still in the linear theory regime. These authors adopted the functional form of the static exchange and correlation potential in LDA. The approximation can be expected to be good only if the time dependence of the density is sufficiently slow. In practice, however, it gives quite good results even for the case of rather rapid time dependence. But the approach of Zangwill and Soven was valid under the assumption that a time-dependent KS theorem exists. After several derivations restricted to a narrow set of time-dependent potentials, a general formulation was given by Runge and Gross [2].

Ordinary time-independent DFT is based on the existence of a one-to-one mapping between densities and external potentials. In the ground state formalism, the existence proof relies on the variational minimum of the energy. Straightforward extension to the time-dependent domain is not possible, since a *minimum* principle is not available in this case. However,

Runge and Gross proved that there is actually a one-to-one mapping between time-dependent external potentials and electronic densities. In other words, if a given initial state with many-body function Ψ_0 evolves in time under the influence of two different potentials $v(\mathbf{r},t)$ and $v'(\mathbf{r},t)$, the resulting electronic densities $n(\mathbf{r},t)$ and $n'(\mathbf{r},t)$ are different as well. Note that in this context, two potentials are considered to be different if they differ by more than a time-dependent, space-independent, constant.

A direct consequence from Runge-Gross theorem is that, for a given interacting system, the expectation value of any time-dependent quantum mechanical operator $\hat{O}(t)$ is a unique functional of the density $n(t)$:

$$O(t) \;=\; < \Psi[n(t)]|\hat{O}(t)|\Psi[n(t)] > , \tag{3.1}$$

because the time-dependent many-body function $\Psi[n(t)]$ is also a unique functional of the system density (up to a time-dependent phase that cancels out in Eq. 3.1).

The one-to-one correspondence between time-dependent densities and time-dependent potentials can be established for *any* given interaction between particles. In particular, it can be applied to a system of non-interacting particles. Thus, for a non-interacting system, there is a unique external potential which reproduces a given time-dependent density.

The previous statement allows to establish a time-dependent Kohn-Sham scheme, following the same philosophy of ordinary time-independent DFT. According to the time-dependent Kohn-Sham scheme, for a system of interacting electrons initially in their ground state and subject to a given time-dependent potential, there is an alternative system of non-interacting identical fermions which gives rise to exactly the same time-dependent electronic density. The non-interacting fermions are subject to an external effective potential $v_{\text{eff}}([n],\mathbf{r},t)$, and the one-particle wave functions fulfill the so-called time-dependent KS equations. These are formally similar to a set of time-dependent Hartree equations but include exchange-correlation effects, in principle, in an exact way. In practice, however, approximations for the exchange-correlation potential are required and happen to be the main source of inaccuracy in real calculations.

Similarly to the KS version of DFT, in TDDFT the time-dependent electronic density can be obtained as a sum over one-particle wave functions

in the following way:

$$n(\mathbf{r},t) \;=\; \sum_{i=1}^{N} \left|\varphi_i(\mathbf{r},t)\right|^2 \;, \tag{3.2}$$

where N is the number of electrons in the system, and $\varphi_i(\mathbf{r},t)$ are wave functions that satisfy the following KS time-dependent equations:

$$i\frac{\partial}{\partial t}\Psi_i(\mathbf{r},t) \;=\; \left(\frac{-\nabla^2}{2} + v_{\text{eff}}([n],\mathbf{r},t)\right)\Psi_i(\mathbf{r},t) \;. \tag{3.3}$$

The time-dependent effective potential $v_{\text{eff}}([n],\mathbf{r},t)$ is built from three terms, namely, the external time-dependent potential $v_{\text{ext}}(\mathbf{r},t)$, the Hartree potential $v_{\text{H}}([n],\mathbf{r},t)$, and the exchange-correlation term $v_{\text{xc}}([n],\mathbf{r},t)$:

$$v_{\text{eff}}([n],\mathbf{r},t) \;=\; v_{\text{ext}}(\mathbf{r},t) + v_{\text{H}}([n],\mathbf{r},t) + v_{\text{xc}}([n],\mathbf{r},t) \;. \tag{3.4}$$

The time-dependent Hartree term is obtained from the electronic density of the system in the following way:

$$v_{\text{H}}([n],\mathbf{r},t) \;=\; \int \frac{d\mathbf{r}'\; n(\mathbf{r}',t)}{|\mathbf{r}-\mathbf{r}'|} \;. \tag{3.5}$$

As in standard DFT, the exchange correlation term $v_{\text{xc}}([n],\mathbf{r},t)$ is the one in which most of the problem complexity is included in practice. Several approximations can be used to include dynamical exchange and correlation effects. The simplest is the one that Zangwill and Soven employed: to consider that $v_{\text{xc}}([n],\mathbf{r},t)$ is a local term that only depends on the value of the electronic density at that given point of space $\mathbf{r}$ and at that given point of time t. This is the so-called adiabatic local density approximation (ALDA), which will be used all through this work with the exchange and correlation functional of Ref. [3].

ALDA should be in principle accurate in the limit of low-frequency and long-wavelength changes in the density. For other cases, the exchange-correlation term should have a non-local dependence both in space and in time. The non-local dependence in space was already discussed in Chapter 2, when referring to the limitations of the static LDA approximation. The non-local dependence in time implies that the exchange-correlation functionals should take into account 'memory effects' [4, 5, 6], i.e. the

dependence of the functional on the value of the density at past times. However, and in a way similar to what happens in static DFT with the LDA approximation, ALDA is often able to provide suprisingly good results in spite of the strong assumpltions implied.

3.2 TDDFT and spherical jellium cluster

In this PhD work, we use TDDFT to describe the time-evolution of the electronic density of a metal cluster when different time-dependent external perturbations are applied. As in the ground state described in Chapter 2, we make use of the spherical jellim approximation, which enables us to study the dynamics of clusters of very different sizes under the same theoretical scheme. A common feature to all time-dependent external potentials considered in this PhD. work is their display of axial symmetry, i.e. with respect to an axis crossing the geometrical center of the cluster.

In Chapter 5, we briefly use TDDFT to identify the main features of the electronic excitations when a short laser pulse is applied to the cluster. The laser pulse that we use is of the following shape:

$$\mathbf{E}(\mathbf{r},t) = E_0 \ \cos(\Omega t) \ exp\{-[(t-t_0)/\Delta]^2\} \ \mathbf{u}_z \tag{3.6}$$

Here, E_0 is the field amplitude, Ω is the frequency of the laser, t_0 the time of maximum amplitude, and Δ a parameter fixing the pulse duration.

In general, the wavelength of the laser fields considered is much larger than typical cluster dimensions. We are thus allowed to work in the dipole approximation. The external potential $v_{\text{ext}}(\mathbf{r},t)$ associated to the pulse can be calculated as:

$$v_{\text{ext}}(\mathbf{r},t) \ = \ \mathbf{E}(\mathbf{r},t)\cdot\mathbf{r}. \tag{3.7}$$

As $\mathbf{u}_z$ is a unitary vector along the z-axis, the problem keeps axial symmetry during the time evolution. Therefore, m is kept as a good quantum number and KS wave functions with different m values evolve differently.

In Chapter 6, we consider the external potential created by a moving bare charge Q and study the electronic excitations created during the collision process with a metal cluster. We also discuss the implications of the electronic excitations in the the energy loss of the moving particle. The external potential $v_{\text{ext}}(\mathbf{r},t)$ can be written as:

$$v_{\text{ext}}(\mathbf{r},t) \ = \ \frac{-Q}{|\mathbf{R}(t)-\mathbf{r}|}, \tag{3.8}$$

where $\mathbf{R}(t)$ is the position of the moving charge at time t. In our case, we consider that the trajectory of the charge follows a straight line that crosses through the geometrical center of the cluster. In this way, axial symmetry is kept again and m is still a good quantum number.

Because of the identical symmetry in the two problems, we use a similar methodology and numerical implementation in both, which we outline in the following paragraphs. Further details about the time-propagation methodology can be found in [9].

The initial conditions for the TDDFT calculation correspond to the ground state of the cluster. This way, the initial KS wave functions are taken as the wave functions calculated within ordinary DFT, $\Psi_i(\mathbf{r}, t = 0) \equiv \varphi_i(\mathbf{r})$. As shown in Chapter 2, these can be expressed in the spherical harmonics basis set:

$$\Psi_{klm}(\mathbf{r}, t = 0) = \varphi_i(\mathbf{r}) = R_{kl} Y_{lm}(\mathbf{\Omega}), \tag{3.9}$$

where the index i groups the set of quantum numbers (k, l, m).

Owing to the cylindrical symmetry of the problem, the projection of the angular momentum m on the quantization z-axis is a good quantum number. Thus, we use cylindrical coordinates, $\mathbf{r} = (\rho, z, \phi)$, where the z-axis is set along the symmetry axis of the system.

It is customary to reexpress the time dependent Kohn-Sham orbitals as

$$\Psi_{klm}(\mathbf{r}, t) = \psi_j^m(\rho, z, t) \frac{e^{im\phi}}{\sqrt{2\pi}}, \tag{3.10}$$

where the index j groups the set of quantum numbers (k, l). Note that each Kohn-Sham orbitals is doubly degenerate with respect to the projection of the electron spin s since we perform spin-restricted calculations.

Numerically, we use a uniform grid in z coordinate, but the convergence can be greatly improved if we introduce a variable change in ρ coordinate, $\rho = f(\xi)$, such that the mesh in ρ is densified in the vicinity of the symmetry axis. In our case, we have used the function $\rho = \xi - (\beta/\sqrt{\alpha})\ atan(\xi/\sqrt{\alpha})$, with α and β being arbitrary parameters in the range of $\alpha \approx \beta \approx 500$, depending on the particular situation.

The $\psi_j^m(\rho, z, t)$ orbitals evolve according to the time-dependent Kohn-Sham equations

$$i \frac{\partial}{\partial t} \psi_j^m(\rho, z, t) = H_m \psi_j^m(\rho, z, t), \tag{3.11}$$

where H_m denotes effective m - dependent one-particle Hamiltonian of the system:

$$H_m = -\frac{1}{2}\frac{\partial^2}{\partial z^2} - \frac{1}{2}\frac{1}{ff'}\frac{\partial}{\partial \xi}\frac{f}{f'}\frac{\partial}{\partial \xi} + \frac{m^2}{2f^2} + v_{\text{eff}}([n], \rho, z, t), \tag{3.12}$$

and $f' = df/d\xi$.

With the initial conditions defined by Eqs. (3.9) and (3.10), the time dependent equations are solved via short-time propagation:

$$\psi_j^m(\rho, z, t + \Delta t) = e^{-i\Delta t H_m}\psi_j^m(\rho, z, t). \tag{3.13}$$

In practice, the time propagation is performed with the split-operator technique [7], separating potential and kinetic energy terms.

$$e^{-i\Delta t H_m} = e^{-i\frac{\Delta t}{2}v_{\text{eff}}(t+\Delta t/2)}e^{-i\Delta t T_z}e^{-i\Delta t T_\xi^m}e^{-i\frac{\Delta t}{2}v_{\text{eff}}(t+\Delta t/2)}, \tag{3.14}$$

where

$$T_z = -\frac{1}{2}\frac{\partial^2}{\partial z^2}, \tag{3.15}$$

and

$$T_\xi^m = -\frac{1}{2}\frac{1}{ff'}\frac{\partial}{\partial \xi}\frac{f}{f'}\frac{\partial}{\partial \xi} + \frac{m^2}{2f^2}. \tag{3.16}$$

Observe that the $\pm m$ states are degenerate in the course of the time evolution. We then only propagate the $m \geq 0$ orbitals assuming double occupation for the $m = 0$ states and quadruple occupation ($\pm m$-degeneracy times spin degeneracy) for the $m > 0$ states.

The action of the exponential operator $e^{-i\Delta t T_\xi^m}$ on the wave function is calculated using the Cayley transform [8] and three point finite difference techniques. A pseudo-spectral approach and Fast Fourier Transform is used the calculate the action of $e^{-i\Delta t T_z}$.

To calculate the action of the exponential opertator $e^{-i\frac{\Delta t}{2}v_{\text{eff}}(t+\Delta t/2)}$, we follow an iterative procedure. This procedure involves $v_{\text{eff}}(t)$ and consecutive estimates of $v_{\text{eff}}(t + \Delta t)$ in order to calculate $v_{\text{eff}}(t + \Delta t/2)$. The procedure is typically repeated 3-4 times to avoid divergences in the total energy of the system.

For the processes encompassed in this PhD. work, typical time steps range between $\Delta t = 0.01$ and 0.08 a.u., depending on the particular process under study.

For completion of the study, an alternative code has been developed using spherical coordinates, by means of expansion of the wave functions in a set of spherical harmonics. The outcoming results are consistent with the ones obtained with the cylindrical code.

The code used in the time-dependent work was designed and developed by A.G. Borisov at CNRS-Universit Paris sud, Orsay.

References

[1] A. Zangwill and P. Soven, *Phys. Rev. A* **21**, 1561 (1980).

[2] E. Runge and E. K. U. Gross, *Phys. Rev. Lett.* **52**, 997 (1984).

[3] O. Gunnarson and B. I. Lundqvist, *Phys. Rev. B* **13**, 4274 (1976).

[4] G. Vignale, C.A. Ullrich and S. Conti, *Phys. Rev. Lett.* **79**, 4878 (1997).

[5] J.F. Dobson, M.J. Bunner and E.K.U. Gross, *Phys. Rev. Lett.* **79**, 1905 (1997).

[6] Y. Kurzweil and R. Baer, *Phys. Rev. B* **73**, 075413 (2006).

[7] M.D. Feit, J.A. Fleck, Jr. and A. Steiger, *J. Comput. Phys* **47**, 412 (1982).

[8] W.H. Press, S.A. Tenkolsky, W.T. Vetterling and B.P. Flannery, *Numerical Recipes in FORTRAN*, Cambridge University Press, Cambridge, 1992.

[9] A.G. Borisov, J.P. Gauyacy and S.V. Shabanov, *Surf. Sci.* **487**, 243 (2001).

4 Lifetime of electronic excitations in metal clusters

Abstract

Density functional theory and the self-energy formalism are used to evaluate the lifetime of electronic excitations in metal clusters of nanometer size. The electronic structure of the cluster is obtained in the jellium model and spherical symmetry is assumed. Two effects that depend on the size of the clusters are discussed: the change in the number of final states to which the excitation can decay, as well as the modification in the screened interaction between electrons. For clusters with density parameter $r_s = 4$ and few nanometers diameter, a lifetime value of ≈ 5 femtoseconds is reached for electronic excitations of $\approx$ 1 eV. This value is of the same order of magnitude of that obtained in the bulk limit at the same level of approximation. For smaller clusters, a distinct non-monotonic behaviour of the lifetime as a function of the cluster size is found and the lifetime of excitations of ≈ 1 eV can vary between 4 and 30 femtoseconds.

4.1 Introduction

One of the most appealing features of nanometer-sized clusters is that their electronic properties are midway between those of small molecular systems and those of bulk condensed matter. This intermediate nature of clusters makes most of their properties depend on size. Valence electrons in metal clusters can be described as occupying discrete levels determined by the cluster size and geometry [1, 2]. Electronic shells similar to those of atomic and molecular systems appear. Metallic clusters in closed-shell configurations are more stable, as measured in pioneering experiments in the field [3]. In the limit of very large clusters, the difference in energy between the discrete levels becomes negligible and the density of electronic levels can be safely approximated by a continuum of states, as in bulk.

In the last years, the development of experimental techniques based on femtosecond lasers has made it possible to study the dynamics of electronic excitations in a wide variety of systems, including clusters [4]. Electronic excitations with energies of few eV usually decay in a time scale of the order of femtoseconds, making their analysis by other techniques particularly difficult. In clusters, special attention has been paid to the dependence on size of the electron-electron interaction processes [5, 6, 7].

There are two main effects that drastically modify the dynamics of electronic excitations in clusters with respect to the bulk analogous situation. First, the discretization of levels in the electronic structure of the cluster reduces the number of final states to which an electronic excitation can decay enhancing its lifetime. Second, the reduction of dynamic screening in the proximity of the cluster surface changes the interaction potential between electrons and decreases the excitation lifetimes. The interplay between these two effects makes the analysis of electron dynamics in clusters both intricate and appealing.

The theoretical study of electronic excitations in clusters is in general less developed than the analysis of ground state properties. One of the main obstacles is the necessity of analysing systems of very different size under the same approximation grounds, in order to obtain meaningful results. Here, we analyse the size dependence of electron lifetimes in metal clusters. The description of the cluster is simplified by means of the jellium approximation. In this way, we can cover a wide range of cluster radii under the same theoretical scheme. We take as an example the lifetime of ≈ 1 eV electronic excitations in jellium clusters of different size, keeping

fixed the cluster average electronic density. We show that the lifetime of electronic excitations in metallic clusters of few nanometers radii, due to electron-electron scattering processes, are of the same order of magnitude as those of metal bulk at the same level of approximation. This is due to a rough compensation of the two cluster-specific effects mentioned above. We also show that there is a non-monotonic behaviour of the lifetime as a function of the cluster size for clusters with radii of $1-2$ nanometers, due to electron confinement effects. For clusters of bigger size, a lifetime value of ≈ 5 femtoseconds is reached.

The article is organized as follows: the theoretical model and numerical details are provided in Section 4.2, Section 4.3 is dedicated to the presentation and discussion of our results, and Section 4.4 contains our conclusions. Atomic units are used throughout unless otherwise stated.

4.2 Theoretical model

4.2.1 Density functional theory of jellium clusters

The spherical jellium model has been widely used in the description of small metallic clusters [1, 2]. In the jellium model, the background of positive ions is smeared out over the cluster volume and the valence electrons move in the attractive potential created by them. The positive background charge $n^+(\mathbf{r})$ is approximated by a constant value $n^+(\mathbf{r}) = n_0^+$ inside the cluster ($r < R$) and made equal to zero outside it [$n^+(\mathbf{r}) = 0$ for $r > R$]. It is also customary to define the average one-electron radius in the cluster from $r_s = R/N^{1/3}$, where R is the radius of the cluster and N the number of electrons in it. If the cluster is neutral, the equality $1/n_0^+ = 4\pi r_s^3/3$ holds as well. Despite its simplicity, the jellium model is able to describe qualitatively (and even quantitatively in some cases) many experimentally measured electronic properties of small metal clusters [8].

We use density functional theory (DFT) [9] and Kohn-Sham (KS) equations [10]

$$\left\{-\frac{1}{2}\nabla^2 + v_{\text{eff}}(\mathbf{r})\right\}\varphi_i(\mathbf{r}) \;=\; \varepsilon_i\varphi_i(\mathbf{r}) \tag{4.1}$$

$$v_{\text{eff}}(\mathbf{r}) \;=\; v_{\text{jellium}}(\mathbf{r}) + v_{\text{Hartree}}(\mathbf{r}) + v_{\text{xc}}(\mathbf{r}) \tag{4.2}$$

to describe self-consistently the ground state properties of spherical jellium

clusters. The effective potential $v_{\text{eff}}(\mathbf{r})$ is composed of three terms:

$$v_{\text{eff}}(\mathbf{r}) \;=\; -\int d\mathbf{r}'\frac{n^{+}(\mathbf{r}')}{|\mathbf{r}-\mathbf{r}'|} \;+\; \int d\mathbf{r}'\frac{n^{-}(\mathbf{r}')}{|\mathbf{r}-\mathbf{r}'|} \;+\; v_{\text{xc}}(\mathbf{r}), \tag{4.3}$$

where the first two terms account for the electrostatic potentials created by the positive background and the electronic density $n^{-}(\mathbf{r})$ respectively. The third term $v_{\text{xc}}(\mathbf{r})$ is the exchange-correlation potential, calculated in the local density approximation (LDA) with the parametrization of Reference [11]. The electronic density $n^{-}(\mathbf{r})$ is calculated as a sum over occupied wave functions

$$n^{-}(\mathbf{r}) \;=\; \sum_{i\in occ.} |\varphi_i(\mathbf{r})|^2. \tag{4.4}$$

Jellium clusters are finite-size objects in which the electrons are confined. The spectrum of KS energy levels ε_i is thus discrete. Keeping spherical symmetry, the KS wave functions $\varphi_i(\mathbf{r})$ are characterized by the radial quantum number k and the angular momentum quantum number l. Each (k,l) shell accepts up to $2(2l+1)$ electrons, due to angular and spin degeneracy. The work function of the system reaches maximum values whenever a closed-shell configuration is formed [12]. The KS wavefunctions $\varphi_i(\mathbf{r})$ are calculated numerically after expansion in the spherical-harmonic basis set $Y_{lm}(\Omega)$. The set of KS equations are solved self-consistently using an iterative procedure.

4.2.2 GW calculation of electronic lifetimes

Calculating energies and lifetimes of electronic excitations in many-electron systems is a difficult task. The GW method developed by Hedin [13] has proven to be a useful tool to make such calculations. The GW approximation is an improvement over Hartree-Fock-like schemes due to the inclusion of dynamic correlation between electrons [14]. It takes into account the medium polarization, which is an important physical ingredient in extended systems. Despite its success in the description of lifetimes in bulk metals [15] and surfaces [16], applications of GW to the study of cluster excitations have been so far scarce [17, 18].

In the following, we restrict our discussion to neutral clusters in closed-shell configurations. Let us consider one of these neutral clusters and let us add an external electron to it. In a first-order approximation, the one-electron wave function of the added electron can be approximated by

the corresponding KS wave function $\varphi_i(\mathbf{r})$ with KS eigenvalue ε_i, obtained using the self-consistent effective potential $v_{\text{eff}}(\mathbf{r})$ of the neutral cluster. In the framework of many-body theory, the lifetime of this quasiparticle τ_i can be obtained from the projection of the imaginary part of the electron self-energy $\Sigma(\mathbf{r}, \mathbf{r}', \varepsilon_i)$ over the wave function of the electron [15]. The decay probability Γ, i.e., the inverse of the lifetime, in the on-shell approximation, is:

$$\Gamma_i \;=\; \tau_i^{-1} \;=\; -\,2 \int d\mathbf{r} d\mathbf{r}' \varphi_i^*(\mathbf{r}) \mathrm{Im}\Sigma(\mathbf{r}, \mathbf{r}', \varepsilon_i) \varphi_i(\mathbf{r}'). \tag{4.5}$$

We calculate $\Sigma(\mathbf{r}, \mathbf{r}', \varepsilon_i)$ in the GW approximation [13, 14]. The electron self-energy $\Sigma(\mathbf{r}, \mathbf{r}', \varepsilon_i)$ can be obtained as a convolution over energies ω of two functions, namely, the Green function $G(\mathbf{r}, \mathbf{r}', \varepsilon_i - \omega)$ and the dynamically screened interaction between electrons $W(\mathbf{r}, \mathbf{r}', \omega)$. Further approximations are used to calculate both of them. If the exact Green function G is replaced by the independent-electrons Green function G^0, one can show that [15]:

$$\Gamma_i \;=\; -\,2 \sum_{f \notin occ.} \int d\mathbf{r} d\mathbf{r}' \varphi_i^*(\mathbf{r}) \varphi_f^*(\mathbf{r}') \mathrm{Im}W(\mathbf{r}, \mathbf{r}', \omega) \varphi_i(\mathbf{r}') \varphi_f(\mathbf{r}), \tag{4.6}$$

where $\omega = \varepsilon_i - \varepsilon_f$ and the sum over f runs over all unoccupied KS states of energy ε_f below the initial energy ε_i.

The screened interaction $W(\mathbf{r}, \mathbf{r}', \omega)$ can be obtained in terms of the bare Coulomb potential $v(\mathbf{r}, \mathbf{r}') = 1/|\mathbf{r} - \mathbf{r}'|$ and the density-density response function of the cluster $\chi(\mathbf{r}, \mathbf{r}', \omega)$

$$W(\mathbf{r}, \mathbf{r}'\omega) \;=\; v(\mathbf{r}, \mathbf{r}') \;+\; \int d\mathbf{r}_1 d\mathbf{r}_2 \; v(\mathbf{r}, \mathbf{r}_1) \; \chi(\mathbf{r}_1, \mathbf{r}_2, \omega) \; v(\mathbf{r}_2, \mathbf{r}') \; . \tag{4.7}$$

We calculate $\chi(\mathbf{r}, \mathbf{r}', \omega)$ in the random-phase approximation (RPA), in which the following self consistent equation has to be solved:

$$\chi(\mathbf{r}, \mathbf{r}'\omega) \;=\; \chi^0(\mathbf{r}, \mathbf{r}', \omega) \;+\; \int d\mathbf{r}_1 d\mathbf{r}_2 \; \chi^0(\mathbf{r}, \mathbf{r}_1, \omega) \; v(\mathbf{r}_1, \mathbf{r}_2) \; \chi(\mathbf{r}_2, \mathbf{r}', \omega) \; , \tag{4.8}$$

where $\chi^0(\mathbf{r}, \mathbf{r}', \omega)$ is the independent-particle response function that can be built from KS wave functions [19, 20].

At the level of approximation presented above, exchange-correlation effects are included neither in the calculation of $\chi(\mathbf{r}, \mathbf{r}', \omega)$ [Equation (4.8)] nor in the calculation of the screened interaction $W(\mathbf{r}, \mathbf{r}'\omega)$ [Equation

(4.7)]. However, the omission of exchange-correlation effects at both places may not introduce significant variations in the final results. Inclusion of exchange and correlation effects in $W(\mathbf{r},\mathbf{r}'\omega)$ reduces the electron-electron dynamic interaction and hence increases the lifetime. Inclusion of exchange and correlation effects in $\chi(\mathbf{r},\mathbf{r}',\omega)$ reduces the screening supplied by the many-body system and hence decreases the lifetime. A rough compensation of both effects has been shown in bulk metals [15] and other low-symmetry systems, such as metal surfaces [21].

In practice, the spherical symmetry of the problem reduces the complexity of the calculation. Wave functions, response functions and interaction potentials can be expanded in the spherical-harmonic basis set $Y_{lm}(\Omega)$:

$$\begin{aligned}
\varphi_i(\mathbf{r}) &= R_{l_i}(r)Y_{lm}(\Omega_{\mathbf{r}}) \\
\chi(\mathbf{r},\mathbf{r}',\omega) &= \sum_{lm}\chi_l(r,r',\omega)Y_{lm}(\Omega_{\mathbf{r}})Y^*_{lm}(\Omega_{\mathbf{r}'}) \\
v(\mathbf{r},\mathbf{r}') &= \sum_{lm}v_l(r,r')Y_{lm}(\Omega_{\mathbf{r}})Y^*_{lm}(\Omega_{\mathbf{r}'}) \\
&= \sum_{lm}\frac{4\pi}{2l+1}\frac{r^l_<}{r^{l+1}_>}Y_{lm}(\Omega_{\mathbf{r}})Y^*_{lm}(\Omega_{\mathbf{r}'}) \ , \qquad (4.9)
\end{aligned}$$

where $r_<$ ($r_>$) is the minimum (maximum) between r and r'. Similar expansions can be made for $\chi^0(\mathbf{r},\mathbf{r}',\omega)$ and $W(\mathbf{r},\mathbf{r}',\omega)$.

A simplified expression for the decay probability Γ_i is thus:

$$\Gamma_i = \sum_{\varepsilon_f,l_f}(2l_f+1)\gamma_{if} \ , \qquad (4.10)$$

where the sum over ε_f and l_f runs over unoccupied KS states with $\varepsilon_f < \varepsilon_i$. The individual state contribution to the rate γ_{if} is

$$\gamma_{if} = -\frac{1}{2\pi}\sum_l(2l+1)\begin{pmatrix} l & l_i & l_f \\ 0 & 0 & 0\end{pmatrix}^2\int dr r^2\phi^*_l(r)\rho_l(r) \ . \qquad (4.11)$$

The values of l which give non-zero contributions to the partial rate γ_{if} are fixed by the properties of the Wigner $3j$ coefficients. The function $\phi_l(r)$ is calculated from:

$$\phi_l(r) = \int dr' r'^2 R^*_{l_f}(r')R_{l_i}(r')v_l(r,r') \qquad (4.12)$$

and $\rho_l(r)$ is obtained from a self-consistent RPA-type integral equation:

$$\begin{aligned} \rho_l(r) &= \int dr'(r')^2 \chi_l^0(r,r',\omega)\phi_l(r') + \\ &+ \int dr'(r')^2 dr''(r'')^2 \chi_l^0(r,r',\omega) v_l(r',r'')\rho_l(r''). \end{aligned} \tag{4.13}$$

The decay probability written as a sum over ε_f and l_f can be visualized in a simple one-electron picture. An electron in an excited state can decay to several one-electron states of lower energy ε_f and angular momentum l_f at the same time that electronic excitations are created in the medium. The coupling between the angular momenta of the initial and final decaying electron wave functions determines the multipole components of the response function that play a role in the process. We emphasize here that multipole moments with angular momentum higher than the dipolar moment ($l = 1$) are necessary for most of the calculations.

Numerically, we follow a procedure similar to that of Reference [22]. We build one-electron Green functions from the solutions of the KS equation for every ω. We use these Green functions to calculate the multipole components of $\chi^0(\mathbf{r},\mathbf{r}',\omega)$. Integral Equation (4.13) is solved in real space after matrix inversion for every polar component l. Finally, integrals in Equations (4.12) and (4.11) are solved by standard numerical methods.

4.3 Results and discussion

Our analysis is focused into metal clusters with a fixed average electronic density. We choose a value for the one-electron radius $r_s = 4$ a.u., that can represent a free electron sodium cluster. As mentioned above, we restrict our discussion to neutral clusters in closed-shell configurations. We have performed calculations for clusters with these characteristics and a number of electrons that varies from $N = 34$ to $N = 2018$.

The first step of the process is the calculation of the cluster ground state. Our results are in agreement with those previously published in the literature [12]. In Figure 4.1 we see the case of a cluster with $N = 556$ electrons. The upper panel shows the electronic density $n^-(\mathbf{r})$ in units of the average electronic density $n_0^- = 3/(4\pi r_s^3)$. We observe Friedel oscillations due to electron confinement and an exponential decay of the electronic density at the surface of the cluster. In the lower panel, we represent the KS potential

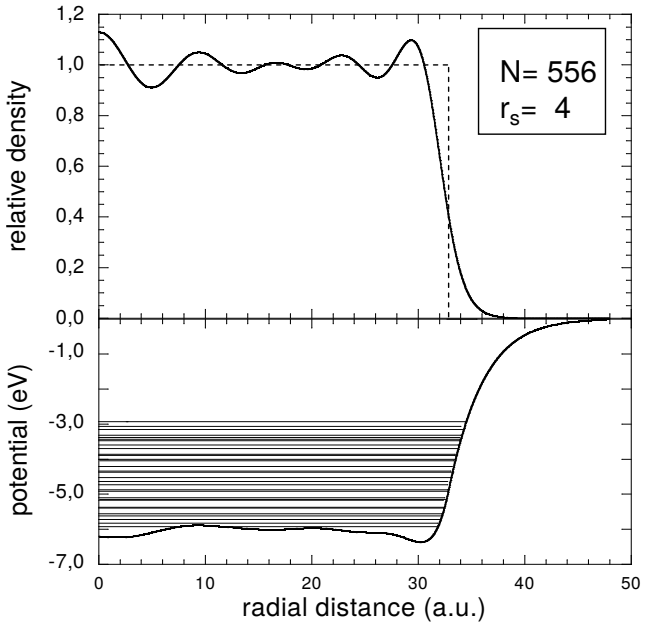

Figure 4.1: Density functional calculation of a jellium cluster with $N = 556$ electrons and density parameter $r_s = 4$. The upper panel shows the electronic density in units of $n_0^- = 3/(4\pi r_s^3)$ as a function of the distance from the centre of the cluster (in atomic units). The lower panel shows the Kohn-Sham potential (in eV) as a function of the same variable. The occupied Kohn-Sham levels are represented with horizontal lines in the lower panel as well.

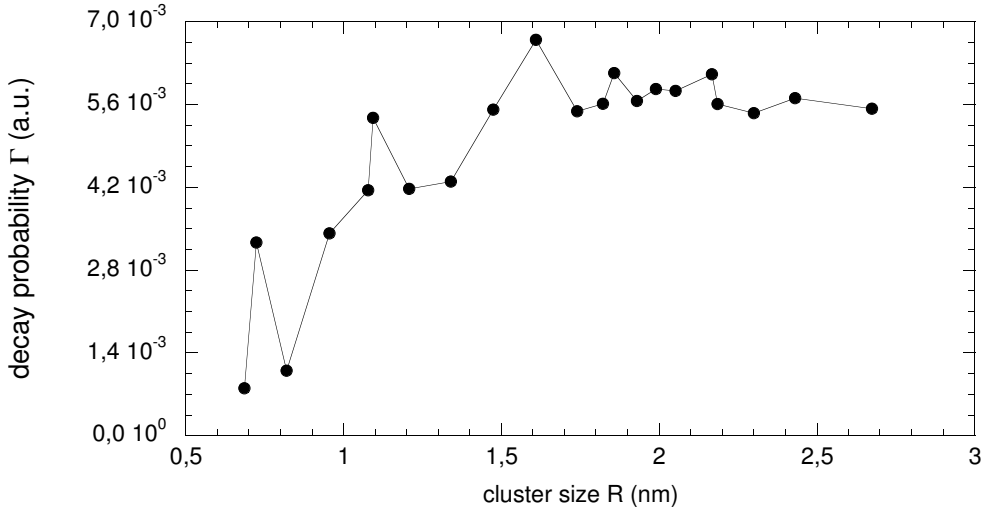

Figure 4.2: Decay probability $\Gamma = \tau^{-1}$ (in atomic units) for electronic excitations of 1 eV in jellium clusters with density parameter $r_s = 4$. The probability Γ is plotted as a function of the cluster radius R (in nanometers).

$v_{\rm eff}(r)$ and the occupied KS electron levels, so that the upper line corresponds to the Fermi energy of the system.

With these results we calculate the lifetime of energy excitations with $\epsilon_i \approx 1$ eV above the Fermi level. Due to the discretization of levels in the cluster, the initial energy of the excitation cannot be fixed exactly to this quantity, but the variation with respect to this reference value is never larger than 10%. The calculation of the response function $\chi(\mathbf{r}, \mathbf{r}', \omega)$ is made by introducing a damping η as an external parameter. The value of η is big enough to give appreciable transition rates but never larger than the distance between the energy levels of different states. We have checked that the results do not have a significant dependence on the value of the damping for values between $\eta = 0.001$ and $\eta = 0.008$ a.u.. Hence we chose a value of $\eta = 0.005$ for all calculations presented here.

We show the results of our calculations in Figure 4.2, in which the transition rate Γ is represented for different cluster sizes. In order to simplify the analysis, we can define here two different regimes. For the smallest clusters, the transition rates show large oscillations. Confinement, which

leads to the discretization of levels, has a strong effect in this region. For instance, an increment of six electrons in the $N = 34$ electron cluster makes the transition rate a factor of 4 bigger. The rate considerably depends on *which* is the initial state, its angular momentum and the features of the energy levels below it. For clusters of $R > 1.5$ nm (i.e., $N > 340$ electrons) variations in the absolute value of Γ are smaller, and the values of Γ are always in the range between $\Gamma = 0.005$ a.u. and $\Gamma = 0.007$ a.u.. Still a few small oscillations show that size effects remain. In particular, the value of Γ for a cluster with $R = 1.82$ nm increases approximately 75% if the transition is calculated with the initial state $\epsilon_i = 0.94$ eV above the Fermi level, instead of the one represented in Figure 4.2, namely $\epsilon_i = 1.08$ eV. The reason for this is twofold: confinement effects and the difference in decaying energies. In the limit of an homogeneous electron gas, such a difference in the initial energy of the excitation would lead to a 40% increase in the final rate.

As a reference, we mention here that a RPA calculation of electron lifetimes in a homogeneous electron gas, with the same parameters that we fix in our calculation ($\epsilon_i = 1$ eV and $r_s = 4$) gives a value $\Gamma = 0.0022$ a.u. [23], still smaller than the one obtained for the biggest of our clusters. Localization in space of the electronic excitation and screening effects are reponsible for this difference. In a homogeneous electron gas, initial states of the excitation are plane waves, extended all over the space. In a cluster, the initial state of the excitation is described by a localized wave function, normalized to unity. Furthermore, screening in the vicinity of the cluster surface is less effective than in bulk, making the electron-electron interaction stronger in this region. Significant overlap between the initial and final wave functions in the surface region enhances the decay probability, reducing the lifetime of the excitation. We also show in Figure 4.3 the partial decay probabilities γ_{if} for an electronic excitation of $\varepsilon_i \approx 1$ eV in a jellium cluster with $r_s = 4$ and $N = 556$ electrons. The probabilities γ_{if} are plotted for all unoccupied KS levels $\varepsilon_f < \varepsilon_i$. The exact values of the KS eigenenergies ε_f are also plotted in the right panel. The total transition rate Γ can be obtained as a sum over all these γ_{if}, after accounting for angular degeneracy [Equation 4.10]. Figure 4.3 shows that the KS final levels that most contribute to the total value of Γ are not necessarily those closest in energy to ε_i.

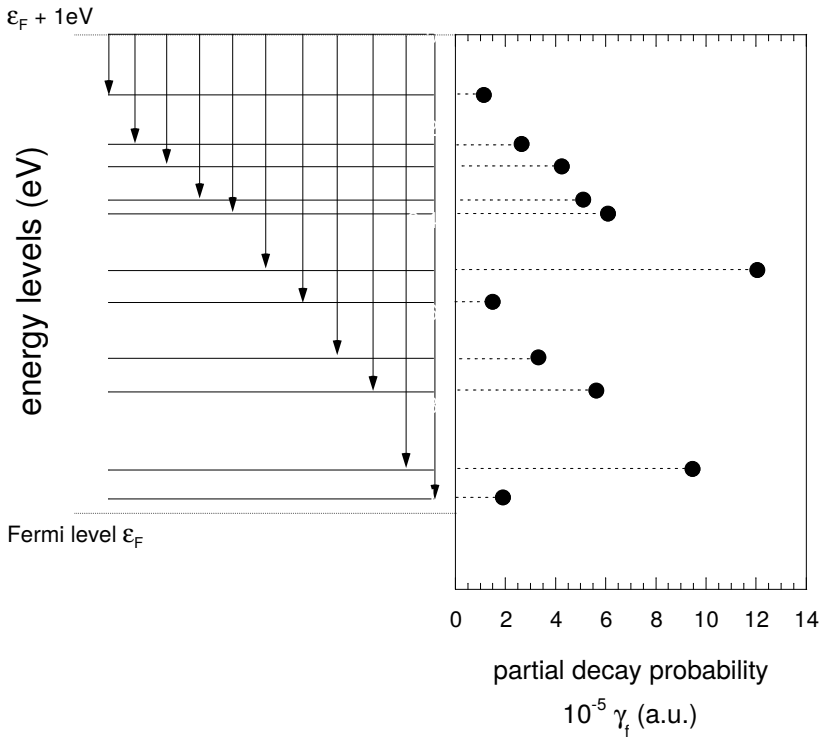

Figure 4.3: Partial decay probabilities γ_{if} (in units of 10^{-5} atomic units) for an electronic excitation of 1 eV in a jellium cluster with $N = 556$ electrons and density parameter $r_s = 4$ (right panel). The left panel shows the eigenenergies ε_f of the unoccupied Kohn-Sham states (in eV).

4.4 Conclusions

In summary, we have calculated the lifetime of electronic excitations of $\varepsilon_i \approx 1$ eV energy in jellium clusters of a fixed electronic density ($r_s = 4$). We have shown that, for small clusters ($R < 1.5$ nm), several maxima and minima appear in the dependence of the lifetime on the cluster size. This non-monotonic behaviour is a consequence of the discrete spectrum of levels as well as of the different filling of electronic shells in the clusters depending on their size. The order of magnitude of the excitation lifetimes in this region can vary between $\tau \approx 4$ and $\tau \approx 30$ femtoseconds. For bigger clusters, effects due to the discretization of levels in the cluster are smoother, and the excitation lifetimes reach a value around $\tau \approx 5$ femtoseconds. This lifetime is smaller than that of electronic excitations with the same characteristics in a homogeneous electron gas. A subtle interplay between screening effects and space localization of the initial excitation is the responsible of this difference.

References

[1] Brack M 1993 *Rev. Mod. Phys.* **65** 677

[2] Alonso J A and Balbás L C 1996 *Topics in Current Chemistry* vol 182 (Springer-Verlag, Berlin-Heidelberg) p 119

[3] Knight W D, Clemenger K, de Heer W A, Saunders W A, Chou M Y and Cohen M L 1984 *Phys. Rev. Lett.* **52** 2141

[4] Vajda Š, Bartelt A, Lupulescu C and Wöste L 2003 *Progress in Experimental and Theoretical Studies of Clusters*, Advanced Series in Physical Chemistry vol 13 (Edited by Kondow T and Mafuné F, World Scientific Publishing, Singapore) c 4

[5] Voisin C, Christofilos D, Del Fatti N, Vallée F, Prével, Cottancin E, Lermé J, Pellarin M and Broyer M 2000 *Phys. Rev. Lett.* **85** 2200

[6] Pontius N, Lüttgens G, Bechtold P S, Neeb M and Eberhardt W 2001 *J. Chem. Phys.* **115** 10479

[7] Gerhardt P, Niemietz M, Dok Kim Y and Ganteför G 2003 *Chem. Phys. Lett.* **382** 454

[8] de Heer W A 1993 *Rev. Mod. Phys.* **65** 611

[9] Hohenberg P and Kohn W 1964 *Phys. Rev.* **136** B864

[10] Kohn W and Sham L J 1965 *Phys. Rev.* **140** A1133

[11] Gunnarsson O and Lundqvist B I 1976 *Phys. Rev. B* **13** 4274

[12] Ekardt W 1984 *Phys. Rev. B* **29** 1558

[13] Hedin L 1965 *Phys. Rev.* **139** A796

[14] Aryasetiawan F and Gunnarsson O 1998 *Rep. Prog. Phys.* **61** 267

[15] Echenique P M, Pitarke J M, Chulkov E V and Rubio A 2000 *Chem. Phys.* **251** 1

[16] Echenique P M, Berndt R, Chulkov E V, Fauster Th, Goldmann A and Höfer U 2004 *Surf. Sci. Rep.* **52** 219

[17] Verdozzi C, Godby R W and Holloway S 1995 *Phys. Rev. Lett.* **74** 2327

[18] Pavlyukh Y and Hübner W 2004 *Phys. Lett. A* **327** 241

[19] Ekardt W 1985 *Phys. Rev. B* **31** 6360

[20] Puska M J, Nieminen R M and Manninen M 1985 *Phys. Rev. B* **31** 3486

[21] Sarria I, Osma J, Chulkov E V, Pitarke PM and Echenique P M 1999 *Phys. Rev. B* **60** 11795

[22] Díez Muiño R, Arnau A, Salin A and Echenique P M 2003 *Phys. Rev. B* **68** 041102(R)

[23] Pitarke J M (private communication).

5 Lifetime of electronic excitations in metal nanoparticles

Abstract

Electronic excitations in metal particles with sizes up to few nanometers are shown to have a one-electron character when a laser pulse is applied off the plasmon resonance. The calculated lifetimes of these excitations are in the femtosecond time scale but their values are substantially different from those in bulk. This deviation can be explained from the large weight of the excitation wave function in the nanoparticle surface region, where dynamic screening is significantly reduced. The well-known quadratic dependence of the lifetime with the excitation energy in bulk breaks down in these finite-size systems.

5.1 Introduction

While structural properties of materials depend on ground state features, electronic and optical properties are largely determined by their electronic excitations. A large amount of theoretical and experimental work has been devoted to understand the dynamics and predict the lifetimes of these excitations in metallic solids [1, 2, 3, 4, 5] and at metal surfaces [6, 7, 8, 9, 10, 11]. Much less is known about the dynamics of electronic excitations in finite-size systems. In metal nanoparticles, electronic properties are very often size-dependent and can be tuned purposely. The modification at wish of the electronic properties of metal systems and the subsequent change in the lifetime of electronic excitations has important implications for many technological applications. In photochemistry, for instance, electronically excited states can act as intermediate steps in various chemical processes[12]. Either enhancement or reduction of the reaction rate should be thus possible through a proper design of the intermediate step lifetime.

The difference between the dynamics of hot electrons in nanoparticles and in bulk has to be discussed in terms of two effects. First, the electron lifetime can be enhanced in metal nanoparticles as compared to bulk because of the discretization of levels that reduces the number of final states to which the electronic excitation can decay. Second, the lifetime can be shortened in the nanoparticle because of the reduction of dynamic screening for low frequencies. Thus, there are no *a priori* reasons to predict whether the lifetime of electronic excitations in nanoparticles is longer or shorter than in bulk.

From the experimental point of view, laser-based pump-probe techniques have been used to analyze the dependence on size of the electron-electron interaction processes [13, 14, 15, 16]. Some of the conclusions extracted from these works are puzzling. Measurements of internal thermalization times suggest that the electron-electron scattering rate is increased in Ag nanoparticles of size smaller than 5 nm as compared with the bulk reference value [13]. However, electron lifetimes in supported Ag nanoparticles were measured to be appreciably higher than those obtained for Ag thick films [16]. These apparently contradictory conclusions show the necessity of further research on the subject.

In this work, we combine time-dependent density functional theory (TDDFT) and the self-energy formalism to characterize the electronic excitations in metal nanoparticles and calculate their decay rates in typical

pump-probe situations. We first show that, when a laser pulse is applied off the plasmon resonance, the electronic excitation exhibits a one-electron character. Afterwards, we calculate the lifetime of the excitation and show that, for particle sizes up to few nanometers, the lifetime does not depend much on size. Still, the lifetime value is surprisingly different from the bulk limit. We explain this fact in terms of the partial localization of the electron excitation in the vicinity of the surface.

We restrict our discussion to neutral nanoparticles in closed-shell electronic configurations. The description of the system is simplified by means of the jellium approximation, which allows us to cover a wide range of particle sizes. The spherical jellium model has been widely used in the description of metal clusters and is able to describe many of their experimentally measured electronic properties [17]. The average one-electron radius in the nanoparticle is defined from $r_s = R/N^{1/3}$, where R is the radius of the nanoparticle and N the number of electrons.

5.2 Theory and results

5.2.1 Time evolution of electronic excitations

The first goal of our work is the analysis of the electronic excitations produced in the nanoparticle when pumping energy with a laser source. For this purpose, we use TDDFT to describe the dynamical evolution of the electronic density $n(\mathbf{r},t) = \sum_{j\in occ.} |\varphi_j(\mathbf{r},t)|^2$, where $\varphi_j(\mathbf{r},t)$ are Kohn-Sham (KS) wave functions (atomic units will be used unless otherwise stated). Numerical details are similar to those of Ref. [18]. In the ground state ($t = 0$), the spectrum of KS energy levels ε_j is discrete and each $\varphi_j(\mathbf{r}, t = 0)$ is characterized by the radial quantum number k and the angular momentum l. A gaussian laser pulse $\mathbf{E} = E_0 \cos(\Omega t)\, exp\{-[(t-t_0)/\Delta]^2\}\, \mathbf{u}_z$ is applied, where $\mathbf{u}_z$ is a unitary vector along the z-axis. E_0 is the field amplitude, Ω the laser frequency, t_0 the time of maximum amplitude, and Δ controls the pulse duration. During the time evolution, the problem becomes axially symmetric and KS wave functions preserve their quantum number m.

Figure 5.1 shows the dipole moment d induced by the laser pulse in a nanoparticle with $N = 556$ and $r_s = 2.07$ (upper panel). The laser frequency is $\Omega = 4.12$ eV. The change in electronic density $\Delta n(\mathbf{r},t) = n(\mathbf{r},t) - n(\mathbf{r}, t = 0)$ is shown at two different times (middle panels), with the induced dipole moments pointing in opposite directions. We define the

projection $P_{ij}(t) = \sum_{m_i,m_j} \delta_{m_i m_j} |< \varphi_{i\in unocc.}(\mathbf{r}, t=0)|\varphi_{j\in occ.}(\mathbf{r}, t) >|^2$ of the time-dependent KS wave functions over those unperturbed KS wave functions which are unoccupied at $t = 0$. The sums over m_i and m_j run over all possible m-values of the energy levels ε_i and ε_j. When the pulse is over, only one projection $P_{ij}(t)$ takes a non-negligible value, as shown in the lower panel. This means that the excitation can be roughly described as a one-electron transition between an initially occupied KS level ε_j and an initially unoccupied KS level ε_i. The excitation energy is close (although not identical) to the energy of the pulse $\varepsilon_i - \varepsilon_j \approx \Omega$. This result strongly supports the use of unoccupied KS wave functions as final one-electron states in the excitation process.

5.2.2 Lifetime of electronic excitations

As a second step, we calculate the lifetime of the electronic excitation created by the laser pulse. The wave function of the excited electron is approximated by the corresponding KS one-electron wave function $\varphi_i(\mathbf{r})$ with KS eigenvalue ε_i. In the framework of many-body theory, the lifetime of this quasiparticle is given by $\tau_i = \Gamma_i^{-1}$, where the decay rate Γ_i can be obtained from the projection of the imaginary part of the electron self-energy $\Sigma(\mathbf{r}, \mathbf{r}', \varepsilon_i)$ over the wave function of the electron. We calculate $\Sigma(\mathbf{r}, \mathbf{r}', \varepsilon_i)$ in the GW approximation [19, 20]. If the exact Green function G is replaced by the independent-electrons Green function G^0, one can show that [21]:

$$\Gamma_i \;=\; -2 \sum_{f\in unocc.} \int d\mathbf{r} d\mathbf{r}' \varphi_i^*(\mathbf{r}) \varphi_f^*(\mathbf{r}') \mathrm{Im} W(\mathbf{r}, \mathbf{r}', \omega) \varphi_i(\mathbf{r}') \varphi_f(\mathbf{r}), \qquad (5.1)$$

where $W(\mathbf{r}, \mathbf{r}', \omega)$ is the screened interaction, $\omega = \varepsilon_i - \varepsilon_f$ and the sum over f runs over all unoccupied KS states of energy ε_f below the energy ε_i. The screened interaction $W(\mathbf{r}, \mathbf{r}', \omega)$ is obtained in terms of the bare Coulomb potential $v_C(\mathbf{r}, \mathbf{r}')$ and the density-density response function of the nanoparticle $\chi(\mathbf{r}, \mathbf{r}', \omega)$, the latter calculated in the random phase approximation (RPA).

The numerical procedure can be found in Ref. [21] and is only summarized here. We build one-electron Green functions for every ω, and use them to calculate the multipole components of $\chi^0(\mathbf{r}, \mathbf{r}', \omega)$. The RPA-type integral equation is solved in real space after matrix inversion for every polar component l. An imaginary damping η is added to the value of ω in the

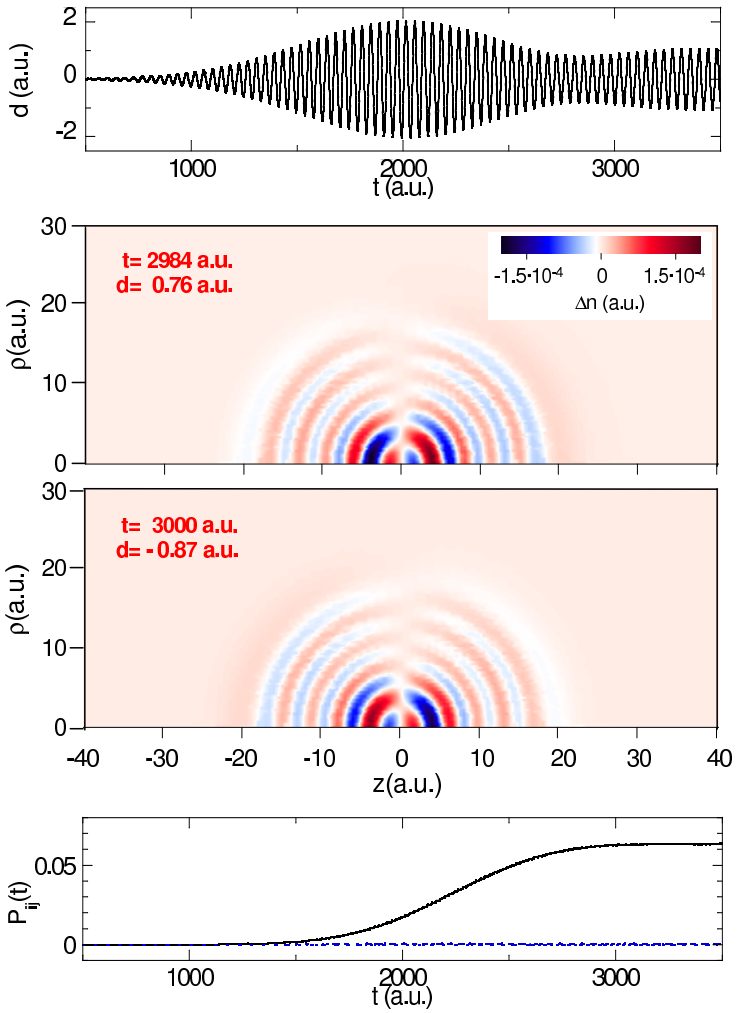

Figure 5.1: Change in electronic density $\Delta n(\mathbf{r}, t)$ induced in a metal nanoparticle by a laser pulse (central panels). $\Delta n(\mathbf{r}, t)$ is shown over a plane (ρ, z) containing the direction of propagation of the field, for $t = 2984$ and $t = 3000$. The nanoparticle is made of $N = 556$ electrons and $r_s = 2.07$. The laser pulse parameters are $E_0 = 2 \times 10^{-4}$, $t_0 = 2000$, $\Delta = 700$, and $\Omega = 4.12$ eV. The upper panel shows the time evolution of the dipole moment d induced in the nanoparticle. The lower panel shows the projections $P_{ij}(t)$ of an initially occupied level j over an initially unoccupied level i (blue dotted lines). The projection with a maximum value over time is plotted with a black solid line.

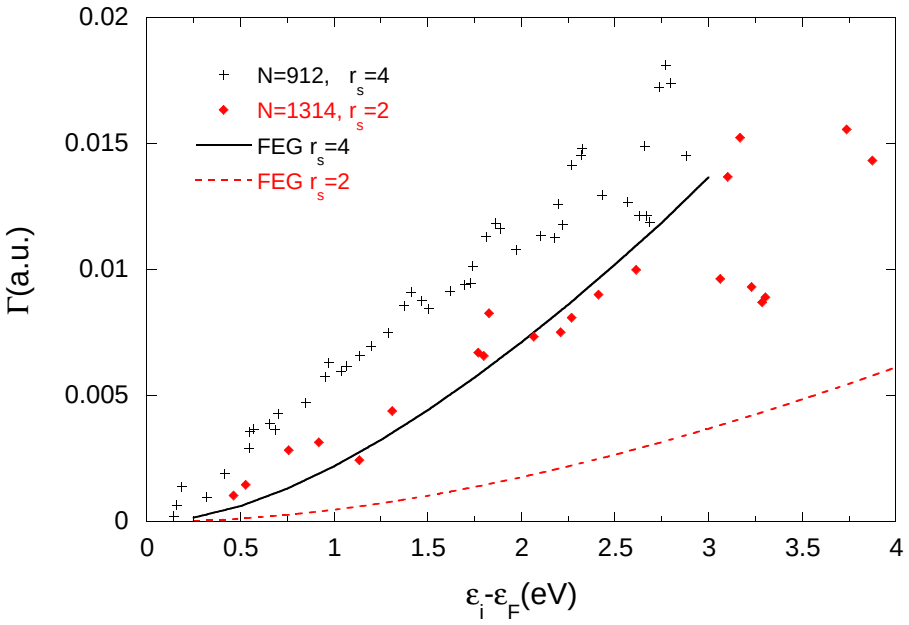

Figure 5.2: Decay rate $\Gamma = \tau^{-1}$ for electronic excitations in nanoparticles as a function of the excitation energy $\varepsilon_i - \varepsilon_F$. (Red) diamonds refer to a nanoparticle of $N = 1314$ and $r_s = 2$ ($R = 1.1$ nm). (Black) crosses refer to a nanoparticle of $N = 912$ and $r_s = 4$ ($R = 1.9$ nm). The dashed (red) line and the solid (black) line show the values of Γ in an infinite electron gas of $r_s = 2$ and $r_s = 4$ respectively.

numerical calculation of $\chi^0(\mathbf{r}, \mathbf{r}', \omega + i\eta)$. Without a certain indeterminacy in the energy value, Γ would be strictly zero for transitions between discrete states. In real systems, physical effects such as temperature and finite duration of the laser pulse account for this indeterminacy. We have checked that the results do not vary more than 3% for values of the damping between $\eta = 10^{-3}$ and $\eta = 10^{-2}$. We choose a value $\eta = 0.005$ for all calculations presented here.

In Fig. 5.2, we show the decay rate Γ as a function of $\varepsilon_i - \varepsilon_F$, where ε_F is the highest occupied state energy. We choose values of $r_s = 2$ ($N = 1314$) and $r_s = 4$ ($N = 912$), representing Al and Na nanoparticles respectively. The present results are compared with the decay rates of electronic excitations in an infinite homogeneous free electron gas (FEG) calculated in the same approximation [22]. Our results show that the values of Γ in a nanoparticle, whereas in the femtosecond time scale, are significantly larger than the values of Γ in a FEG.

In a FEG and for small values of $\varepsilon_i - \varepsilon_F$, the decay rate is known to depend on the excitation energy ε_i through a quadratic function $\Gamma \propto (\varepsilon_i - \varepsilon_F)^2$ [24]. This scaling law arises from the phase space available for the electronic excitation to decay [23]. Fig. 5.2 shows that the quadratic dependence breaks down in a nanoparticle. The discrete spectrum of excitation energies in a finite system modifies the available phase space and thus the dependence with the energy. In addition, the dependence of Γ on r_s is also smoother in a nanoparticle, as can be seen in Fig. 5.2. In other words, and according to our calculation, lifetimes of electronic excitations in nanoparticles are less material-dependent than those in bulk. Further experimental evidence would be useful to gain insight into these points.

An interesting question for confined systems is always the size for which the properties merge into those of bulk. We analyze the dependence of the decay rate $\Gamma = \tau^{-1}$ on the particle radius R in Fig. 5.3. Values of Γ are plotted for three different excitation energies ε_i in nanoparticles with $r_s = 4$. An exact matching in energy is not possible because of the discretization of energy levels in finite-size systems. For the largest sizes considered in this work ($\approx$ 5 nm diameter), there is still a significant difference between the lifetime of electronic excitations in nanoparticles and bulk, even if the density of final states in the decay can be considered roughly as a continuum. The first reason for this deviation is that the dynamic screening between electrons in a nanoparticle of this size is still different to the one in bulk, even in the inner regions of the nanoparticle. The second and most important reason

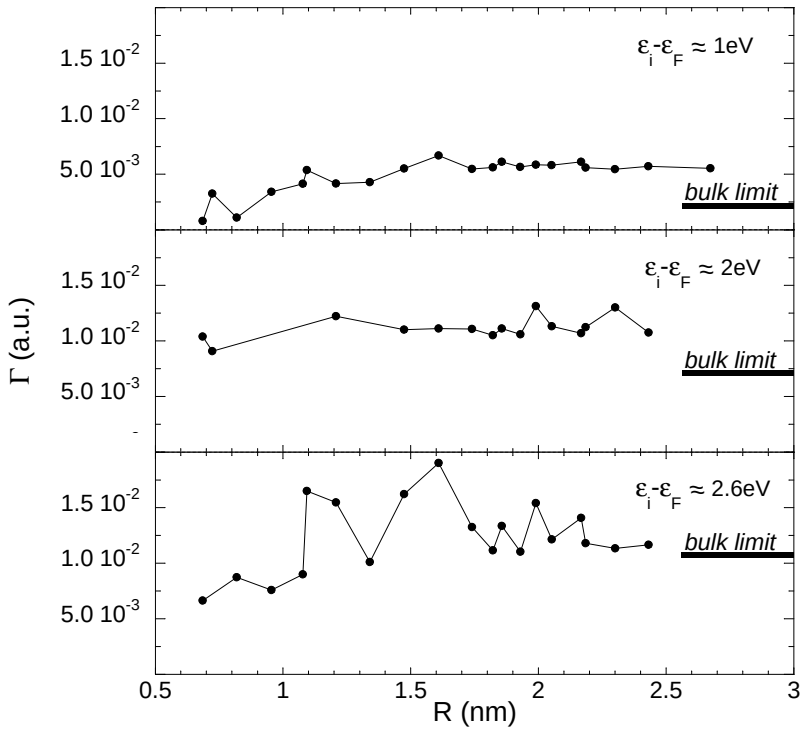

Figure 5.3: Decay rate $\Gamma = \tau^{-1}$ for electronic excitations in nanoparticles of $r_s = 4$ as a function of their radius R. Three different excitation energies are shown. The values for the free electron gas are also shown (bulk limit).

for the difference is the localization in space of the electronic excitation. In an infinite homogeneous system, the initial states of the excitation can be considered as plane waves, extended all over the space. In a nanoparticle, we have shown above that unoccupied KS wave functions appropriately describe the excited state after laser excitation. Figure 5.4 shows that the unoccupied KS wave functions have a large weight nearby the surface. Dynamic screening in the vicinity of the surface is less effective than in bulk, making the electron-electron interaction stronger. Significant overlap between the initial and final wave functions in the surface region modifies the decay probability as compared to the bulk case.

Let us now discuss our results in connection with the aforementioned experimental evidence. The decay rates calculated above for nanoparticles correspond to lifetimes τ between 1 and 100 femtoseconds. Experimental results for Ag nanoparticles [16] are in between these values. Our theoretical results also show that the decay rate is larger in nanoparticles than in bulk. This is in agreement with the conclusions extracted from the measurements of thermalization times in Ag nanoparticles [13], but it does not help to understand the opposite behavior obtained in supported Ag nanoparticles [16]. Further research is thus needed to clarify this point.

5.3 Summary

In summary, our results show that the lifetimes of electronic excitations in nanoparticles are in the femtosecond time scale. We also show that the well-known quadratic dependence of the lifetime with the excitation energy in bulk $\tau \propto (\varepsilon - \varepsilon_F)^{-2}$ breaks down in metal nanoparticles. This peculiar quasilinear behavior has been also predicted in other low-dimensional systems [25], and would require experimental evidence to be confirmed. Finally, substantial quantitative variations appear between the lifetime of electronic excitations in metal nanoparticles and bulk. Electron excitations have a significant weight in the nanoparticle surface region, where dynamic screening is largely reduced, and the lifetime of these excitations is subsequently shortened. Finite-size effects thus play a major role in the decay of electronic excitations in metal nanoparticles.

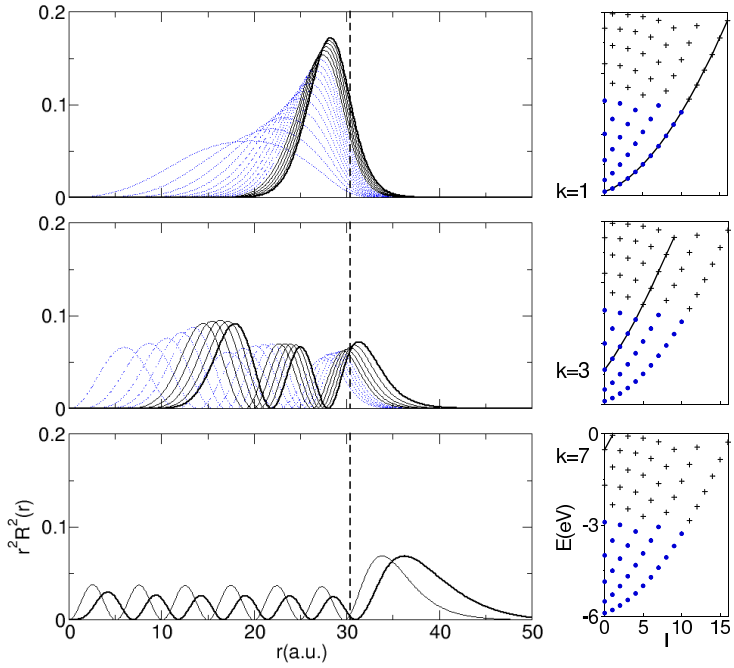

Figure 5.4: Left panels: Radial distributions for the wave functions in a nanoparticle with $N = 440$ and $r_s = 4$ ($R = 1.6$ nm). Blue dotted (black solid) lines represent occupied (unoccupied) states. The unoccupied state of highest energy is represented with a thick solid line. The nanoparticle surface is indicated with a dashed line. Right panels: Energy levels as a function of angular momenta. Blue circles (black crosses) indicate occupied (unoccupied) states. Lines are plotted joining the energy levels for which radial distributions are shown on the left panels.

References

[1] M. Aeschlimann *et al.*, Phys. Rev. Lett. **79**, 5158 (1997).

[2] H. Petek, S. Ogawa, Prog. Surf. Sci. **56**, 239 (1997).

[3] E. Knoesel, A. Hotzel, M. Wolf, Phys. Rev. B **57**, 12812 (1998).

[4] R. Knorren *et al.*, Phys. Rev. B **61**, 9427 (2000).

[5] E. V. Chulkov *et al.*, Chem. Rev. **106**, 4160 (2006).

[6] U. Höfer *et al.*, Science **277**, 1480 (1997).

[7] M. Weinelt, J. Phys.: Condens. Matter **14**, R1099 (2002).

[8] J. Kröger *et al.*, Prog. Surf. Sci. **80**, 26 (2005).

[9] J. Güdde and U. Höfer, Prog. Surf. Sci. **80**, 49 (2005).

[10] I. Sarria *et al.*, Phys. Rev. B, **60**, 11795 (1999).

[11] J. Osma *et al.*, Phys. Rev. B, **59**, 10591 (1999).

[12] K. Watanabe *et al.*, Chem. Rev. **106**, 4301 (2006).

[13] C. Voisin *et al.*, Phys. Rev. Lett. **85**, 2200 (2000).

[14] N. Pontius *et al.*, J. Chem. Phys. **115**, 10479 (2001).

[15] P. Gerhardt *et al.*, Chem. Phys. Lett. **382**, 454 (2003).

[16] M. Merschdorf, C. Kennerknecht, W. Pfeiffer, Phys. Rev. B **70**, 193401 (2004).

[17] J. A. Alonso, *Structure and properties of atomic nanoclusters* (Imperial College Press, London 2005).

[18] M. Quijada *et al.*, Phys. Rev. A **75**, 042902 (2007).

[19] L. Hedin, Phys. Rev. **139**, A796 (1965).

[20] F. Aryasetiawan and O. Gunnarsson, Rep. Prog. Phys. **61**, 267 (1998).

[21] M. Quijada, R. Díez Muiño, and P. M. Echenique, Nanotechnology **16**, S176 (2005).

[22] E. Zarate, PhD thesis, University of the Basque Country (1999).

[23] E. Zarate, P. Apell, and P.M. Echenique, Phys. Rev. B **60**, 2326 (1999).

[24] D. Pines and P. Nozières, *The Theory of Quantum Liquids* (Benjamin, New York, 1966).

[25] P. M. Echenique *et al.*, Prog. in Surf. Sci. **67**, 271 (2001).

6 TDDFT calculation of the stopping power for protons and antiprotons in metals

Abstract

Time-dependent density functional theory is used to calculate the energy loss of antiprotons and protons traversing metal clusters of variable size. We find that the effective energy loss per unit path length inside the cluster shows no significant cluster size effects over the wide range of projectile velocities studied. This allows us to compare the calculated stopping power with the experimental values for a solid metal target. Excellent agreement between the theoretical results and recent experimental data is found for velocities below the inner-shell excitation threshold. We thus present a non-perturbative quantum-mechanical approach to obtain the energy loss of charges in solids.

6.1 Introduction

Charged particles penetrating solid media give rise to electronic excitations in the target and thus lose kinetic energy. The slowing down of charged particles in matter is a key phenomenon in applied materials science, in medical physics, as well as being an important ingredient in many experimental techniques used in fundamental research on solids, surfaces, and nanostructures. However, and despite numerous attempts, the complexity of the dynamic interaction between charges and solids has made it difficult to apply theoretical schemes at the level of accuracy achieved in other condensed matter problems. For such accuracy, a detailed description of electronic excitations, dynamic screening, and possible charge transfer processes is required.

So far, self-consistent calculations for the slowing down of ions in metal targets have been reported only in the low-velocity limit. A combination of scattering theory with the results of static density functional theory (DFT) can successfully describe the energy loss in this case [1, 2, 3, 4, 5]. For higher projectile velocities, only model calculations based on velocity-dependent screening [6, 7] or perturbative expansions in terms of screened higher-order response functions [8] are available at present. There has been no quantal self-consistent theoretical framework able to describe the stopping power of solids for charged projectiles over a wide range of velocities. Only theories based on classical mechanics [9, 10] have been applied. Particularly challenging is the case in which the projectile velocity is similar to the Fermi velocity v_F of the target electrons. In this velocity range, quasi-static or perturbative approximations break down even for unit-charge projectiles.

The development of time-dependent methods in recent years has opened new perspectives in the theoretical description of the slowing down of charged projectiles in matter. In particular, time-dependent density functional theory (TDDFT) provides a self consistent, non-perturbative, time-domain treatment of electron dynamics in many body systems. TDDFT has been successfully applied to the calculation of energy transfer in collisions between charged atomic particles and small molecules and clusters in the gas phase [11, 12, 13, 14]. Two-dimensional targets of finite size [15] and metal surfaces [16] have been addressed as well.

In this article, we develop a quantal method based on TDDFT in order to obtain the contribution of the valence band electrons to the slowing down of charges in solids over a wide range of velocities. The stopping

power of Al for antiprotons is taken as an illustration to demonstrate the capabilities of the method. There are several reasons for this choice. First, the valence electrons of Al are the paradigm of a free-electron-like band, so that numerical effort can be much reduced. Second, point-like projectiles of negative charge have often been under scrutiny since the pioneering paper of Fermi and Teller [17]: the absence of charge exchange processes between the projectile and the target simplifies the analysis in this case. Finally, accurate experimental data have recently been obtained for this system [18, 19, 20]. It is worth mentioning that our method is not limited to free electron-like targets: the methodology is general and could be in principle applied to any weakly-correlated material.

The core of our method consists of TDDFT calculations of the energy loss of projectiles traversing target clusters of variable sizes. We then show that the energy loss per unit path length inside the cluster is nearly independent of the cluster size. This allows us to link this quantity to the stopping power of an infinite system. Our theoretical results for the stopping power of Al for antiprotons reproduce recent experimental measurements [18, 19, 20] for the range of projectile velocities below the inner-shell excitation threshold. Extension of the present approach to the stopping of Al for protons agrees quantitatively with experimental data [19, 20] as well.

6.2 Theoretical Approach

To calculate the stopping power of a cluster of Al atoms, a spherical jellium model is used to represent the valence electrons. The contribution of inner-shell excitations to the stopping is thus not included. The jellium positive background density is defined by $n_0^+(\mathbf{r}) = n_0^+\theta(R_{\rm cl} - r)$. Here, $R_{\rm cl}$ is the cluster radius and $\theta(x)$ is the Heaviside function. The electron density of the cluster is described by the density parameter r_s ($4\pi r_s^3/3 = 1/n_0$). The number of electrons in the cluster N_e is $N_e = (R_{cl}/r_s)^3$.

The time evolution of the electron density in response to the field of the moving projectile, $n(\mathbf{r}, t)$, is calculated within the Kohn-Sham (KS) scheme of TDDFT (Hartree atomic units are used everywhere unless otherwise stated):

$$i\frac{\partial\psi_j(\mathbf{r},t)}{\partial t} \;=\; \{T + V_{\rm eff}([n],\mathbf{r},t)\}\,\psi_j(\mathbf{r},t)\;, \tag{6.1}$$

where $\psi_j(\mathbf{r}, t)$ are the KS orbitals and T is the kinetic energy operator. The effective KS potential, $V_{\rm eff}([n], \mathbf{r}, t)$ is a function of the electron density of

the system: $n(\mathbf{r},t) = \sum_{j\in occ.} |\psi_j(\mathbf{r},t)|^2$. Here, $V_{\rm eff}$ is obtained as the sum of the external potential $V_{\rm ext}$, the Hartree potential $V_{\rm H}$, and the exchange correlation potential $V_{\rm xc}$: $V_{\rm eff} = V_{\rm ext} + V_{\rm H} + V_{\rm xc}$. $V_{\rm ext}$ is the Coulomb potential created by a point charge Q moving with constant velocity v along a straight trajectory that goes through the geometrical center of the cluster. The initial position of the projectile is such that the projectile/cluster interaction can be neglected. $V_{\rm xc}(\mathbf{r},t)$ is treated in a standard adiabatic local density approximation (ALDA) with the exchange-correlation functional of Ref. [21].

The numerical procedure used is very similar to that of Refs. [15] and [22]. For $t = 0$, $n(\mathbf{r},0)$ is the electron density of the unperturbed cluster. The KS wave functions $\psi_j(\mathbf{r},0)$ are expanded in a basis set of spherical harmonics. A radial mesh of equidistant points is used, allowing the Fourier Grid representation of the Hamiltonian matrix [23]. The static KS equations are then solved by direct diagonalization. Afterwards, the KS orbitals are projected onto a cylindrical grid, $\mathbf{r} = (\varrho, \varphi, z)$, with the z-axis along the projectile trajectory. The time propagation is performed by means of the split-operator technique [24].

6.3 Results and Discussion

Figure 6.1 shows several snapshots of the change in electron density $\Delta n(\mathbf{r},t) = n(\mathbf{r},t) - n(\mathbf{r},0)$ induced by an antiproton ($Q = -1$) of velocity $v = 1.5$ colliding with a cluster of $N_e = 254$, $R_{cl} = 12.7$, and $r_s = 2$. This value of r_s is close to that describing the screening radius in bulk Al. The density is plotted in a plane that contains the particle trajectory. A polarization effect is clearly visible before the antiproton reaches the cluster surface. Once inside the cluster, a depletion of charge develops in the vicinity of the antiproton. The self-consistent dynamic rearrangement of charge in the vicinity of the moving particle results in a wake potential similar to that in bulk metal targets [25]. Our results show that the collision of the antiproton with the cluster is followed by electron emission from the cluster.

Figure 6.2 shows the force acting on the antiproton during the collision process. It is directly obtained from the time-dependent charge density, $n_0^+(\mathbf{r}) - n(\mathbf{r},t)$. Due to the cylindrical symmetry of the problem, the only nonzero component of the force is along the projectile trajectory (z-axis), $F_z(t)$. When the antiproton is located outside the cluster, it is attracted by the induced dipole. Crossing the surface into the cluster results in a rapid rearrangement of electron density to screen the projectile charge. Inside the

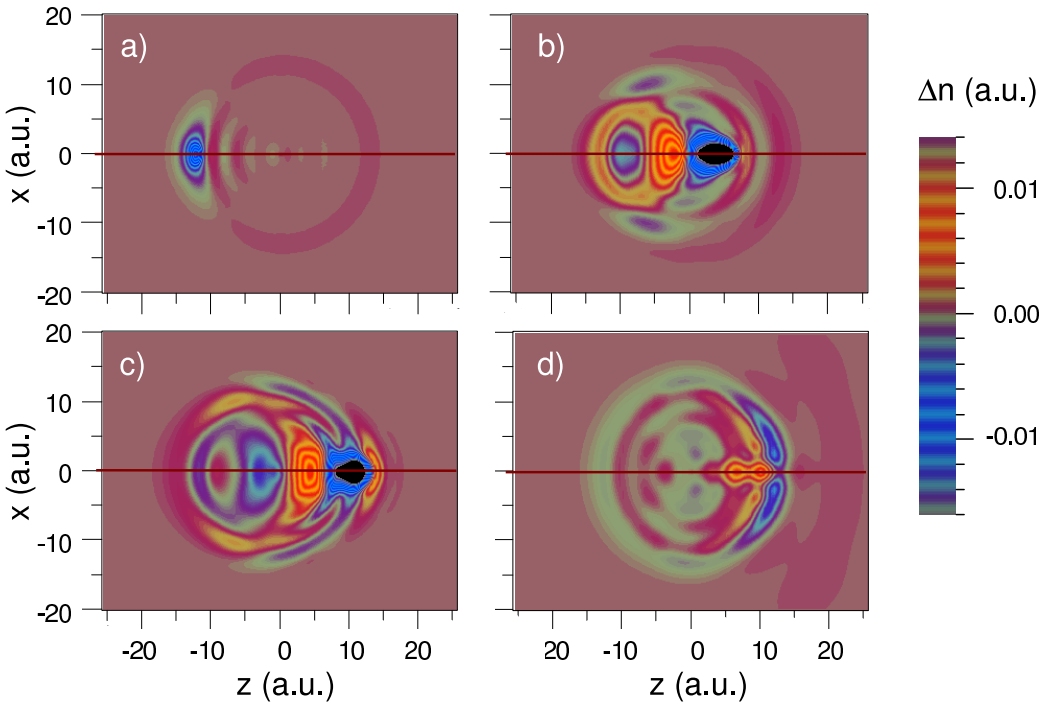

Figure 6.1: Contour plots for the antiproton-induced change $\Delta n(\mathbf{r}, t)$ in the electron density of the spherical cluster. The cluster parameters are: $r_s = 2$, and $N_e = 254$. Results are shown in the (x, z) plane. The center of the cluster is at $(0, 0)$. The projectile trajectory is shown as a horizontal line in each plot. The projectile velocity is $v = 1.5$. Plots a) to d) correspond to antiproton positions z = -12.7, 5.8, 12.6, and 42.5. Color codes are shown at the right side of the figure.

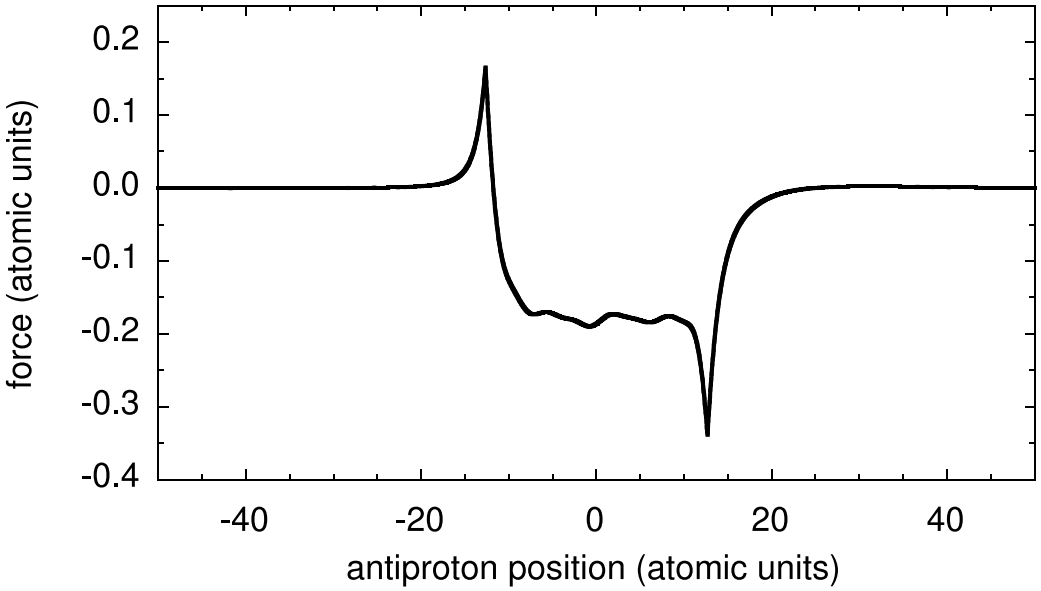

Figure 6.2: Force on an antiproton moving with $v = 1.5$ as a function of its position with respect to the center of the cluster. The cluster parameters are: $r_s = 2$, $N_e = 254$, and $R_{cl} = 12.7$.

cluster, F_z shows minor oscillations around a constant (mean) value.

The energy lost by the projectile during the collision is given by:

$$\Delta E \;=\; v \int_{-\infty}^{\infty} F_z(t) dt. \tag{6.2}$$

We have explicitly checked that $|\Delta E|$ calculated from Eq. 6.2 corresponds to the increase of the total energy of the cluster. However, the magnitude we are interested in is the effective stopping power inside the cluster S. For this purpose, we define S as the ratio of the energy loss to the trajectory length inside the cluster, i.e., the diameter of the cluster: $S = \Delta E/(2R_{\rm cl})$.

Figure 6.3 shows S as a function of projectile speed for antiprotons colliding with clusters of $r_s = 2.07$ and size ranging from $N_e = 18$ ($R_{\rm cl} = 5.42$) to $N_e = 556$ ($R_{\rm cl} = 17.02$). The valence electrons of bulk Al can be well represented by this value of r_s. Size effects are only significant for the two smallest clusters considered ($N_e = 18$ and $N_e = 58$). For the largest ones, the results merge roughly into a universal curve. We estimate that deviations from this universal behavior for larger clusters amount to a maximum of

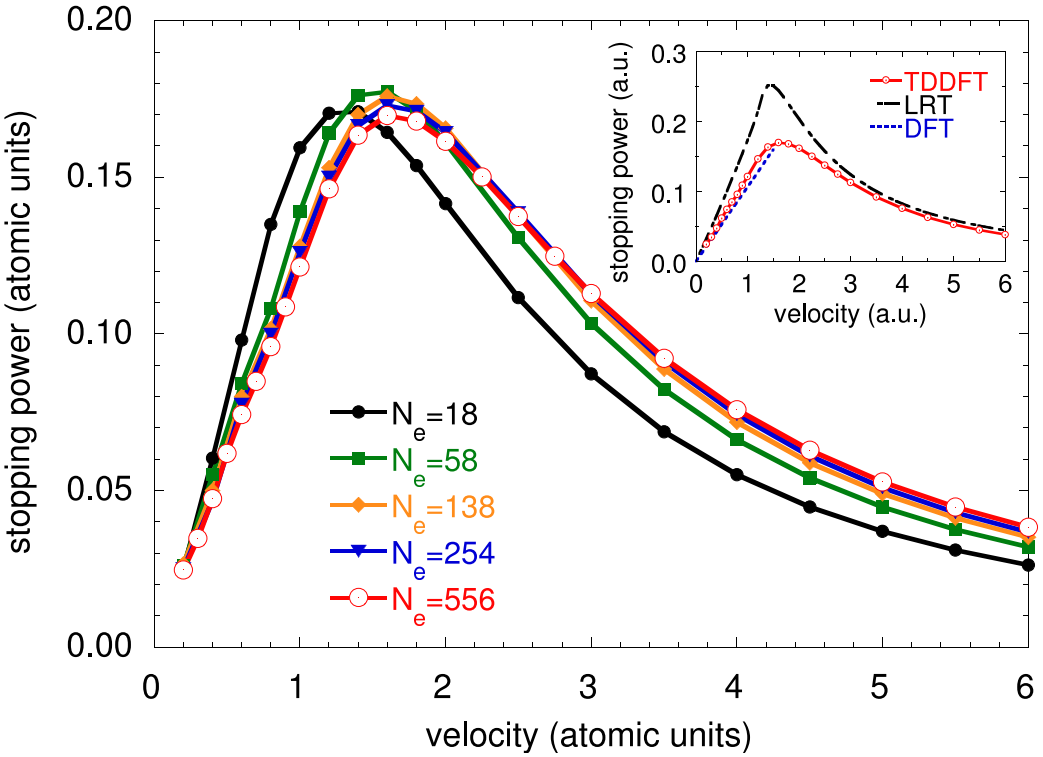

Figure 6.3: Stopping power S of antiprotons moving inside clusters with $r_s = 2.07$ and of different sizes (see legend), as a function of velocity. Lines are drawn to guide the eye. The inset compares the $N_e = 556$ results with those of LRT and DFT.

$\approx 5\%$. The similarity of the results for different clusters reflects important features of the dynamics of the interaction within the studied velocity range: (i) The contributions to ΔE from the ingoing and outgoing trajectory paths, as well as from the surface region, are small. Most of the energy loss is suffered while moving inside the cluster. (ii) The size independence suggests that the dynamic screening within the cluster is essentially that for a homogeneous system in the velocity range considered. This implies that the discreteness of electronic states in the cluster does not play an important role in the screening process.

The independence of the value of S on the cluster size allows us to consider S as representative of the stopping power in an infinite free electron gas with the same electron density parameter r_s. In the inset of Fig. 6.3,

we compare our TDDFT results with other theoretical approximations for the infinite system, which are known to be accurate under more restricted conditions. The LRT result provides the high velocity limit. It is obtained using a Mermin linear response function [26] with an empirical damping factor of $\gamma = 1.35$ eV. The DFT result [2] assumes a linear dependence of S on v, and provides the low-velocity limit. Both the low-velocity limit and the high-velocity limit for the infinite system are well-described by our calculation.

In Fig. 6.4, we compare our TDDFT results for the $N_e = 556$ cluster with experimental measurements recently reported for bulk Al [18, 19, 20]. The TDDFT results quantitatively agree with the experimental data, up to velocities beyond the stopping power maximum. Deviations arise at $v \approx 1.8$, when the excitation of the Al inner-shell electrons starts to contribute to the projectile energy loss. This channel is not included in our calculation. For low-velocity projectiles, our results show a linear dependence of S on v, roughly up to the maximum in S: deviations from the linear dependence are smaller than 6% for velocities $v < 1.4$.

The description of the interaction between negatively charged atomic particles and metals is simplified by the absence of charge exchange. For positive ions, and particularly for velocities lower than v_F, electron capture and loss processes come into play. In order to test the accuracy of the TDDFT-ALDA model for positive ions, we have performed additional calculations for the stopping of Al for protons ($Q = +1$). The procedure is identical to that used for antiproton projectiles. The results are shown in Fig. 6.4. They are compared with recent experimental measurements [19, 20]. Reference tabulations of stopping ranges in solids are shown as well [27, 28, 29]. The agreement is good up to the velocity for which the excitation of the Al inner-shells starts to contribute. According to our TDDFT result, the difference between the stopping power for protons and that for antiprotons due to the excitation of the Al valence band is small ($< 10\%$) for $v \geq 3$, suggesting a small valence Barkas effect.

6.4 Summary and Conclusions

In summary, we conclude that finite sized systems can be used to study the energy loss of charged projectiles moving inside metallic solids. The local character of the interaction makes it possible to define an effective stopping power that is shown to be comparable to that of an infinite target.

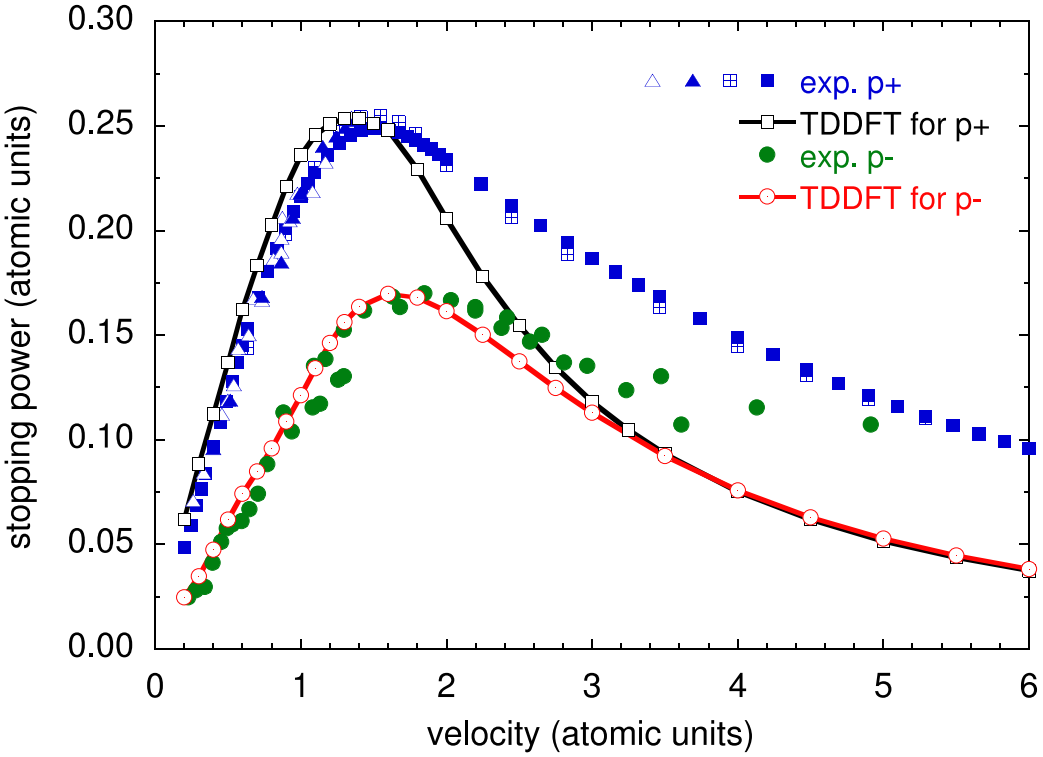

Figure 6.4: TDDFT calculation of the stopping power S of Al ($r_s = 2.07$) for protons (black empty squares) and antiprotons (red empty circles) as a function of projectile velocity. Experimental results for antiprotons (green filled circles [18, 19, 20]) and protons (blue filled and empty triangles [20]), as well as tabulated stopping powers for protons (blue crossed [27] and filled [28, 29] squares) are also shown.

The specific example of the free-electron metal is treated here, but the methodology developed in the present work is general. It can be applied to any material for which the electronic structure can be well characterized within a DFT framework. Further studies should be made to investigate whether our conclusions are also applicable to semiconductors and insulators, where the adiabatic approximation for correlations may also have limitations [30].

Furthermore, we have shown that TDDFT is a promising approach for the calculation of the mean energy loss of point-charges in matter. It is a quantal, non-perturbative method, which is able to describe projectile/target energy transfer over a wide range of projectile velocities. The support for this statement is twofold: (a) Our TDDFT calculations reproduce stopping powers in the well-known limits of low- and high-velocity projectiles, and (b) they quantitatively agree with recent data for the stopping power of Al for protons and antiprotons. The agreement in the case of protons is particulary interesting and worthy of more detailed analysis, as it suggests that charge transfer processes are reasonably well described within the ALDA.

References

[1] P. M. Echenique, R. M. Nieminen, and R. H. Ritchie, Solid State Commun. **37**, 779 (1981).

[2] I. Nagy, A. Arnau, P. M. Echenique, and E. Zaremba, Phys. Rev. B **40**, R11983 (1989).

[3] A. H. Sørensen, Nucl. Instrum. Methods B **48**, 10 (1990).

[4] A. Narmänn, R. Monreal, P. M. Echenique, F. Flores, W. Heiland, and S. Schubert, Phys. Rev. Lett. **64**, 1601 (1990).

[5] A. Salin, A. Arnau, P. M. Echenique, and E. Zaremba, Phys. Rev. B **59**, 2537 (1999).

[6] I. Nagy and B. Apagyi, Phys. Rev. A **58**, R1653 (1998).

[7] N. R. Arista and A. F. Lifschitz, Phys. Rev. A **59**, 2719 (1999).

[8] J. M. Pitarke, R. H. Ritchie, and P. M. Echenique, Phys. Rev. B **52**, 13883 (1995).

[9] P. Sigmund and A. Schinner, Eur. Phys. J. D **12**, 425 (2000).

[10] F. Grüner, F. Bell, W. Assmann, and M. Schubert, Phys. Rev. Lett. **93**, 213201 (2004).

[11] K. Yabana, T. Tazawa, Y. Abe, and P. Bozek, Phys. Rev. A **57**, R3165 (1998).

[12] U. Saalmann and R. Schmidt, Phys. Rev. Lett. **80**, 3213 (1998); T. Kunert and R. Schmidt, Phys. Rev. Lett. **86**, 5258 (2001).

[13] R. Baer and N. Siam, J. Chem. Phys. **121**, 6341 (2004).

[14] T.A. Niehaus, D. Heringer, B. Torralva, and Th. Frauenheim Eur. Phys. J. D **35**, 467 (2005).

[15] A. G. Borisov, J. I. Juaristi, R. Díez Muiño, D. Sánchez-Portal, and P. M. Echenique, Phys. Rev. A **73**, 012901 (2006).

[16] M. Lindenblatt, E. Pehlke, A. Duvenbeck, B. Rethfeld, and A. Wucher, Nucl. Instrum. Methods B **246**, 333 (2006).

[17] E. Fermi and E. Teller, Phys. Rev. **72**, 399 (1947).

[18] S. P. Møller, E. Uggerhøj, H. Bluhme, H. Knudsen, U. Mikkelsen, K. Paludan, and E. Morenzoni, Phys. Rev. A **56**, 2930 (1997).

[19] S. P. Møller, A. Csete, T. Ichioka, H. Knudsen, U. I. Uggerhøj, and H. H. Andersen, Phys. Rev. Lett. **88**, 193201 (2002).

[20] S. P. Møller, A. Csete, T. Ichioka, H. Knudsen, U. I. Uggerhøj, and H. H. Andersen, Phys. Rev. Lett. **93**, 042502 (2004).

[21] O. Gunnarson and B. I. Lundqvist, Phys. Rev. B **13**, 4274 (1976).

[22] A. Borisov, D. Sánchez-Portal, R. Díez Muiño, and P. M. Echenique, Chem. Phys. Lett. **387**, 95 (2004).

[23] R.Kosloff, J.Phys.Chem. **92**, 2087 (1988).

[24] M. D. Feit and J. A. Fleck, Jr., J. Chem. Phys. **78**, 301 (1982);

[25] J. Neufeld and R. H. Ritchie, Phys. Rev. **98**, 1632 (1955).

[26] N. D. Mermin, Phys. Rev. B **1**, 2362 (1970).

[27] H. Paul, D. Semrad, and A. Seilinger, Nucl. Instrum. Methods B **61**, 261 (1991).

[28] H. H. Andersen and J. F. Ziegler, *Hydrogen Stopping Powers and Ranges in all Elements* (Pergamon Press, Elmsford NY, 1977).

[29] International Commission on Radiation Units and Measurements, *Stopping Powers and Ranges for Protons and Alpha-Particles, ICRU Report 49* (Bethesda, MD 20814, USA, 1993).

[30] J. Tao and G. Vignale, Phys. Rev. Lett. **97**, 036403 (2006).

7 TDDFT calculation of the energy loss of antiprotons colliding with metallic nanoshells

Abstract

Time-dependent density functional theory is used to study the interaction between antiprotons and metallic nanoshells. The ground state electronic properties of the nanoshell are obtained in the jellium approximation. The energy lost by the antiproton during the collision is calculated and compared to that suffered by antiprotons traveling in metal clusters. The resulting energy loss per unit path length of material in thin nanoshells is larger than the corresponding quantity for clusters. It is shown that the collision process can be interpreted as the antiproton crossing of two nearly bi-dimensional independent metallic systems.

7.1 Introduction

The understanding of phenomena taking place in the interaction of charged projectiles with matter is of paramount importance for fundamental and applied science. Experimental techniques using charges as probes of matter are widely used in research on solids, surfaces, and nanostructures. In general, charged particles penetrating solid media create electronic excitations within the latter. The excitation of the target is accompanied by a loss of projectile kinetic energy and, in some cases, by a change in the internal state of the projectile. As an example one can consider stopping and Auger neutralization of ions colliding with metallic targets. The complexity of the dynamic interaction between charges and solids has made it difficult to apply theoretical schemes at the same level of accuracy already achieved in other condensed matter problems. Indeed, a detailed description of electronic excitations, dynamic screening, and possible charge transfer processes is required [1, 2, 3, 4]. This is a formidable task particularly under non-perturbative conditions, when the modification of the electronic density induced by the external time-dependent perturbation cannot be considered as small.

Time-dependent density functional theory (TDDFT) has been shown to be a successful tool to face up such strong perturbations. In the time domain, TDDFT has been used to study the dynamic screening of charges in finite-size systems [5, 6] and the absorption properties of complex metallic nanostructures [7]. It has been applied to the calculation of the energy transfer between atomic particles and small gas-phase clusters [8, 9, 10, 11, 12, 13, 14]. Finite-sized bi-dimensional targets [15] and bulk insulators [16] have been addressed as well . In a different context, the contribution of electron-hole pair excitations to energy dissipation during adsorption processes at metal surfaces is currently under strong debate [17, 18, 19, 20] and TDDFT may offer new insights into the problem. For instance, Lindenblatt *et al.* have used TDDFT to estimate the electron-hole pair excitation during the chemisorption of hydrogen atoms on an Al(111) surface [21, 22, 23].

In the particular case of the interaction of protons and antiprotons with metal clusters, it was recently shown that the effective energy loss per unit path length inside the cluster is nearly independent of the cluster size over a wide range of projectile velocities [13]. The quantity so calculated can thus be linked to the stopping power of an infinite system. The main reasons for the

size independence are minimal surface effects and the local character of the interaction. On the characteristic time scales of the collision the information from the cluster boundaries does not reach the projectile and the cluster essentially appears as a homogeneous system. Whether these features are general and can be extended to other cluster geometries is the subject of this contribution. We present a study of the antiproton interaction with spherical hollow clusters, described within the jellium approximation. This geometry can qualitatively represent either relatively small systems, such as fullerenes [24], or larger ones, such as nanoshells [25, 26].

We will show in the following that the energy loss per unit path length of antiprotons going through jellium shells of nanometer size is larger than the corresponding quantity in jellium clusters. Confinement effects are much more important in the former case, and this is reflected in the energy loss suffered by the incident particle. For the nanoshell dimensions considered in this study, the process resembles the collision of an antiproton with two independent nearly bi-dimensional metallic systems. Details about the calculation procedure are presented in Section 7.2, the results are shown and discussed in Section 7.3, and we finish with a summary and some concluding remarks in Section 8.

Atomic units will be used throughout the article unless specifically indicated.

7.2 Theory

7.2.1 Calculation of the ground state of a metallic nanoshell

We use a jellium model to represent a spherical metallic nanoshell. In this model, the core ions are substituted by a uniform background of positive charge with density defined by

$$n_0^+(\mathbf{r}) = n_0\theta(r - R_{\text{int}})\theta(R_{\text{ext}} - r), \tag{7.1}$$

where R_{int} and R_{ext} denote the nanoshell internal and external radius respectively, $\theta(x)$ is the Heaviside function, and n_0 is given by the average screening radius r_s ($1/n_0 = 4\pi r_s^3/3$). The system is filled with a given number of electrons $N = (R_{ext}^3 - R_{int}^3)/r_s^3$ so that total neutrality is preserved.

The electronic density $n(\mathbf{r})$ of the nanoshell is calculated by means of

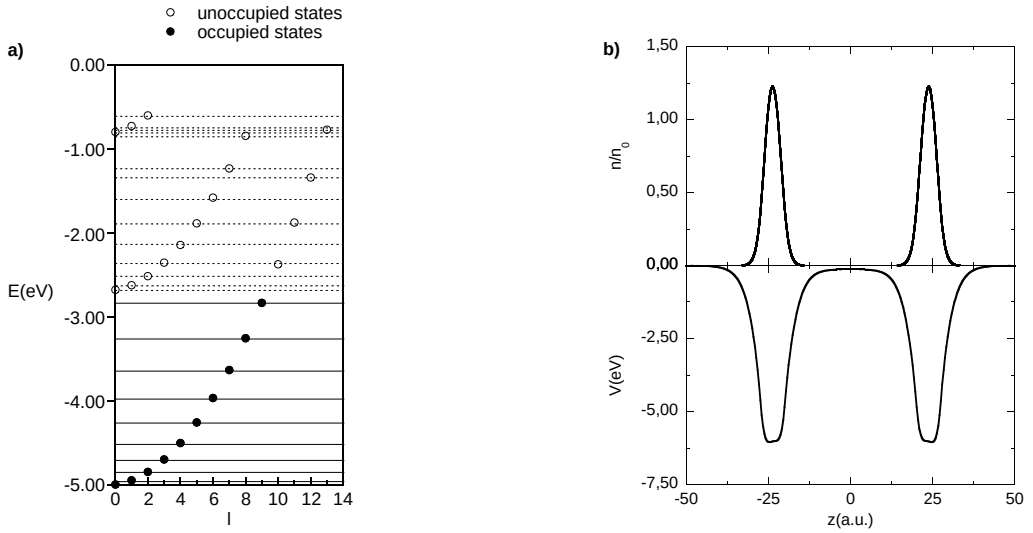

Figure 7.1: Ground state of a nanoshell with $r_s = 4$, $N = 200$ and $R_{int} = 20$ ($R_{ext} = 27.50$) a) One-electron energy levels plotted as a function of the angular momentum b) Electronic density and effective potential.

density functional theory (DFT), solving the Kohn-Sham (KS) equations:

$$\left\{-\frac{1}{2}\Delta + V_{\rm eff}([n],\mathbf{r})\right\}\psi_j(\mathbf{r}) \;=\; \varepsilon_j\psi_j(\mathbf{r}) \tag{7.2}$$

$$V_{\rm eff}([n],\mathbf{r}) \;=\; V_+(\mathbf{r}) + V_{\rm H}([n],\mathbf{r}) + V_{\rm xc}([n],\mathbf{r}) \tag{7.3}$$

which give the one-electron KS wave functions $\psi_j(\mathbf{r})$ and energy levels ε_j. Here, $V_+(\mathbf{r})$ and $V_{\rm H}([n],\mathbf{r})$ are the electrostatic potentials created by the positive background and the electronic density respectively (H stands for Hartree potential). $V_{\rm xc}([n],\mathbf{r})$ is the exchange-correlation potential, calculated in the local density approximation (LDA) with the parametrization of Ref.[27]. The electronic density $n(\mathbf{r})$ is given by the sum over occupied wave functions

$$n(\mathbf{r}) \;=\; \sum_{j\in occ.} |\psi_j(\mathbf{r})|^2. \tag{7.4}$$

The electronic wave functions $\psi_j(\mathbf{r})$ are expanded in the spherical harmonic basis and a mesh of equidistant points is used for the radial coordinate. For each value of the angular momentum l, the KS equations

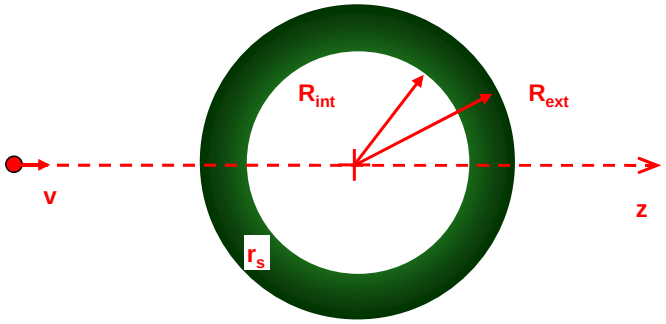

Figure 7.2: Schematic view of the collision process showing the coordinates and parameters which come into play

are solved by direct diagonalization of the Fourier Grid Hamiltonian (FGH) matrix [28]. Figure 7.1a) shows the calculated energy levels in the case of a nanoshell with $N = 200$ electrons, $r_s = 4$, $R_{int} = 20$ and $R_{ext} = 27.50$. They are labeled in terms of their angular momentum l and energy ε_j. Each level fits $2(2l + 1)$ electrons. Observe the formation of three bands with parabolic dispersion on l. These bands originate from three quantized states corresponding to the electron confinement in the radial direction between external and internal nanoshell radii. The parabolic dispersion with l reflects the link between the angular momentum l and the free electron momentum k for the motion inside a layer of finite thickness $L = R_{\rm ext} - R_{\rm int}$ (the limit of the nanoshell for fixed L and $R_{\rm int} \to \infty$). The converged effective potential $V_{\rm eff}$ and the normalized electronic density n/n_0 are plotted in Fig. 7.1b) along the z axis in a coordinate system with the origin at the geometrical center of the system (see Fig. 7.2).

7.2.2 TDFFT description of the collision process of antiprotons with metallic nanoshells

The present study is restricted to collision processes where an antiproton follows a trajectory which goes through the geometrical center of the nanoshell. Such a geometry allows one to strongly reduce the computational effort because of the cylindrical symmetry of the problem. As shown in Fig. 7.2, the coordinate system is chosen such that the z axis is along the projectile trajectory $Z(t) = -Z_{ini} + vt$. v is the projectile velocity. The initial distance Z_{ini} is set large enough so that the electron density obtained

from static DFT is unperturbed in the beginning of the collision. The time evolution of the electron density in response to the field of the moving projectile $n(\mathbf{r},t)$ is calculated within the KS scheme of TDDFT:

$$i\frac{\partial\psi_j(\mathbf{r},t)}{\partial t} \;=\; \left\{-\frac{1}{2}\Delta + V_{\rm eff}([n],\mathbf{r},t) + V_{\rm ext}(t)\right\}\psi_j(\mathbf{r},t)\;, \qquad (7.5)$$

The effective KS potential $V_{\rm eff}$ is treated within standard adiabatic local density approximation (ALDA) with the exchange-correlation functional of Ref. [27]. $V_{\rm eff}$ is time-dependent through the time dependence of the electron density $n(\mathbf{r},t) = \sum_{j\in occ.} |\psi_j(\mathbf{r},t)|^2$. $V_{\rm ext}$ is the Coulomb potential created by the moving antiproton. The initial conditions for the KS wave functions $\psi_j(\mathbf{r},t=0) = \psi_j(\mathbf{r})$ correspond to the ground state KS wave functions obtained from Eq.(7.2).

The KS wave functions are represented on a discrete mesh in spherical coordinates $\mathbf{r} = (r,\theta,\varphi)$. Because of the symmetry, the projection m of the angular momentum on the quantization axis is preserved in due course of the collision. Thus, the time dependent KS wave functions are calculated in the form $\psi_j(\mathbf{r},t) \to \psi_{jm}(r,\theta,t)$. The time evolution is obtained via short-time split-operator propagation [29], where the action of the kinetic energy operator is calculated in two steps: (1) projection on the spherical harmonics basis (we use Gaussian quadrature with corresponding mesh in θ coordinate); (2) FGH method for the radial part (we use equidistant mesh in r coordinate).

The only nonzero component of the Coulomb force acting on the antiproton during the collision process is along the projectile trajectory:

$$F_z(t) \;=\; -\int d^3\mathbf{r}'\;\frac{\left[n_0^+(\mathbf{r}') - n(\mathbf{r}',t)\right]}{\left|\hat{\mathbf{e}}_\mathbf{z}Z(t) - \mathbf{r}'\right|^3}\;[Z(t)-z'], \qquad (7.6)$$

where $\hat{\mathbf{e}}_\mathbf{z}$ is the unit length vector in z-direction.

The energy lost by the projectile during the collision is given by:

$$E_{loss} \;=\; v\int_0^\infty F_z(t)dt. \qquad (7.7)$$

In TDDFT, the total energy of the nanoshell in the presence of the antiproton $E(t)$ can be obtained at any time. The energy change during the collision is given by: $\Delta E(t) = E(t) - E(t=0)$, where $E(t=0)$ is the total energy of the nanoshell in its ground state. $\Delta E(t\to\infty)$ corresponds to the increase of the

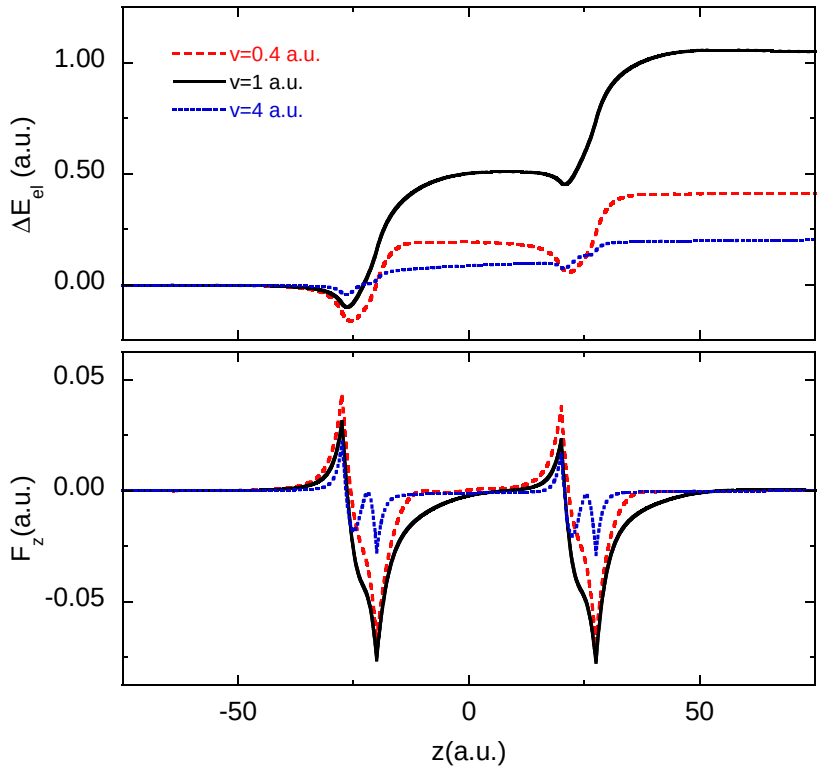

Figure 7.3: Electronic energy change in the nanoshell and force on the projectile for several collision processes. The nanoshell parameters are $r_s = 4$, $N = 200$, $R_{int} = 20$ and $R_{ext} = 27.50$.

electronic energy of the nanoshell at the end of the collision. One can show that it exactly equals to the energy loss calculated from Eq. 7.7. We have explicitly checked from our calculations that the two values are in agreement.

7.3 Results and Discussion

In this section, results of the calculation of the energy loss for several collision processes are reported for two nanoshells with different electron density parameters, $r_s = 2$ and 4.

Figure 7.3 shows the details of the collision process of an antiproton with a nanoshell characterized by $r_s = 4$ (corresponding to the density parameter of sodium), $N = 200$, $R_{int} = 20$ and $R_{ext} = 27.50$. Data for three different projectile velocities: $v = 0.4$, 1 and 4 a.u. are presented. The upper panel

of Fig. 7.3 shows the change in the total energy of the nanoshell during the collision process. The lower panel shows the force on the projectile along its trajectory. Figure 7.3 illustrates that the collision process takes place in two distinct steps. These correspond to the first and second crossing of the nanoshell by the projectile, and are very similar one to another. The energy rises approximately by the same amount in both steps, and the force has the same features. Thus the curvature of the surfaces of the nanoshell and the fact that they form a closed object is not important, at least for the sake of the energy loss calculation. This suggests that the collision process can be similar to that of an antiproton with two independent slabs of thickness $L = R_{ext} - R_{int}$.

Figure 7.3 also gives details on the screening process during the collision. When the antiproton is approaching the nanoshell surface, the attractive polarization lowers the total energy. The polarization force in each of the collision steps is not symmetric for the 'in' and 'out' trajectory paths, due to the electronic excitations left behind. This feature is most appreciable for the maximum energy loss velocity (see Fig. 7.3), for which the asymmetry on the force contributes to the total energy loss as much as the trajectory path inside the material. The screening inside the material also depends on the projectile velocity. For the highest velocity, the oscillations visible in the force give account for the interference effects due to the slower (as compared to the projectile) rearrangement of the electrons inside the material. For the lower velocities, the screening hole has time to be created [5], [13] and the oscillating features disappear.

Figure 7.4 shows the antiproton energy loss per unit path length within the nanoshell $E_{loss}/2L$ as a function of projectile velocity. Two systems have been studied. Figure 7.4a) shows the results of the calculations for the sodium nanoshell ($N = 200$, $r_s = 4$, $R_{int} = 20$ and $R_{ext} = 27.50$), and Fig. 7.4b) shows the ones corresponding to the case of a denser system ($N = 180$, $r_s = 2$, $R_{int} = 10$ and $R_{ext} = 13.5$). The present results are compared to previously reported theoretical data obtained for antiprotons colliding with spherical jellium clusters [13]. The maximum energy loss corresponds to the same projectile speed in the two systems. However, the energy loss per unit path length is larger for nanoshells than for clusters. For the nanoshells considered in this study, the asymmetry of the force outside the material provides a contribution to the total energy loss much larger than the corresponding contribution in the cluster case. In this respect, the energy loss process for thin nanoshells resembles more the collision of

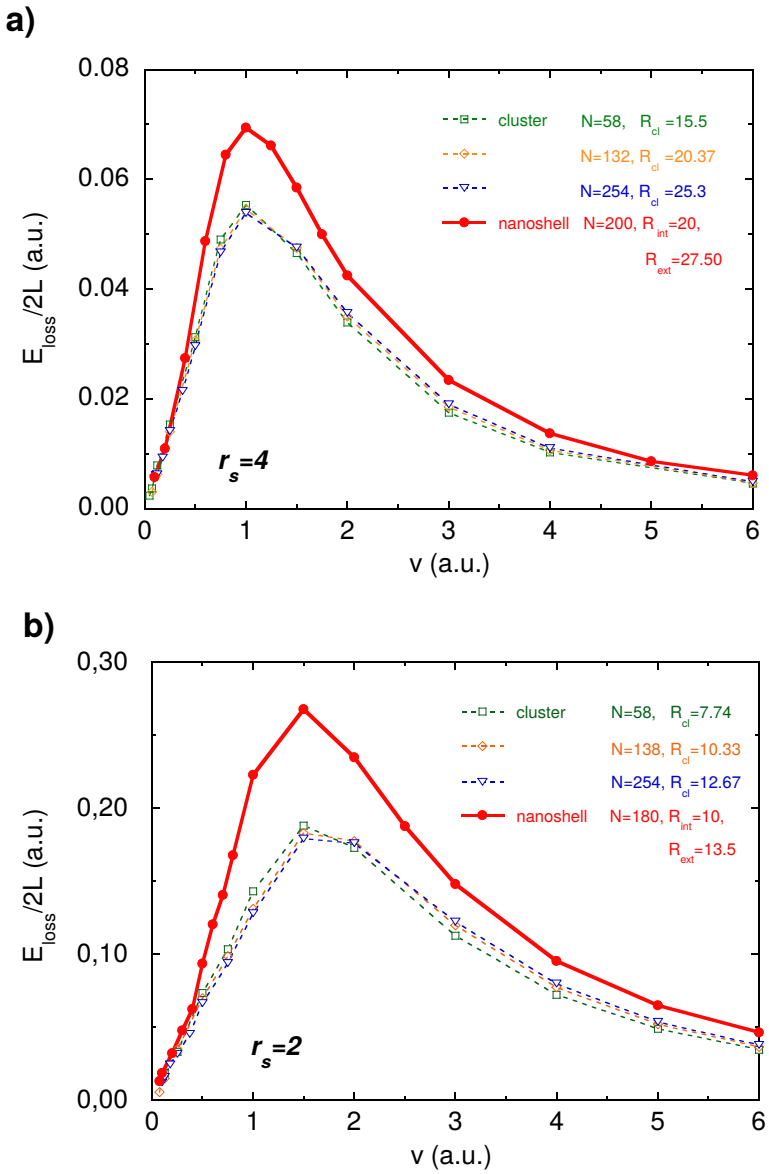

Figure 7.4: Energy loss per unit path length within the nanoshell as a function of projectile speed for collision processes of an antiproton with nanoshells of parameters a) $r_s = 4$, $N = 200$, $R_{int} = 20$ and $R_{ext} = 27.50$, and b) $r_s = 2$, $N = 180$, $R_{int} = 10$ and $R_{ext} = 13.5$. Lines are drawn to guide the eye. The results of the TDDFT calculation for clusters of several sizes and $r_s = 4$ are also shown for comparison.

two consecutive bi-dimensional systems [15]. In antiproton collisions with confined 2D systems, the energy loss comes out only from the asymmetry on the force and not from a dynamical screening process inside the material, as in the 3D case. This makes that, when dividing the total energy loss E_{loss} by the total path length inside the material of the nanoshell $2L$, the result does not give something assimilable to a stopping power as in the case of clusters. Moreover, for a thin nanoshell the energy difference between the quantized states corresponding to the electron motion in the radial direction is large (See Fig.7.1a)). Then, primarily the angular motion is excited with an electron moving parallel to the surface of the nanoshell. This feature further supports the analogy to the bi-dimensional case.

7.4 Conclusions

In this study, TDDFT has been used to calculate the energy loss of antiprotons colliding with thin metal jellium nanoshells of different electronic density parameters. The results show that the calculated energy loss per unit path length inside the material is higher than the corresponding quantity for antiproton collisions with jellium clusters. For thin nanoshells, the process resembles the collision of an antiproton with two independent nearly bi-dimensional metallic systems. The contribution to the energy loss coming from the asymmetry of the force, which is the only one appearing in 2D systems, has an important weight to the total energy loss inside the material. This is the main reason for the difference in the energy loss between thin nanoshells and spherical clusters.

References

[1] A. Närmann, R. Monreal, P. M. Echenique, F. Flores, W. Heiland, and S. Schubert, Phys. Rev. Lett. **64**, 1601 (1990).

[2] T. L. Ferrell and R. H. Ritchie, Phys. Rev. B **16**, 115 (1977).

[3] P. M. Echenique, I. Nagy, and A. Arnau, Int. J. of Quant. Chem. **23**, 121 (1989).

[4] J. I. Juaristi, A. Arnau, P. M. Echenique, C. Auth, and H. Winter, Phys. Rev. Lett. **82**, 1048 (1999).

[5] A. G. Borisov, D. Sánchez-Portal, R. Díez Muiño, and P. M. Echenique, Chem. Phys. Lett. **387**, 95 (2004).

[6] A. G. Borisov, D. Sánchez-Portal, R. Díez Muiño, and P. M. Echenique, Chem. Phys. Lett. **393**, 132 (2004).

[7] R. Baer, D. Neuhauser, and S. Weiss, Nano Lett. **4**, 85 (2004).

[8] K. Yabana, T. Tazawa, Y. Abe, and P. Bozek, Phys. Rev. A **57**, R3165 (1998).

[9] U. Saalmann and R. Schmidt, Phys. Rev. Lett. **80**, 3213 (1998).

[10] T. Kunert and R. Schmidt, Phys. Rev. Lett. **86**, 5258 (2001).

[11] R. Baer and N. Siam, J. Chem. Phys. **121**, 6341 (2004).

[12] T.A. Niehaus, D. Heringer, B. Torralva, and Th. Frauenheim Eur. Phys. J. D **35**, 467 (2005).

[13] M. Quijada, A. G. Borisov, I. Nagy, R. Díez Muiño, and P. M. Echenique, Phys. Rev. A **75**, 042902 (2007).

[14] A. V. Krasheninnikov, Y. Miyamoto, and D. Tománek, Phys. Rev. Lett. **99**, 016104 (2007).

[15] A. G. Borisov, J. I. Juaristi, R. Díez Muiño, D. Sánchez-Portal, and P. M. Echenique, Phys. Rev. A **73**, 012901 (2006).

[16] J. M. Pruneda, D. Sánchez-Portal, A. Arnau, J. I. Juaristi, and Emilio Artacho, Phys. Rev. Lett **99**, 235501 (2007).

[17] R. Díez Muiño and A. Salin, Phys. Rev. B **62**, 5207 (2000).

[18] J. D. White, J. Chen, D. Matsiev, D. J. Auerbach, and A. M. Wodtke, Nature **433**, 503 (2005).

[19] P. Nieto, E. Pijper, D. Barredo, G. Laurent, R. A. Olsen, E. J. Baerends, G. J. Kroes, and D. Farias, Science **312**, 86 (2006).

[20] C. Díaz, J. K. Vincent, G. P. Krishnamohan, R. A. Olsen, G. J. Kroes, K. Honkala and J. K. Nørskov, J. Chem. Phys. **125**, 114706 (2006).

[21] M. Lindenblatt, E. Pehlke, A. Duvenbeck, B. Rethfeld, and A. Wucher, Nucl. Instrum. Methods B **246**, 333 (2006).

[22] M. Lindenblatt, J. van Heys, and E. Pehlke, Surf. Sci. **600**, 3624 (2006).

[23] M. Lindenblatt and E. Pehlke, Surf. Sci. **600**, 5068 (2006).

[24] M. J. Puska and R. M. Nieminen, Phys. Rev. A **47**, 1181 (1993).

[25] E. Prodan and P. Nordlander, Chem. Phys. Lett. **349**, 153 (2001).

[26] E. Prodan and P. Nordlander, Chem. Phys. Lett. **3529**, 140 (2002).

[27] O. Gunnarson and B. I. Lundqvist, Phys. Rev. B **13**, 4274 (1976).

[28] R.Kosloff, J.Phys.Chem. **92**, 2087 (1988).

[29] M. D. Feit and J. A. Fleck, Jr., J. Chem. Phys. **78**, 301 (1982).

8 Conclusions

Electron dynamics is a topic of interest in many different areas of physics and chemistry, ranging from the interpretation of different characterization techniques to the control of photoinduced chemical processes. The design and control of nanoscale systems achieved in the last decades has triggered the necessity to tackle the study of electron dynamics in nanoparticles. This thesis covers two main topics in this respect, namely the study of the decay of electronic excitations and the collision processes of charges with nanoparticles.

Despite its simplicity, the spherical jellium model used throughout this work has allowed to obtain meaningful results. It is worth remarking here as well the broad spectrum of methodologies used in this work to approach the complicated problem of many-body physics: on one hand, linear response theory, which can also be considered as a first order approximation in TDDFT, has been involved in the calculation of lifetimes. On the other, fully non-perturbative time-dependend density functional theory has been employed to follow the time-evolution of excited states. In addition to that the GW approximation has been used for the calculation of lifetimes.

Chapter 4 presents a first study of the decay of electronic excitations in clusters within linear response theory and the GW approximation. The study is focused on the calculation of the lifetime of electronic excitations of $\approx$ 1 eV energy above the Fermi level in jellium clusters of increasing size. Sodium clusters ($r_s = 4$) are used as paradigmatic systems to approach for the first time the study of size effects in electronic properties of metal nanoparticles. For clusters smaller than 1.5 nm, strong oscillations are found when representing the lifetimes as a function of the system size. Lifetimes in this size scale vary between $\tau \approx 4$ and $\tau \approx 30$ femtoseconds. This non-monotonic behaviour is a consequence of the discrete spectrum of levels. For clusters with radius $R \gtrsim 2$ nm, these effects are smoother, and the excitation lifetimes show minor oscillations around $\tau \approx 5$ femtoseconds. The order of magnitude of the calculated lifetime is consistent with that of electronic excitations in a homogeneous electron gas with the same characteristics. However, its numerical value is significantly smaller. A subtle interplay between screening and the space localization of the initial excitation is foreseen to be responsible of this difference.

This question is further developed in Chapter 5. Here, the lifetimes of electronic excitations in metal clusters of different materials are calculated

for several excitation energies. The order of magnitude of the calculated lifetimes is confirmed to be on the femtosecond scale. However, its numerical value is still substantially smaller than the one corresponding to bulk metals. With the aid of TDDFT, we show that the Kohn-Sham one-electron wave functions are suitable to represent initial states of electronic excitations. As predicted in Chapter 4, these wave functions have a significant weight in the region close to the nanoparticle surface. In this region, dynamic screening is largely reduced, and the lifetime of the electronic excitations is subsequently shortened. Finite-size effects thus play a major role in the decay process of excited electrons in metal nanoparticles. Additionally, we observe a quasi-linear behaviour in the the lifetime as a function of the excitation energy. The well-known quadratic dependence of the decay rate on the excitation energy in a free electron gas $\Gamma \propto (\varepsilon - \varepsilon_F)^2$ thus breaks down in metal nanoparticles. This quasi-linear behaviour has been also predicted in other low-dimensional systems , and would require experimental evidence to be confirmed.

The second main topic addressed in this thesis is the study of the collision processes of charged projectiles with metallic nanoparticles. Calculations have been made both for protons and antiprotons colliding with aluminium clusters of different size. Due to the non-perturbative character of the external potential, a fully time dependent density functional approach is used. As a result, we find out that the screening around the projectiles is rapidly built, resulting in an interaction with the target electrons in the collision process which is quite local. The local character of the interaction makes it possible to define an effective stopping power which is shown to be comparable to that of an infinite target. This result has the direct implication that finite sized metallic systems can be used to study the energy loss of charged projectiles inside bulk metals. Our results reproduce calculations of stopping powers in bulk matter in the well-known low and high velocity regimes.

The fully non-perturbative character of our TDDFT approach enables us to calculate the stopping power in the intermediate velocity regime as well. Moreover, our calculated data agree quantitatively with experimental measurements for the stopping power of protons and antiprotons in aluminium. The agreement in the case of protons is particularly interesting and worthy of further analysis, as it suggests that charge transfer processes are reasonably well described within the ALDA. The methodology developed is general and could in principle be applied to any material well described

within DFT framework. Further studies should be made to investigate whether our conclusions are also applicable to semiconductors and insulators, where the adiabatic approximation for correlations may also have limitations.

To further explore the possibilities offered by the non-perturbative TDDFT approach, we have briefly addressed at the end of this PhD. work the study of collision processes with thin metal nanoshells. Our results show that, in such case, the process resembles the collision of an antiproton with two independent nearly bi-dimensional metallic systems. In parallel with it, the main contribution to the energy loss comes from the asymmetry of the force on each path inside the shell.

Finally, it can be concluded from this thesis that nano-sized systems can behave similarly to solids, or intrinsically different, depending on the particular property under study. In the study of lifetimes, the cuasiparticle representing the electronic excitation has a significant weight on the surface of the cluster, yielding results that cannot be compared with bulk materials. In the case of collision processes, the interaction with the traversing charged particle is very local and yields results comparable to those of infinite systems. Thus, it is not possible to determine *a priori* the minimum size of the systems at which confinement effects are no longer significant. Each individual electronic property needs to be studied separately to conclude at what size confinement effects become relevant.

9 Resumen

La dinámica electrónica es un tema de interés en diferentes áreas de la física y la química, tanto a nivel fundamental como aplicado: a nivel fundamental, el estudio de las excitaciones electrónicas constituye toda una rama de la física del estado sólido así como de la física atómica y molecular. En cuanto a sus aplicaciones, éstas abarcan un amplio espectro, desde la interpretación de diferentes técnicas de caracterización de materiales hasta el control de procesos químicos fotoinducidos. Por otra parte, el diseño y control en la fabricación de nanomateriales logrado en las últimas décadas ha propiciado el interés por las propiedades electrónicas de estos sistemas, que a menudo están a caballo entre las de átomos y/o moléculas, y las de materiales macroscópicos.

Un tipo de sistemas a escala nanométrica en auge desde los comienzos de la nanociencia y la nanotecnología son los agregados atómicos, también llamados *clusters* o nanopartículas. Esta tesis aborda el estudio de los efectos de tamaño en dos propiedades fundamentales ligadas a la dinámica electrónica en nanopartículas metálicas: por una parte, el tiempo de vida de excitaciones electrónicas en *clusters* metálicos y por otra, la pérdida de energía de proyectiles cargados en procesos de colisión con nanopartículas metálicas.

Entre los obstáculos para obtener resultados significativos en el estudio de los efectos de tamaño está la necesidad de analizar sistemas de muy diferentes dimensiones dentro de un mismo marco teórico. En este trabajo, se ha utilizado como punto de partida el modelo de *jellium* esférico [1, 2], en el que se sustituye el conjunto de iones positivos por un fondo de densidad de carga positiva constante. Este modelo permite manejar incluso sistemas constituidos por varios miles de átomos, y a pesar de su simplicidad, permite obtener resultados significativos tanto a nivel cualitativo como cuantitativo en propiedades ópticas, dinámica electrónica o plasmónica [3, 4, 5].

En este trabajo, se ha hecho uso de un amplio espectro de metodologías para abordar el complejo problema de la física de muchos cuerpos: para la caracterización del estado fundamental, se ha hecho uso de la teoría del funcional de la densidad (DFT, del inglés "density functional theory"). En el cálculo de los tiempos de vida se ha utilizado teoría de la respuesta lineal y la aproximación GW [6] para estudiar el decaimiento de estados electrónicos excitados. En el cálculo de la pérdida de energía, se ha hecho uso de la teoría del funcional de la densidad dependiente del tiempo (TDDFT, del

inglés "time dependent density functional theory"). En este último caso, cabe destacar que los cálculos se han realizado sin recurrir a la teoría de perturbaciones, a partir de la evolución en tiempo real de los estados excitados monoelectrónicos.

Estudio de los tiempos de vida

El primer problema abordado en esta tesis es el estudio de los tiempos de vida de excitaciones electrónicas en nanopartículas metálicas. Dicho estudio se encuentra recogido en los Capítulos 4 y 5. El Capítulo 4 es un primer estudio del decaimiento de las excitaciones electrónicas en clusters de diferentes tamaños. Dicho estudio se centra en el tiempo de vida de excitaciones electrónicas con energía aproximada $(\varepsilon - \varepsilon_F) \approx 1$ eV por encima del nivel de Fermi. Los cálculos se realizan para nanopartículas de sodio ($r_s = 4$) de radios R entre 0.7 nm y 2.7 nm. Al representar el tiempo de vida de en función del tamaño en clusters con radio menor que 1.5 nm, se observan oscilaciones entre $\tau \approx 4$ fs y $\tau \approx 30$ fs. Este comportamiento se debe a la discretización de los niveles energéticos, que impide asignar un valor idéntico a la energía de excitación para todos los sistemas, además de modificar el espacio de fases al que decae el electrón excitado. Para clusters de radio $R \gtrsim 2$ nm, estos efectos son menos acusados, y los tiempos de vida muestran pequeñas oscilaciones en torno a un valor de $\tau \approx 5$ fs. El orden de magnitud de este valor es consistente con el correspondiente a excitaciones electrónicas en un gas de electrones libres de sodio. Sin embargo, su valor numérico es significativamente menor. Esto sugiere una relación entre el apantallamiento y la localización espacial de la función de onda del estado inicial [7].

La cuestión arriba expuesta se explora en detalle en el Capítulo 5. En él, se calculan los tiempos de vida de excitaciones electrónicas en *clusters* metálicos de diferentes materiales y tamaños, para diferentes energías de excitación. El orden de magnitud de los tiempos de vida calculados es equiparable al de los correspondientes a materiales macroscópicos, pero sus valores numéricos continúan siendo apreciablemente menores. Con la ayuda de la teoría del funcional de la densidad dependiente del tiempo (TDDFT), se observa que las funciones de onda monoelectrónicas de Kohn-Sham representan adecuadamente los estados iniciales de las excitaciones electrónicas. Para ello, se introduce como perturbación externa el potencial creado por un pulso láser de frecuencia coincidente con la de una excitación electrónica determinada, y se observa la evolución temporal

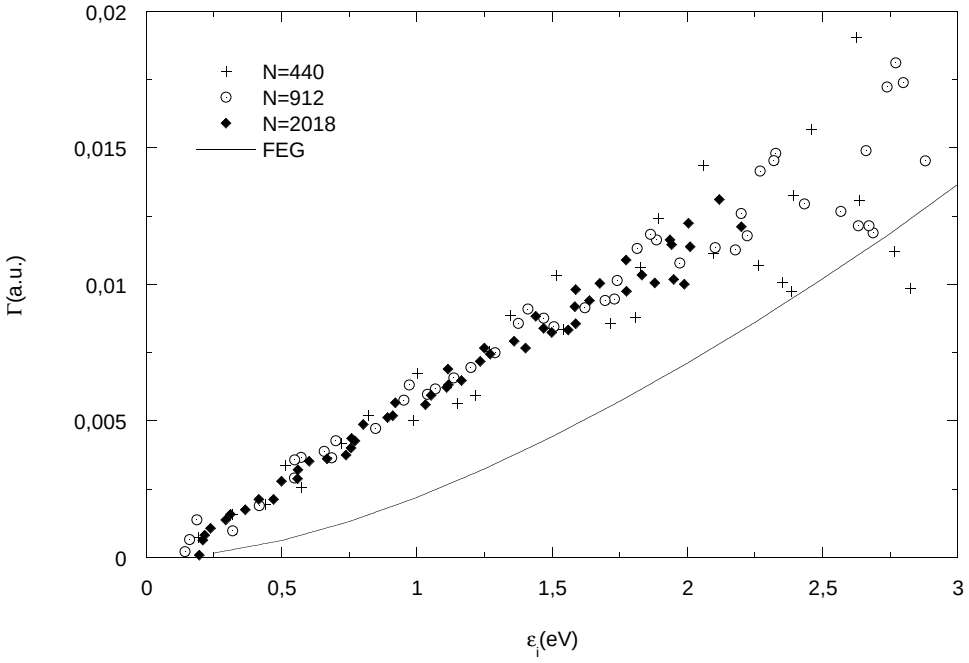

Figure 9.1: Inverso del tiempo de vida $\Gamma = \tau^{-1}$ para excitaciones electrónicas ($r_s = 4$) en nanopartículas de sodio en función de la energía de excitacion ε_i tomando como referencia el nivel de Fermi. Las cruces hacen referencia a nanopartículas con $N = 440$ electrones, los círculos a nanopartículas con $N = 912$ electrones, y los rombos a nanopartículas with $N = 2018$ electrones. La línea sólida muestra los valores de Γ para un gas de electrones libre con parámetro de densidad electrónica $r_s = 4$.

de las funciones de onda monoelectrónicas, obteniendo como resultado que la función de onda correspondiente a la excitación es la que sobrevive al pulso láser.

El resultado es el predicho en el Capítulo 5: las funciones de onda que representan los estados iniciales de las excitaciones electrónicas tienen un peso significativo en la región de la superficie de la nanopartícula. En esta región, el apantallamiento dinámico se reduce de manera considerable, y en consecuencia, el tiempo de vida de las excitaciones eleć tronicas disminuye con respecto al equivalente en un gas de electrones libres. Podemos decir, pues, que los efectos de tamaño juegan un papel importante en el proceso de decaimiento de electrones excitados en nanopartículas metálicas [4].

Otro resultado novedoso sobre la cuestión de los tiempos de vida en

nanopartículas es el siguiente: al representar el inverso del tiempo de vida frente a la energía de excitación se observa un comportamiento cuasilineal, en oposición a la conocida dependencia cuadrática de Quinn-Ferrel $\Gamma \propto (\varepsilon - \varepsilon_F)^2$ para un gas de electrones libres (ver Fig. 9.1). El comportamiento cuasilineal, observado en nanopartículas de diferentes materiales ($r_s = 2$ y $r_s = 4$), ha sido predicho en otros sistemas de baja dimensión como pozos cuánticos en superficies [8], y necesitaría de evidencias experimentales para ser confirmado.

Estudio de procesos de colisión

El segundo problema abordado en esta tesis es el estudio de los procesos de colisión de partículas cargadas con nanopartículas metálicas. Los cálculos se realizan para protones y antiprotones en colisión con *clusters* de aluminio de diferentes tamaños. Debido al carácter no perturbativo del potencial externo, se hace uso del TDDFT no perturbativo para calcular la evolución de las funciones de onda; es decir, sin hacer uso de la aproximación lineal.

Como resultado, se observa que el apantallamiento de los proyectiles se construye rápidamente, resultando en una interacción con los electrones de la nanopartícula de un carácter marcadamente local. Este carácter hace posible definir un poder de frenado efectivo en nanopartículas equiparable al correspondiente a materiales macroscópicos. El resultado tiene como implicación directa la posibilidad de utilizar sistemas metálicos de dimensiones reducidas para estudiar la pérdida de energía por unidad de longitud de proyectiles cargados en materiales macroscópicos [5].

Los resultados obtenidos reproducen los cálculos realizados en un gas de electrones libres con $r_s = 2.07$ (corresponciente al aluminio) en los ya estudiados regímenes de bajas y altas velocidades, mediante la utilización de la teoría del funcional de la densidad (DFT) estática y la teoría de la respuesta lineal respectivamente. Pero además, el carácter no perturbativo de nuestro planteamiento TDDFT nos permite calcular el poder de frenado en el régimen intermedio de velocidades. Los resultados obtenidos para aluminio están en concordancia con medidas experimentales para protones y antiprotones (ver Fig. 9.2). El acuerdo en el caso de protones es especialmente interesante y merecedor de un análisis más detallado, ya que sugiere que los procesos de transferencia de carga se pueden describir adecuadamente mediante la aproximación local adiabática de la densidad (ALDA). La metodología desarrollada es general y podría en principio ser aplicada a cualquier material descrito dentro del marco de la teoría del funcional de la densidad. Se

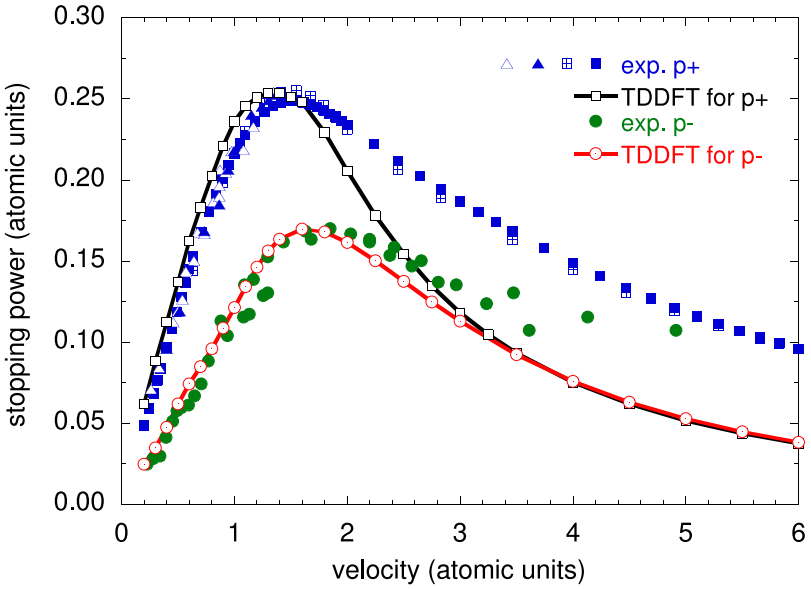

Figure 9.2: Cálculo TDDFT del poder de frenado del aluminio ($r_s = 2.07$) para antiprotones ($p-$) y protones ($p+$) en función de la velocidad de los proyectiles, comparado con resultados experimentales para antiprotones (círculos, exp. $p-$) [9, 10, 11]) y protones (triángulos, exp. $p+$) [11]. Se muestran también valores tabulados para protones (cuadrados, exp. $p+$) [12, 13, 14].

requeriría un estudio más a fondo para investigar si estas conclusiones se pueden aplicar a semiconductores y aislantes, donde la aproximación ALDA para el término de canje y correlación puede tener limitaciones [15].

Con el propósito de explorar las posibilidades ofrecidas por tratamiento no perturbativo de la teoría del funcional de la densidad dependiente del tiempo (TDDFT), al final de este trabajo doctoral se ha abordado el estudio de procesos de colisión de proyectiles cargados con *nanoshells* o nanocáscaras delgadas. En este caso, los resultados muestran que el proceso se asimila a la colisión de un proyectil a través de dos láminas delgadas casi bidimensionales separadas una distancia determinada. Al igual que en el caso de dos sistemas bidimensionales separados, la contribución principal a la pérdida de energía en colisiones con nanocáscaras delgadas proviene de la asimetría de la fuerza en el trayecto de entrada y salida de cada "cáscara" o lámina delgada curvada [16].

Para finalizar, puede extraerse una conclusión general del conjunto de este trabajo doctoral: los sistemas en la escala nanométrica pueden comportarse de manera similar a sólidos o intrínsecamente diferente, dependiendo de la propiedad concreta bajo estudio. Esto se ve reflejado en las dos principales propiedades estudiadas en esta tesis: En el caso de los tiempos de vida, por una parte, la cuasipartícula que representa la excitación electrónica tiene un peso significativo en la superficie del *cluster*, dando lugar a resultados muy distintos a los de un material a escala macroscópica. Por otra parte, en el caso de los procesos de colisión, la interacción del proyectil con la nanopartícula tiene un carácter marcadamente local y da lugar a resultados equiparables a los de un sistema infinito. Así pues, no es posible determinar *a priori* las dimensiones mínimas de un sistema para las cuales los efectos de tamaño dejan de ser relevantes. Cada propiedad electrónica individual debe ser estudiada separadamente para poder llegar a conclusiones respecto a la relevancia o no de hallarse en la nanoescala.

References

[1] Alonso J A and Balbás L C, *Topics in Current Chemistry* vol 182, Springer-Verlag, Berlin-Heidelberg (1996) p 119.

[2] Brack M 1993 *Rev. Mod. Phys.* **65** 677

[3] W. A. de Heer, Rev. Mod. Phys. **65**, 611 (1993).

[4] M. Quijada, R. Díez Muiño, A. G. Borisov, J. A. Alonso , and P.M. Echenique, *New. Jour. Phys.* **12**, 053023 (2010)

[5] M. Quijada, A. G. Borisov, I. Nagy, R. Díez Muiño, and P.M. Echenique, *Phys. Rev. A* **75**, 042902 (2007)

[6] L. Hedin, *Phys. Rev. B*, **139**, A796 (1965)

[7] M. Quijada, R. Díez Muiño, and P.M. Echenique, *Nanotechnology* **16**, S176 (2005).

[8] A. Zugarramurdi, N. Zabala, V. M. Silkin, A. G. Borisov, and E. V. Chulkov, *Phys. Rev. B* **80**, 115425 (2009)

[9] S. P. Møller, E. Uggerhøj, H. Bluhme, H. Knudsen, U. Mikkelsen, K. Paludan, and E. Morenzoni, Phys. Rev. A **56**, 2930 (1997).

[10] S. P. Møller, A. Csete, T. Ichioka, H. Knudsen, U. I. Uggerhøj, and H. H. Andersen, Phys. Rev. Lett. **88**, 193201 (2002).

[11] S. P. Møller, A. Csete, T. Ichioka, H. Knudsen, U. I. Uggerhøj, and H. H. Andersen, Phys. Rev. Lett. **93**, 042502 (2004).

[12] H. Paul, D. Semrad, and A. Seilinger, Nucl. Instrum. Methods B **61**, 261 (1991).

[13] H. H. Andersen and J. F. Ziegler, *Hydrogen Stopping Powers and Ranges in all Elements* (Pergamon Press, Elmsford NY, 1977).

[14] International Commission on Radiation Units and Measurements, *Stopping Powers and Ranges for Protons and Alpha-Particles, ICRU Report 49* (Bethesda, MD 20814, USA, 1993).

[15] J. Tao and G. Vignale, Phys. Rev. Lett. **97**, 036403 (2006).

[16] M. Quijada, A.G. Borisov, and R. Díez Muiño, *Physica Status Solidi A*, **205**, 4546 (2007).

10 Agradecimientos

Una tesis doctoral, como trabajo de varios años que es, lleva consigo una gran cantidad de gente que ha participado de una manera u otra en el camino. A lo largo de estos años de trabajo son muchas las personas que me han ayudado, acompañado y animado a llegar hasta aquí.

En primer lugar, quiero agradecer a mis directores de tesis, los profesores Pedro Miguel Echenique y Ricardo Díez Muiño, su excelente supervisión científica y su apoyo y ánimo incondicionales. A Ricardo, su afabilidad y optimismo contagioso, su buen humor y su buen hacer. A Pedro, la oportunidad de trabajar en un centro como el Donostia International Physics Center, que me ha aportado mucho tanto a nivel personal como profesional.

Quiero agradecer también al Prof. Andrey Borisov, por su acogida en la Universidad de Orsay, donde se desarrolló el código del TDDFT utilizado en este trabajo, y por la colaboración continuada en el DIPC. También a los profesores Julio Alonso e Istvan Nagy, por las interesantes y útiles discusiones científicas en el mismo centro.

No quiero olvidarme de los compañeros de mi quinta en Donostia, de mis amigas de Bilbao, de mi familia en Vitoria. Ni de Martina, Laura, Enara, Maruxa... Gracias también a Stefan Mastel, por su ayuda a la hora de dar formato a esta tesis.

Por último, agradezco a mis padres, a mis hermanas y a Rainer. Su ánimo, apoyo y cariño incondicionales tienen mucho que ver con que este trabajo esté hoy aquí.

11 List of published articles

The present manuscript is based on the following publications (in order of appearance in the manuscript):

- **The lifetime of electronic excitations in metal clusters**
  M. Quijada, R. Díez Muiño, and P. M. Echenique,
  Nanotechnology **16**, S176 (2005).

- **Lifetime of electronic excitations in metal nanoparticles**
  M. Quijada, R. Díez Muiño, A. G. Borisov, J. A. Alonso, and P. M. Echenique,
  New Journal of Physics **12**, 053023 (2010).

- **Time-dependent density-functional calculation of the stopping power for protons and antiprotons in metals**
  M. Quijada, A. G. Borisov, I. Nagy, R. Díez Muiño, and P. M. Echenique,
  Physical Review A **75**, 042902 (2007).

- **Time-dependent density functional calculation of the energy loss of antiprotons colliding with metallic nanoshells**
  M. Quijada, A. G. Borisov, and R. Díez Muiño,
  Physica Status Solidi A **205**, 1312 (2008).

The following articles were published as well during the PhD.:

- **Dynamic screening and electron-electron scattering in low-dimensional metallic systems**
  V. M. Silkin, M. Quijada, R. Díez Muiño, E. V. Chulkov, and P. M. Echenique,
  Surface Science **201**, 4546 (2007).

- **Dynamic screening and electron dynamics in low-dimensional metal systems**
  V. M. Silkin, M. Quijada, M. Garcia-Vergniory, M. Alducin, A. G. Borisov, R. Díez Muiño, J. I. Juaristi, D. Sanchez-Portal, E. V. Chulkov, and P. M. Echenique,
  Nuclear Instruments and Methods in Physics Research B **258**, 72 (2007).